Kazakh National Research Technical University named after Satbayev K.I.

UDC 622.32

DURMAGAMBETOV BERIK ORALOVICH

Hydraulic fracturing efficiency study and optimization of reservoir performance at the Arystan field

8D07202 – Petroleum Engineering

Thesis for the degree of
doctor of philosophy (PhD)

Scientific Advisors
doctor PhD,
professor assistant
D.A. Ismailova

doctor PhD,
professor
I.V. Panfilova

Republic of Kazakhstan
Almaty, 2023

CONTENTS

ABBREVIATIONS

A – Total Fracture Area created after pumping for tp minutes (ft2)
C – Fluid Loss Coefficient (ft)
ΔP – Pressure Difference (psi)
ΔP * – Match pressure for pressure decline analysis (psi)
δ – Dimensionless Shut-In Time
δ_c – Dimensionless Closure Time
e_f – Fracture Fluid Efficiency = Fracture Volume at Shut-In (V)/Total Volume
E – Young's Modulus of Formation (psi), Typical Values - 2x106 psi to 8x106 psi
E' – Crack Opening Modulus
f – Fraction
fp – Pad Fraction or Pad Percentage
fpr – Proppant Fraction of Job, Vpr/Vp
H – Total or Gross Fracture Height (ft)
Hp – Permeable or Leakoff Height (ft)
pc – Fracture Closure Pressure (psi)
pnet – Net Fracturing Pressure
ps – Net Pressure at Shut-In (e.g., ISIP - pc)
ϕ – Porosity of Proppant Pack (typically on the order of 0.40)
Q – Total Injection Rate (barrels/minute, bpm)
qLoss – Fluid Loss Rate (bpm)
rp – Ratio of permeable or leakoff area to total fracture area for P&K or Geertsma rp =
ρ – Loss Ratio = efficiency/ (1 - efficiency)
ρ_{pr} – Specific Gravity of Proppant (e.g., 2.65 gm/cc or 22 lb gal for sand)
S – Fracture "Stiffness" for Pressure Decline Analysis
tc – Closure Time, e.g., Shut-In Time to Fracture Closure (minutes)
tp – Pump Time (minutes)
ts – Shut-In Time (e.g., incremental time since pumping stopped) (minutes)
τ – Time when an incremental element of fracture area is first exposed to fluid loss
V – Fracture Volume (ft3)
VLoss – Total Fluid Loss Volume During Pumping (ft3)
Vp – Total Slurry Volume Pumped (ft3)
Vpr – Total Proppant Volume Pumped (ft3), including porosity of proppant
Vfl – Total Fluid Volume Pumped (ft3)
δ – Dimensionless Shut-In Time, ts/tp or (t-tp)/tp
W – Total weight of proppant pumped (pounds)
υ – Poisson's Ratio for Formation (dimensionless), Typical Values - 0.15 to 0.25
μ – Fluid Viscosity (centipoise)
BHCP – Bottomhole closure pressure in psi

BHTP – Bottomhole treating pressure in psi
bpm – Barrels per minute
C – Fracturing fluid leakoff coefficient. It is also equal to Ct in ft/minute
E – Modulus of Elasticity in psi
FCD – A dimensionless fracture capacity
FOI – Folds of Increase
H – Total or gross fracture height in feet
hhp – Hydraulic Horse Power in hp
k – Reservoir permeability in millidarcies (md)
kf – Fracture permeability in md
kfw – Fracture conductivity in md-ft
K' – A property of gelled frac fluids
L – Hydraulic fracture length from tip to tip
μ – Viscosity in cp
n' – A property of gelled frac fluids called Power Law
OB – Overburden pressure in psi. Generally, it is one times TVD in psi
Pc – Critical Pressure or Pressure Capacity
re – Drainage radius in feet. Generally, it is one-half the distance to the next well
rw – Wellbore radius in feet
r'w – The stimulated wellbore radius effect due to the fracture in feet
S.G. – Specific Gravity relative to water
TVD – True Vertical Depth in feet
w – Fracture Width in feet (may also be in inches)
xf – Fracture radius in feet (or fracture half-length)

INTRODUCTION

The Arystan field reservoirs are characterized by low permeability [1], heterogeneity, and variability of the lithological and mineralogical composition of rocks both in section and area. In this regard, it is necessary to solve an urgent problem, which consists of the development and implementation of new methods for intensifying oil and gas production processes. Take into account the main sensitive parameters which mainly affect OPEX and overall project profitability. Oil production significantly depends on the creation of new technologies for influencing the near-wellbore formation zone (NWF). The diversity and complexity of the phenomena in the bottomhole zone have caused the use of various technologies and methods of oil recovery and intensification of oil production, which are described in domestic and foreign literature. In recent years, in the Arystan field, one of the most effective methods for increasing well productivity is hydraulic fracturing (HF). Despite the high performance and success of hydraulic fracturing, practical experience shows that its effectiveness mainly depends on Reservoir condition such as Kh values, formation pressure, and thermobaric condition that triggers scale and corrosion issue. The flow rates of producing wells are declining, despite repeated hydraulic fracturing

In the context of the depletion of traditional hydrocarbon reserves, increasing attention is being paid to deposits with hard-to-recover reserves (HRR). Currently, HRR accounts for about 70% of Commonwealth of Independent States countries reserves, the majority of which belong to deposits with deteriorated filtration and reservoir properties The profitable involvement of such objects in exploitation requires special technologies capable of increasing well productivity. One of the most commonly used technologies is hydraulic fracturing (HF).

The HF frac allows a combination of a set of thin pay zones into a single development object and improves the quality of the opening under conditions of deep penetration zones, increasing the drainage area compared to the opening without HF .

The history of the practical application of hydraulic fracturing (HF) in the oil and gas industry counts more than 70 years. Over this period, HF has become one of the main technologies for opening low-permeability formations, the development of which is not profitable by "standard" methods due to low well flow rates.

The specifics of both the drainage conditions of the fractured reservoir and control of its development depend on the nature and degree of complexity of the development object, which requires careful study.

Finally, when talking about the problem of controlling the development of a complex–tight reservoir opened up by artificial macro- fracs, it is impossible not to mention wells with depleted pressure conditions and scale problems. In conditions of abnormally low reservoir pressure, scale precipitation, and the operational problem with Artificial lift is playing a key role in the strategic forecast of producing company.

Thus, the effective development of tight reservoirs in hydraulic fracturing conditions requires effective monitoring. Its basis is comprehensive hydrodynamic (well-testing) and field-geophysical research.

The complexity of the objects being studied (heterogeneous formation structure, low formation evaluation saturation, complex well completion methods) has necessitated the improvement of existing approaches to describing these objects and the development of comprehensive interpretation methods for geophysical and hydrodynamic data.

Therefore, for the successful development of low-permeability and heterogeneous objects, a scientifically based approach is required not only for the selection of wells for hydraulic fracturing and its parameters that affect the efficiency but also for the variety of factors and reasons that reduce its productivity during operation. Therefore, the main direction of the dissertation work is related to the development and justification of effective integrated technologies.

Objective

The objective of this dissertation was to introduce advanced methods of fracture geometry analysis, and fracture parameters sensitivity study by using integrated laboratory, software, and research study. The Research and Scientific nature of this work is supported by the fact that Lagrangian approach-based Multiphysics hydraulic fracturing modelling software in combination with fracture height measurement techniques is a new approach to the production stimulation industry in Kazakhstan [2].

To implement a methodology for conducting comprehensive field geophysical and hydrodynamic studies of reservoirs with microheterogeneities opened by artificial microfractures to justify measures to improve efficiency and optimize formation development. This research study focused on the optimization of hydraulic fracturing in the oilfield. The aim was to understand the geometry and characteristics of hydraulic fractures and to optimize them using an advanced numerical matrix flow simulator and Multiphysics hydraulic fracturing simulator. One of the main challenges was to develop a meaningful research component, which required the use of software with outstanding or new algorithms and workflows.

To address this challenge, the research team collaborated with Schlumberger Research Centers and developed an integrated Field-Software-Analytic workflow. This workflow consisted of three main steps. Firstly, a hydraulic-fracture-induced rock anisotropy survey was performed in a fractured well using a dipole acoustic tool. Then, a reservoir-centric Multiphysics fracturing simulator was employed to run a digital sensitivity study of the fracture parameters. The main part of the study scale issue was also examined for fracturing or workover operation to clarify the short-term scaling tendencies that can occur during these operations. This can include understanding the types of scales that can form due to the fracturing or workover operations, and the chemical composition of the fluids used Finally, the hydrodynamic simulation using Intersect, with subsequent analysis, closed the loop [3].

By applying this workflow, the research team was able to reveal that the fracture effective length was overestimated by 40%, which significantly affected the profitability estimations of the fracturing projects. Furthermore, the advanced particle transport algorithm inside the Multiphysics Fracturing Simulator allowed for a detailed understanding of proppant distribution inside hydraulic fractures for the first time in the region. Optimization recommendations were made based on this understanding [4].

The example of this study clearly demonstrated how the integration of the latest digital Multiphysics solutions (Ksinetix based on the recognized reservoir-centric platform Petrel) with advanced surveys (induced anisotropy detection) can yield reasonable conclusions on hydraulic fracturing strategy. Overall, this research study provided valuable insights into the optimization of hydraulic fracturing in the oilfield, which can have significant economic implications [4, p. 694-711].

Main research tasks:

1. A literature review on the use of hydraulic fracturing as a method of extracting oil and natural gas from tight sand rock formations.

2. Analysis and justification of the factors that determine the effectiveness of hydraulic fracturing and identifying the reasons that reduce the productivity of wells during operation.

3. Develop a novel method for Hydraulic fracturing design that includes reservoir geomechanics with respect to pressure depletion.

4. Analytical and numerical studies of the Arystan field in order to understand the main reservoir drive mechanism.

5. Laboratory studies of the composition of mechanical impurities and the nature of deposits that reduce the permeability [5].

6. Development of a new design strategy for well stimulation respectively to reservoir thermobaric condition.

7. Investigation of key parameters that contributes to the well PI index.

Research methodology

To solve the tasks set in the dissertation work, an analysis of domestic and foreign publications on these topics was carried out and summarized; Hydrodynamic modeling of pressure decline and well productivity; processing, interpretation, and analysis of petrophysical data and scale precipitation study.

In the course of the work, the author used software: "Eclipse 100", "Intersect " "Petrel", and "Techlog " (Schlumberger).

The reliability of scientific conclusions and recommendations is confirmed by generalization and analysis of the results published in domestic and foreign publications; evaluation of the information content of the proposed research methods and the reliability of the revealed patterns of behavior of the studied geophysical fields based on mathematical modeling and numerous studies in wells; the results of practical application and implementation of the proposed approaches to the study of macro-homogeneous formations with macro- fracs [6].

Scientific novelty

The novelty of this study lies in the development of a new approach for optimizing the design and operation of hydraulic fractures with respect to aggressive field pressure depletion and thermobaric conditions with high scale formation probability. To develop more effective and efficient fracturing strategies the Eulerian-Lagrangian approach is a mathematical framework used to model hydraulic fracturing. In this approach, the rock formation is modeled using a fixed Eulerian grid, which represents the spatial coordinates of the rock. The fluid and proppant particles, on the other hand, are modeled using a Lagrangian approach, which tracks the motion and deformation of the individual particles as they move through the rock.

The Research and Scientific nature of this work is supported by the fact that. Moreover, running simulations for scaling study evaluation enables understanding long-term scaling tendencies (during water injection projects) or short-term scale tendencies (during fracturing or workover operations), and gives recommendations based on tests and the Schlumberger database. The Research and Scientific nature of this work is supported by the fact that Scale analysis scientific software and Lagrangian approach-based Multiphysics hydraulic fracturing modelling software in combination with fracture height measurement techniques is a new approach to the production stimulation industry in Kazakhstan.

Advanced methods of fracture geometry analysis and fracture parameters sensitivity study performed by the integrated laboratory, software, and research study under the dissertation scope. As the result .it was practically proved that as the reservoir pressure is depleted, the geomechanical stress on the rock surrounding the wellbore will change its maximum direction. By controlling the injection pressure and the properties of the fracturing fluids, the effectiveness of the refracturing operation will much higher despite the decrease in reservoir pressure.

Defending hypotheses:

1. Based on the prepared well model, the main hypothesis to check was: Do we correctly predict the Fracture geometry, and if not – how to optimize it?

2. Proved that the surface readings showed underestimated kh. The surface readings of kh (the permeability of the rock to the flow of fluids) can sometimes underestimate the true value because they are based on measurements taken at the surface of the well, which may not accurately reflect the conditions in the wellbore. In contrast, downhole gauges can measure the conditions directly in the wellbore, which can provide a more accurate picture of the transmissibility of the well.

3. Sensitivity study on the Actual Fracture length.

4. It is noted in some publications in the industry, e.g. SPE-106140 (picture below), that fracture reorientation may happen in a locally depleted zone. Thus, for refracturing candidates, it is recommended to observe the fracture efficiency. If fracture efficiency is close to that of during the initial fracture, then probably fracture is created in the new plane. However, if fracture efficiency is significantly lower, then, probably, the fracture is created along the initial fracture.

Practical value

Development the most effective strategy for scale control and the main strategy to deal with depleting reservoir to increase the effective fracture half-length via several options.

Numerical model

The simulation model develops valuable insights into the behavior of the reservoir in different conditions such as pressure depletion, gas liberation water injection optimization.

Recommendations on scale control methods

The main strategy to deal with scale is to perform pre-heating of injected water with subsequent removal of the precipitated scale may decrease the tendency to the scaling., an increase of pH with subsequent removal of the precipitated scale has a somewhat similar effect to temperature methods for Calcium carbonate or change of water source to the one with two times less Calcite content .

Fracturing treatment strategy recommendation in depleting formation

The main strategy to deal with depleting reservoir is to increase the effective fracture half-length via several options, the most remarkable are: i) to minimize fluid volumes pumped into formation, use more aggressive PAD percentage, eliminate extra pumping stages like SRT, double injection test, because injection combined with SDT or SRT may be enough; ii) use cleaner fluids, like the ones based on Cellulose or on the Viscoelastic Surfactants; iii) use bigger proppants whenever possible, or more conductive proppant type .

Publications. The main hypotheses of the dissertation have been published in 5 articles:

1. Advanced methods of fracture geometry analysis and parameters sensitivity study // News of the National Academy of Sciences of the Republic of Kazakhstan. Series of geology and technical sciences. – 2022. – Vol. 6, Issue 456. – P. 45-57 (ISSN 2224-5278).
2. Geological and hydrodinamic modeling of an oil field of the pricaspian region of the republic of Kazakhstan // News of the National Academy of Sciences of the Republic of Kazakhstan. Series of geology and technical sciences. – 2022. – Vol. 5, Issue 456. – P. 266-288 (ISSN 2224-5278).
3. Geological and geochemical features of an oil field of Precaspian region // Scientific and technical Journal Oil and Gas. – 2022. – №2. – P. 32-41.
4. Problem Research salt formation at the field Caspian region // Scientific and technical Journal Oil and Gas. – 2022. – №5. – P. 40-64.
5. Using a special complex logging to study the properties of reservoir fluids and reservoir ocks Cretaceous and Jurassic deposits periods of the Arystan field // Scientific and technical journal Oil and Gas. – 2022. – №6 (УДК 550.8).

An overview of the entire dissertation

Overall, the main task of the dissertation was to analyze production history to determine the identity if the decline was mainly due to pressure depletion or if it started at a later time due to scale precipitation or hydraulic fracture degradation.

In order to differentiate 3 phenomena and understand the main reason the following step was performed:

1. Reservoir simulation model was created to understand main material balance issue and drive mechanism with respect to time.
2. Selection and adjustment of hydraulic fracturing modeling process that fit for simulation model.
3. Thermobaric condition of wellbore was analyzed to understand main mechanism of scale deposits affecting production.
4. Cause of main hydraulic fracture degradation parameters and design for refracturing treatments.
5. Chapter I, provide information about the Arystan oilfield geology and reservoir development features.
6. Chapters II, describe simulation model construction that was used to

evaluate the reservoir and determine if the decline in production is due to pressure depletion or if there are other factors affecting the reservoir performance such as the presence of scale or hydraulic fracture degradation. describe material balance and analysis of main uncertain parameters to understand main factors that contribute for liquid and pressure decline. As a result, list of suggestions about further acquisition study was created.

7. Chapters III describe the novel approach for hydraulic modeling that fits for Intersect model.

8. Finally, Chapter V includes main outcomes and novel approach for the analysis of wells productivity decrease both hydraulic fracture degradation and pressure depletion sensitivity studies.

Structure of the Thesis. The total volume is 120 pages, including 137 figures, 11 tables, references of 86 titles.

1 THE ARYSTAN OILFIELD OVERVIEW

1.1 The Arystan oilfield geology and reservoir development features

The Arystan field is geographically located within the north-western part of the Usturt plateau at 300 km northeast of Aktau city (figure 1). It is administratively located in Mangystau region of the Mangystau oblast. The nearest developed field is Karakuduk. Arystan field is located in the central part of Arystan tectonic step (figure 2).

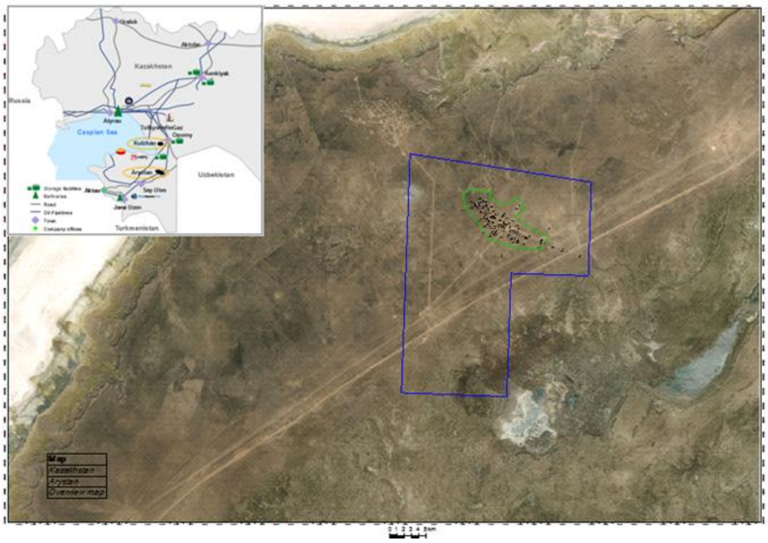

Figure 1 – General map

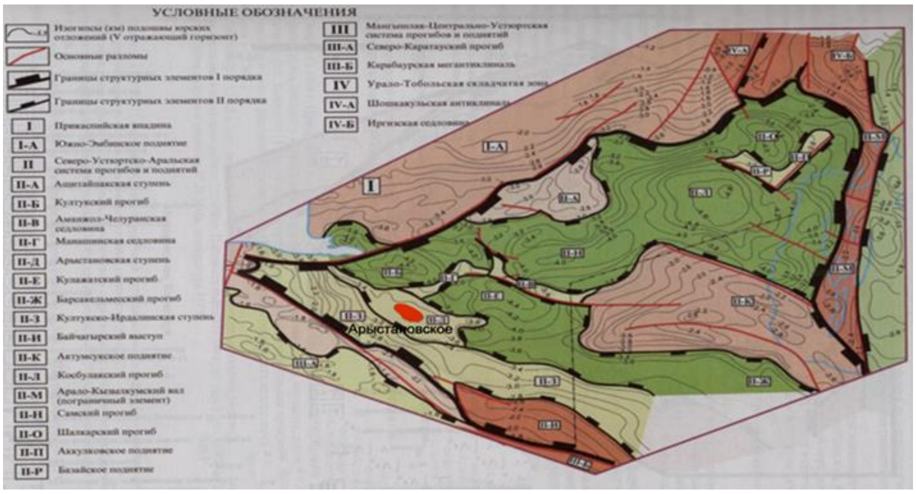

Figure 2 – Tectonic scheme

Seismic Interpretation

A complex of geological and geophysical studies covers the territory of the Arystan field. Seismic survey was carried out in the second part of the last century 50’s-90’s to determine the geological and structural features of the area and the allocation of structures for exploratory drilling. In 2006 3D seismic work was performed in order to clarify the geological and structural setting of the field. The work materials were analyzed, processed, and interpreted in 2006, and structural maps for the five horizons were constructed based on the results of the work (III, J-VII, J-VIII, J-IX, V1). As a result, the structural-tectonic model of the field was substantially refined.

In 2008 additional 3D seismic interpretation was performed. The scope of work included calibration of seismic data with logging data, VSP tie-in for 53 wells, and adjustment of velocity model, seismic inversion, and seismic facial analysis. In addition to this, correlation and maps for new horizons were built (J-X, J-XI) (figure 3).

In 2011, reinterpretation of 3D seismic was done based on new drilled wells.

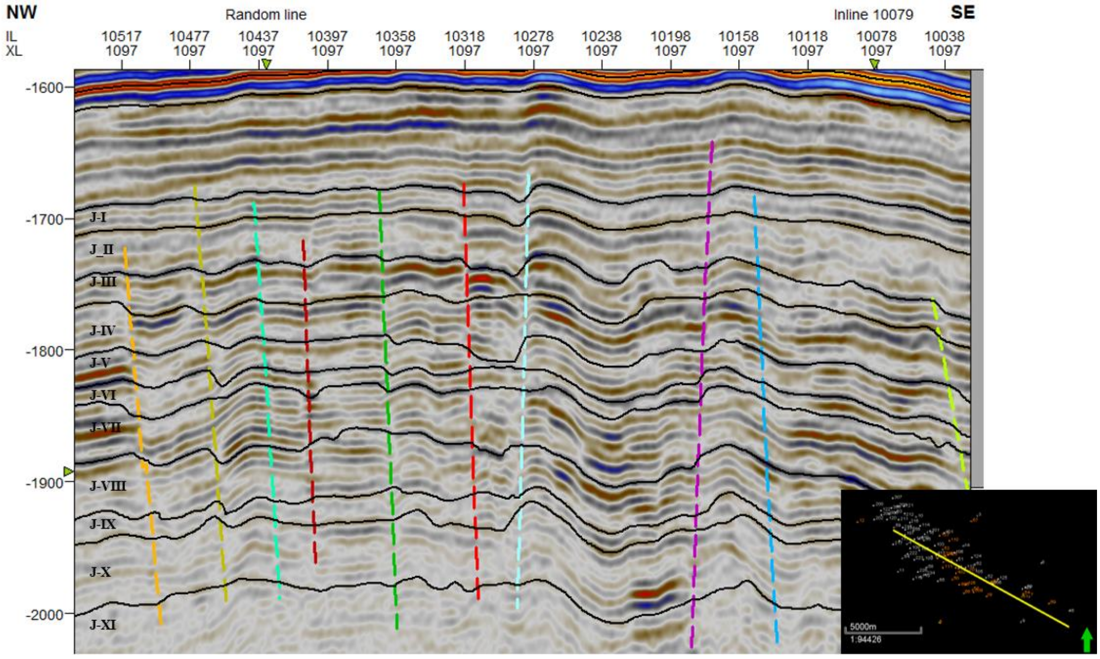

Figure 3 – Time seismic profile _1097

Geological Description

Within the structure of the field, the wells penetrated sediments from Triassic to Quaternary. The Mesozoic deposits on the Arystan field are represented by the Triassic, Jurassic, and Cretaceous systems. Deposits of the Triassic are represented by terrigenous rocks with a penetrated thickness of 929 m.

The Jurassic system is divided into the lower, middle, and upper series. Terrigenous sandy-argillaceous rocks with a thickness variation from 0 to 88 m represent the composition of the Lower Jurassic deposits. The Middle Jurassic series deposits are represented by terrigenous sandy-argillaceous rocks with a thickness variation from 0 to 88 m. The Middle Jurassic series is divided into Aalenian-Bajocian, Bathonian, and Callovian stages. The Upper Jurassic series is divided into Oxfordian, and Volgian stages.

The Cretaceous system is divided into lower and upper series. The deposits of the Cretaceous system is represented by clastic and carbonate rocks. The Lower Cretaceous series is divided into Valanginian, Hauterivian, Barremian, and Aptian stages. The Upper Cretaceous series is divided into Cenomanian, and Turon-Senon stages.

The Cenozoic deposits on the Arystan field are represented by Paleogene, Neogene, and Quaternary systems. Paleogene system is represented by the Danian stage with up to 17m thickness of carbonate rocks. The neogene system is represented by argillaceous-carbonate rocks and limestones with thicknesses up to 126 m. The quaternary system is represented by conglomerates and continental rocks with thickness up to 15 m.

Log Analysis

The company Ken Sary has provided log data (including the following types: Gamma-ray, Lateral log, Microlaterlog, Acoustic, Photoelectric, Neutron, Density, and Resistivity) and its interpretation (with the results of the shale volume, porosity, and oil saturation) for many wells of the Arystan field. To assess the STOIIP, the methodology of wireline interpretation was considered and generally accepted. The methodology of wireline log data interpretation is described.

Determination of clay volume: Clay volume coefficient was determined from the gamma-ray with the use of Larionov relationships. Within the reservoir, it varies from 4 to 40%.

Calculation of porosity: Porosity is determined based on D.T. Neutron, and G.R. Within the reservoir, it varies from 0.1 to 0.22 with a mean of 0.13.

Saturation calculation: The water saturation coefficient was determined by the method of electrical resistance using petrophysical connections Dakhnov-Archi, built on data from the core study of the field Arystan. The oil saturation coefficient is defined as (Soil = 1-Sw) Oil saturation varies from 0.4 to 0.79, with a mean of 0.55.

Fluid Contacts

Several sources of data were analyzed to identify the contacts and estimate the ranges of uncertainty in contact depths. These include the analysis of the lowest known hydrocarbon in oil producing wells, the highest known water in water-tested wells, and the perforation intervals during the testing. Under each horizon, fluid contacts were limited by the lowest estimation (the lowest known oil). Ranges are between -2432 m and -2882.

Reservoir Fluid Properties

Since the beginning of the field development, many bottomhole and surface samples of oil and gas were collected for PVT analysis. The range and average PVT properties of oil for different horizons are shown in the table below (table 1). The average values of the formation volume factor were used in estimating initial oil in place.

Table 1 – Average PVT properties

Description	Range	Average
Saturation pressure, Mpa	6.29-20.11	13.2
GOR, m3/ton	58.46-189.71	124.1
Density at reservoir cond., g/cc	0.6881-0.7292	0.7087
Density at surface cond. (20 Deg C), g/cc	0.8029-0.8253	0.8141
Viscosity, cP	0.27-1.58	0.925
Formation Volume Factor	1.203-1.473	1.338

Production History and Forecast

All producing wells are equipped with Electrical submersible pumps (ESP) and tested periodically through existing group metering systems. The Cumulative oil productions are shown in the figure 4 below.

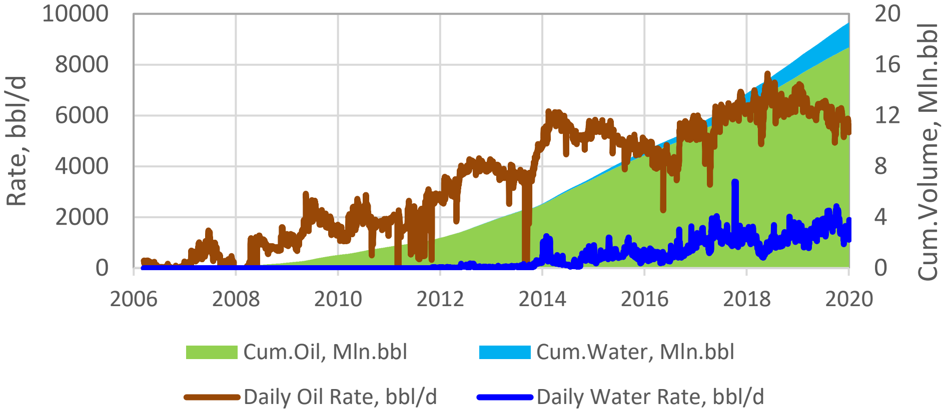

Figure 4 – Field Historical Production

Production Forecast

Production forecasts were generated till April 2038 (end of the license agreement) for Arystan field at three levels of confidence; low, mid, and high (figure 5).

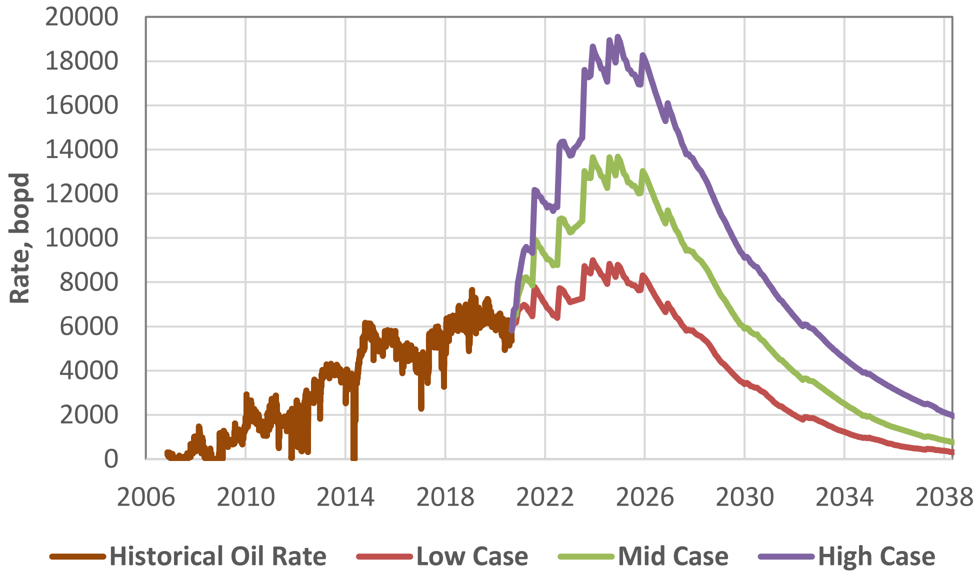

Figure 5 – Total Field Production Forecast

The foundation of the production forecast work is a decline curve analysis based on historical performance. The low and mid cases have been generated using exponential decline, while the high case assumed hyperbolic decline in order to favor future water flooding system [4, p. 694-711].

1.2 Arystan field simulation study approach

This study demonstrates the results of the work under Optimization of Arystan Field and is supposed to include fine-tuning of full field dynamical model and massive simulation of prediction scenarios to increase oil recovery by optimizing pressure maintain and produce upswept oil.

The project plan included three stages: Base Case Scenario with Sensitivity Study, Production Forecasting, and Optimized Development Scenario.

Fine-tuning of the full field dynamic model has been made on wells level. The base scenario of drilling new wells and injection strategy provided by the Customer. A sensitivity study of the base case's production helped to identify key hitters' uncertainty parameters which were included in the further forecast uncertainty study and helped to formulate suggestions for the data acquisition program. Economic model setup.

The production forecasting stage included massive simulation scenarios running with economical evaluation and uncertainty study. The main purposes of the study were maximization of oil recovery with paying attention to the project's economic benefits. The first circle of simulation used automated INTERSECT logic. The second circle of the forecasting stage included an additional manual correction to achieve the goals of maximizing oil production and economic efficiency. All simulation scenarios have been investigated with economical evaluation.

During the last stage of the project the agreed "best scenario" was manually modified including recompletions producers to upper horizons target's zones or/and transferring to injectors to maximize oil recovery by optimizing waterflooding. The optimized scenario of the field development strategy includes the placement of new wells for drilling, completion scenarios, water flooding, and economical calculation results.

The creation of a system of distributed fractures along the length of the well (multi-stage hydraulic fracturing or MSHF) has significantly increased the productivity of wells, thus providing profitable production from reservoirs with abnormally low permeability. Abroad, this technology is called MZST (Multizone stimulation technology). The essence of MSHF is to increase the contact of the well with the target reservoir over the entire length of the horizontal well.

The technology involves the use of packer assemblies. In the horizontal section of the well, a set of equipment is lowered to isolate the intervals - a tailstock with couplings and set packers. During the fluid injection, the couplings are sequentially opened by dropping balls and isolating the lower intervals after hydraulic fracturing is carried out in them. The main advantage of this system is that it allows for simplified completion of the well without cementing and perforating tailstocks .

1.3 Arystan Field Geological feature

The static model used in the current project is based on the static model 2019 year with some updates associated with new wells, drilled in 2019-2021 years. The project plan was not included any static model changes. The components of the static model used in this project consist of:

– structure grid;

– seismic horizons;
– configurations of sand channels;
– two lithology types of sandstone and tight shaly sandstone in model;
– porosity property modeling used a petrophysical interpretation of the 2019-year static model with revision in the 2020-year included new wells drilled in 2019-2020 years (figure 6).

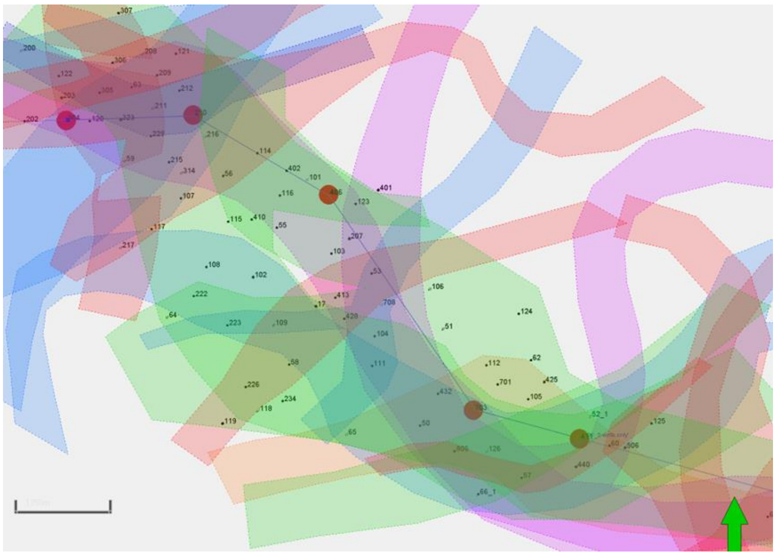

Figure 6 – Five new wells location on 14 Arystan field channels

Conclusions on the 1st section

Developing an oil field with tight reservoir properties can present several challenges. Tight reservoirs are characterized by low permeability, which makes it difficult for oil to flow through the rock and into the wellbore. This can make it challenging to produce oil from these fields and can require specialized techniques and technologies to be successful.

One of the main challenges of developing an oil field with tight reservoir properties is the high cost of drilling and completion. Tight reservoirs require more wells to be drilled and completed compared to conventional reservoirs to achieve the same level of production. This can lead to higher drilling costs and longer completion times, which can increase project costs.

Another challenge is the need for specialized drilling and completion techniques. Hydraulic fracturing is commonly used in tight reservoirs to stimulate the flow of oil and gas. These techniques require specialized equipment and skilled personnel to execute successfully. Hydraulic fracturing has been a game-changer in the development of tight reservoirs, making it possible to access previously inaccessible reserves. However, it is also a controversial technique due to concerns about its economic impact and challenge to sustaining profitable production.

2 THE ARYSTAN OILFIELD SIMULATION STUDY

2.1 Dynamic model initialization

Dynamic model initialized with equilibrium. Irreducible water as SWL property calculated in Petrel property calculator. The regression of water saturation and porosity derived from core analysis. That approach was used in the 2020-year dynamic modeling and described in the previous year's project report. For the creation SWL property of ARYSTAN horizon was used results of centrifugation core analysis were made with samples from ARYSTAN intervals in wells 56, 115, 120. Study of samples from J-X horizons in wells 53, 42, 43, 45, 46 used for J-X SWL modeling. Samples in intervals of J-IX horizon were studied in wells 51 and 53. Horizons J-VIII, J-VII, J-VI and J-V don't have studies of samples covering separate intervals of that horizons but there are two wells where together J-VIII+J-IX intervals' samples studied (well 55) and J-VII interval in well 51. Due to a lack of data all measurements from those two wells were used for SWL modeling of upper horizons from J-VIII up to J-V. The uncertainty of SWL modeling and as a result ambiguousness of oil volumes calculation is the reason for the additional revision of water saturation. In the Petrel modeling 2018-2019 years and static model OIIP volume calculation there is another way of water saturation estimation used. The Archi equation is a method of water saturation calculation in wells logs and petrophysical modeling of grid property after that was used. The volume calculations result with both methods have been compared. Since the STOIIP in the static model with Archi equation Sw and dynamic model SWL from core analysis used in the 2020-year model had significant differences in J-IX and upper horizons was decided to adjust porosity-irreducible water regressions used in the dynamic model to minimize the differences of OIIP up to ±10% in channels bodies.

The final regressions shown on figure 7, 8. The ARYSTAN and J-X horizons SWL modeling with the equation used in 2020-year model (figure 7, 8) without any changes. The maximum SWL of J-IX in 2020-year model corresponded to high porosity 9% which significantly underestimated OIIP – grey line on figure 8. To correct it and achieve more consistency with Archi method of water saturation modeling was decided to use two correlations for SWL modeling: linear for porosity less than 15% (green line) and exponential equation for porosity higher than 15% (red line) (figure 9).The correlation for SWL modeling of J-VIII, J-VI and J-V used as in 2020-year model. It is grey line on figure 10. The red line of power correlation on the same figure 10 used for J-VII SWL modeling.

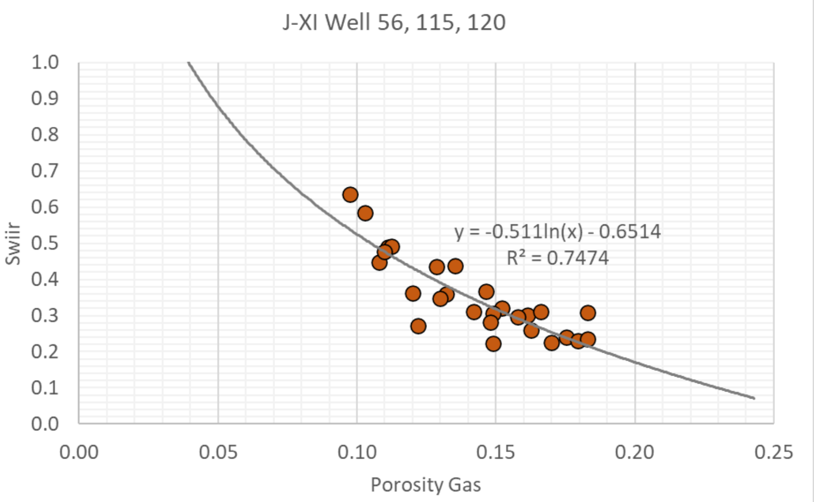

Figure 7 – Logarithmic correlation used for ARYSTAN SWL modeling

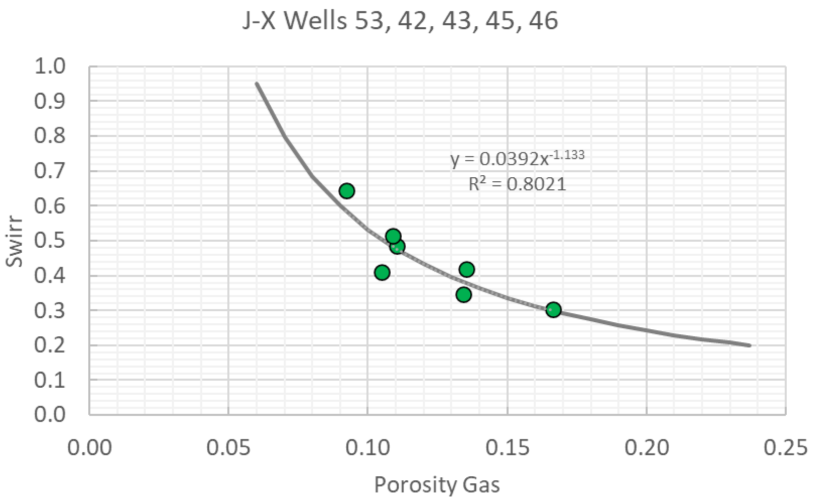

Figure 8 – Power correlation used for J-X SWL modeling

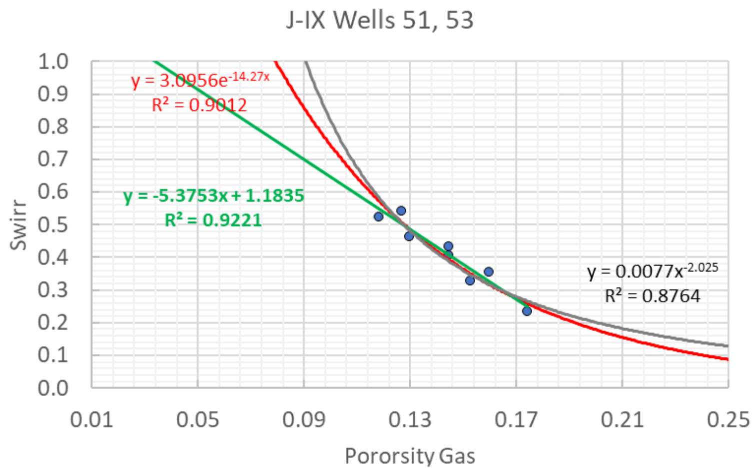

Figure 9 – Correlation used for J-IX SWL modeling

Notes:

1. Linear Green for Porosity <0.15 and exponential red for Porosity >0.15.
2. Grey used in the 2020-year dynamic model

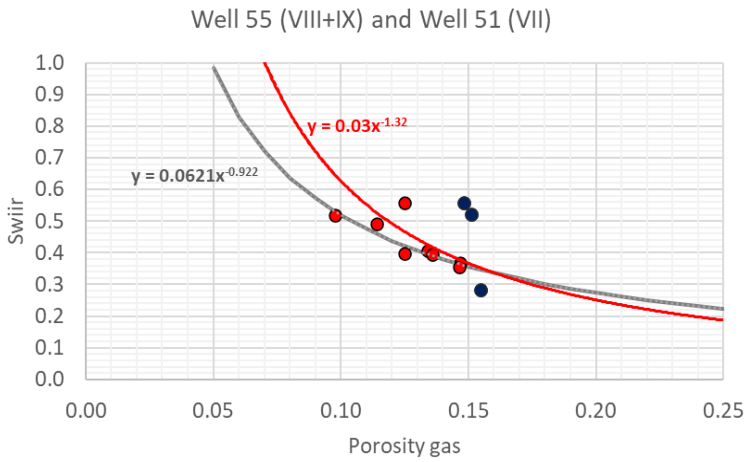

Figure 10 – Grey power correlation used for J-VIII, J-VI, J-V SWL modeling. Red power correlation used for J-VII SWL modeling

Oil-Water transition zone created by using drainage capillary pressure curves from capillary pressure core analysis. The study has been performed with cores from three wells 51, 53 and 120. The maximum capillary pressure as per results are 4,2 bar and 2,36 bar (figure 11).

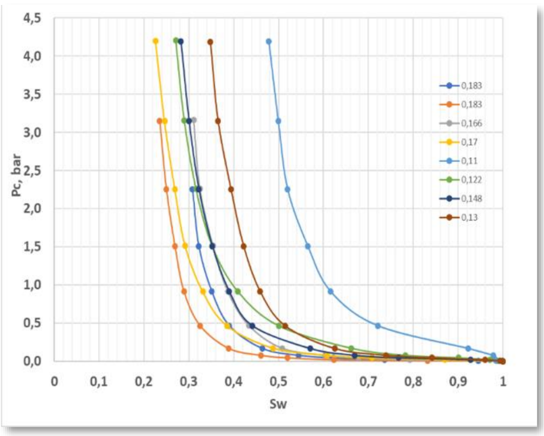

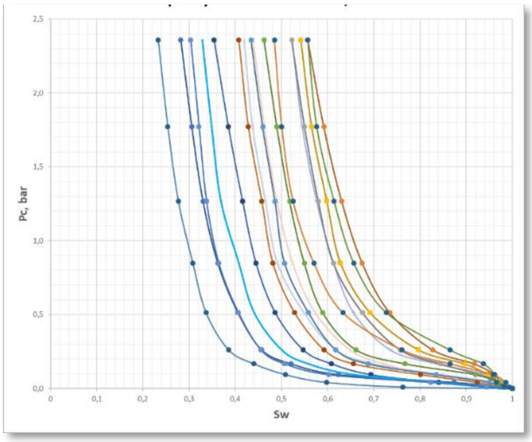

a b

a – capillary pressure, well 120, J-XI; b – capillary pressure, well #51, #53

Figure 11 – Capillary pressure core analysis

Initially OWC estimated by well production tests and well logs interpretation results. During fine tuning to water production history some OWC were modified, and it will be described in figure 12.

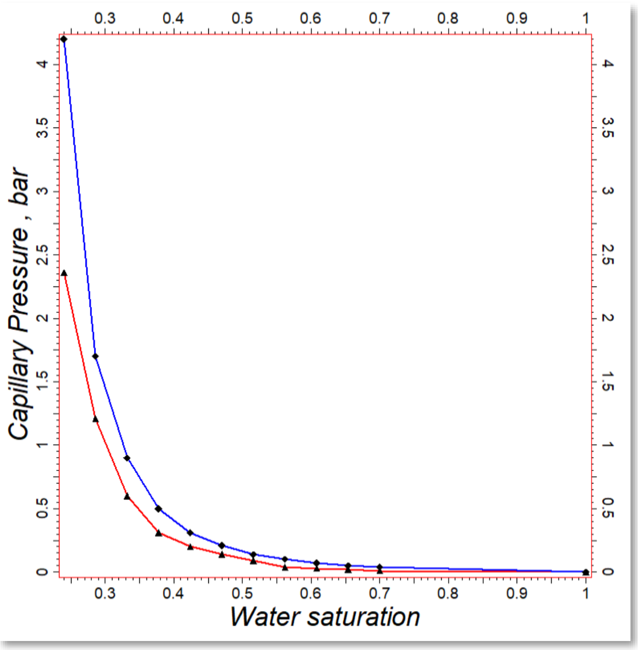

Figure 12 – Capillary pressure used in the modeling

The results of oil volumes calculation will show after fine tuning of dynamic model.

2.2 Permeability modeling

As porosity and permeability are the key reservoir characteristics that determine specificities of the reservoir properties, equation for permeability calculation was provided from petrophysics study: PERM = 10^(38.57*POR-5.026).

On top of all, taking into consideration the big range of the permeability values for the specified porosity value (for instance, 15% effective porosity sample can have the range from 1 to 80mD permeability), it was decided to build additional two dependencies (figure 13) to cover the uncertainty ranges. Maximum Permeability in 3D Models was limited at max value 500 mD [7].

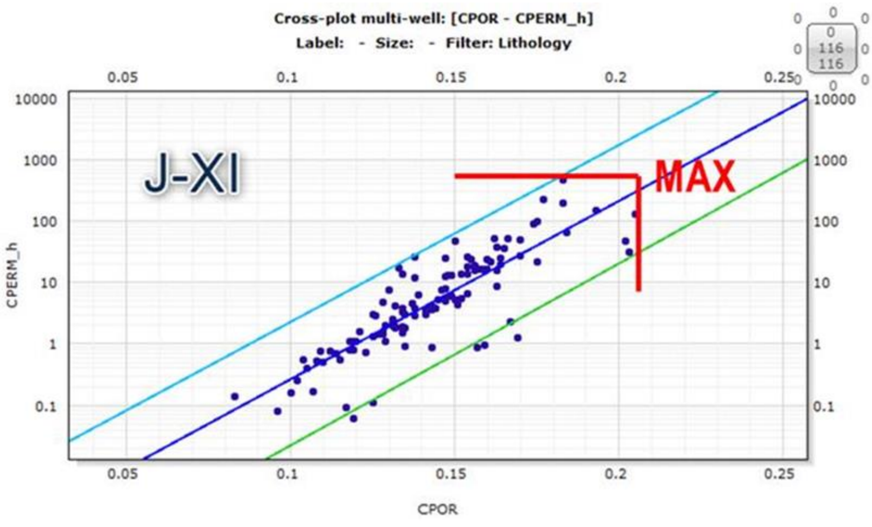

Figure 13 – The porosity vs permeability relationship for reservoir J-XI

For the horizons J-XI, J-X, J-IX, J-VIII and J-VII for lithofacies “sandstone” and “tight shaly sandstone” used separate regressions as on the figure 14. The blue line represents “sandstone” lithotype and green line is “tight shaly sandstone”. More detailed information provided in the report of 2020 year.

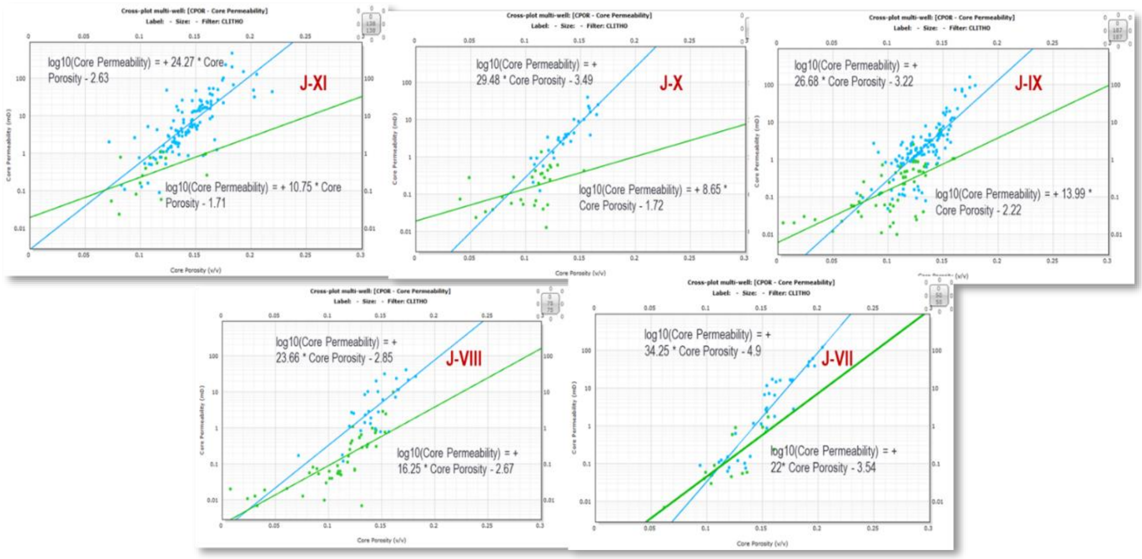

Figure 14 – Porosity-Permeability petrophysical regressions

The uncertainty of porosity-permeability relationship has been accounted by random values changing in specified ranges as shown on the figure 15, for J-XI, on the figure 16, for J-X, on the figure 17 for J-IX, on the figure 18 for J-VIII, on the figure 19 for all others upper horizons J-VII, J-VI and J-V.

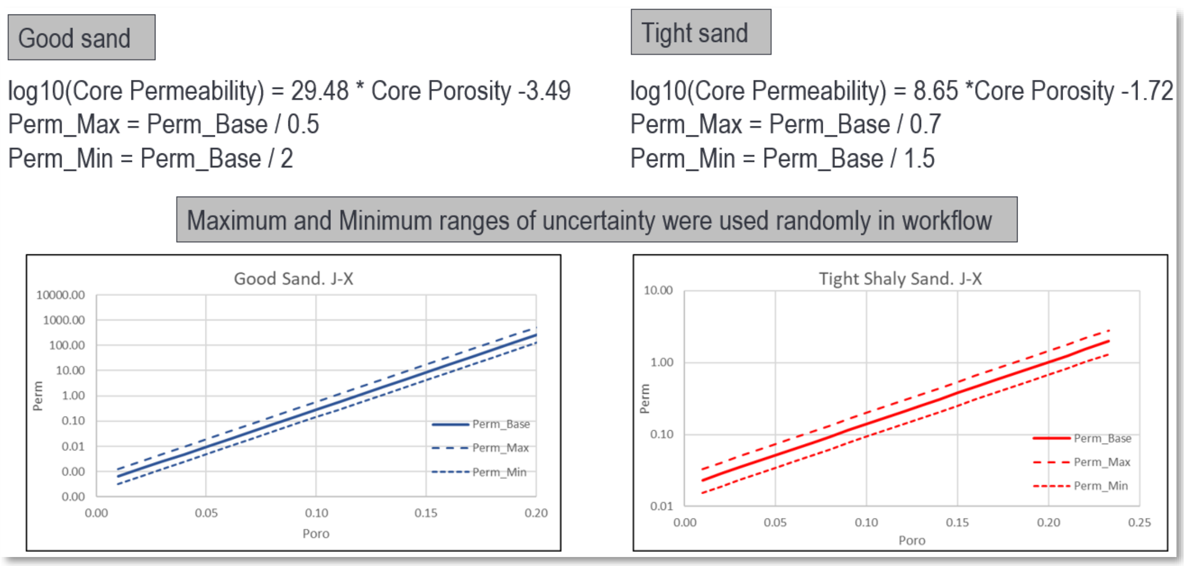

Figure 15 – ARYSTAN Porosity-Permeability petrophysical regressions with uncertainty used in modeling

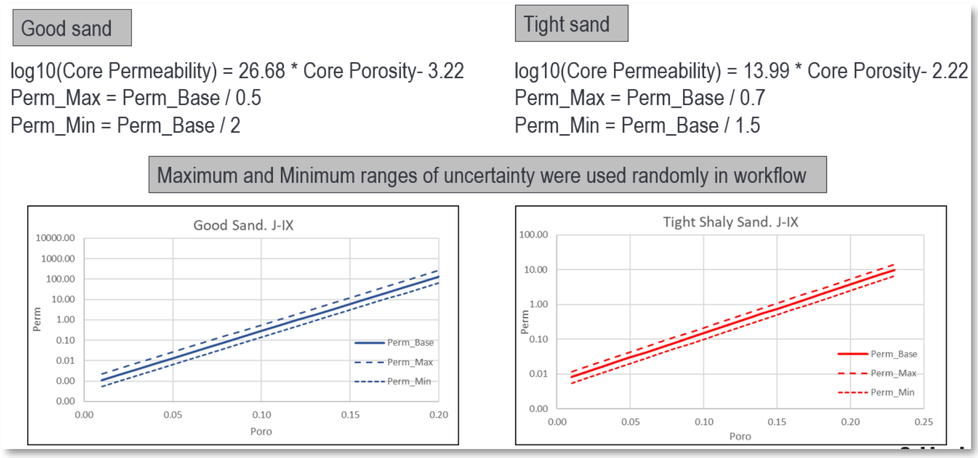

Figure 16 – J-X Porosity-Permeability petrophysical regressions with uncertainty used in modeling

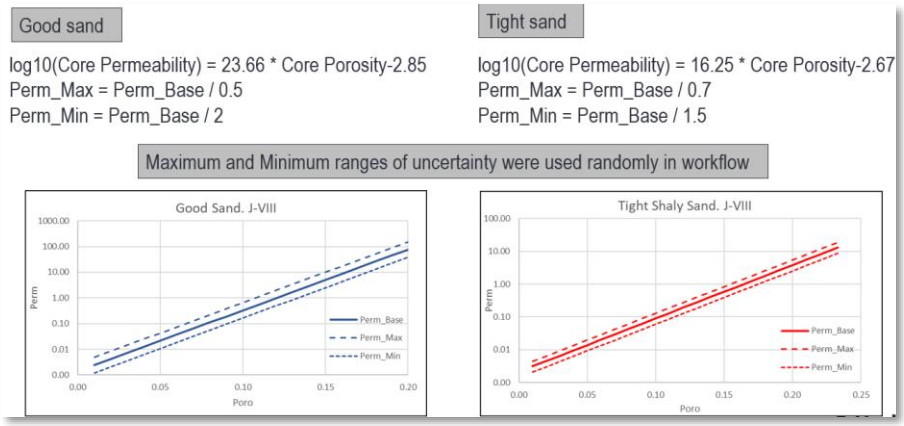

Figure 17 – J-IX Porosity-Permeability petrophysical regressions with uncertainty used in modeling

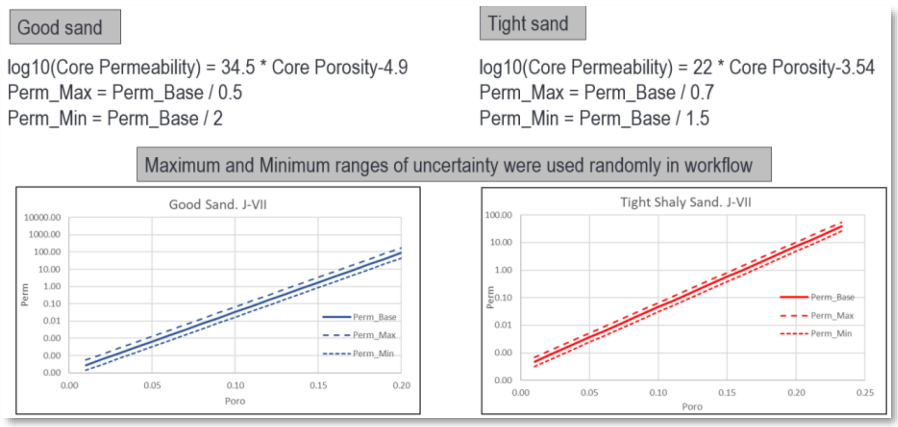

Figure 18 – J-VIII Porosity-Permeability petrophysical regressions with uncertainty used in modeling

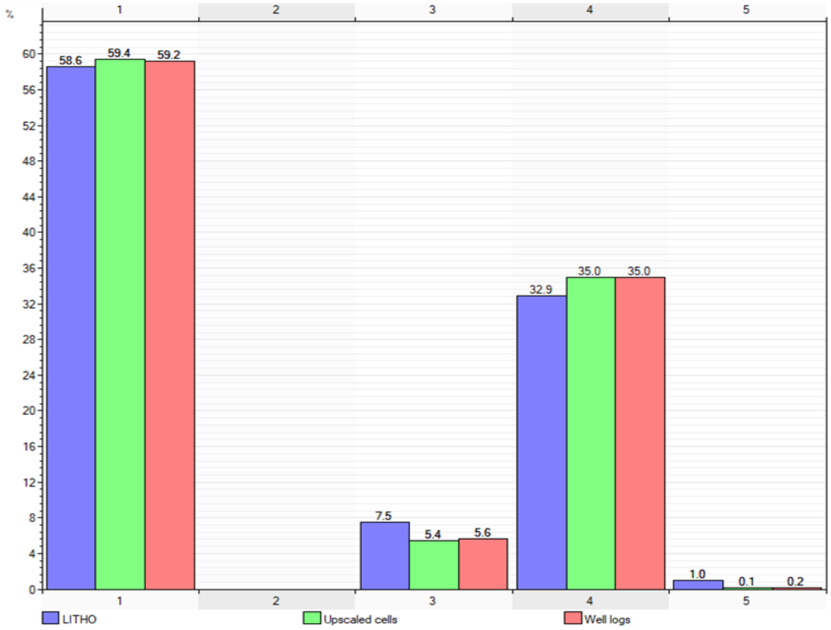

Figure 19 – J-VII, J-Vi and J-V Porosity-Permeability petrophysical regressions with uncertainty used in modeling

Simulation lithology and porosity distribution (figure 20, 21).

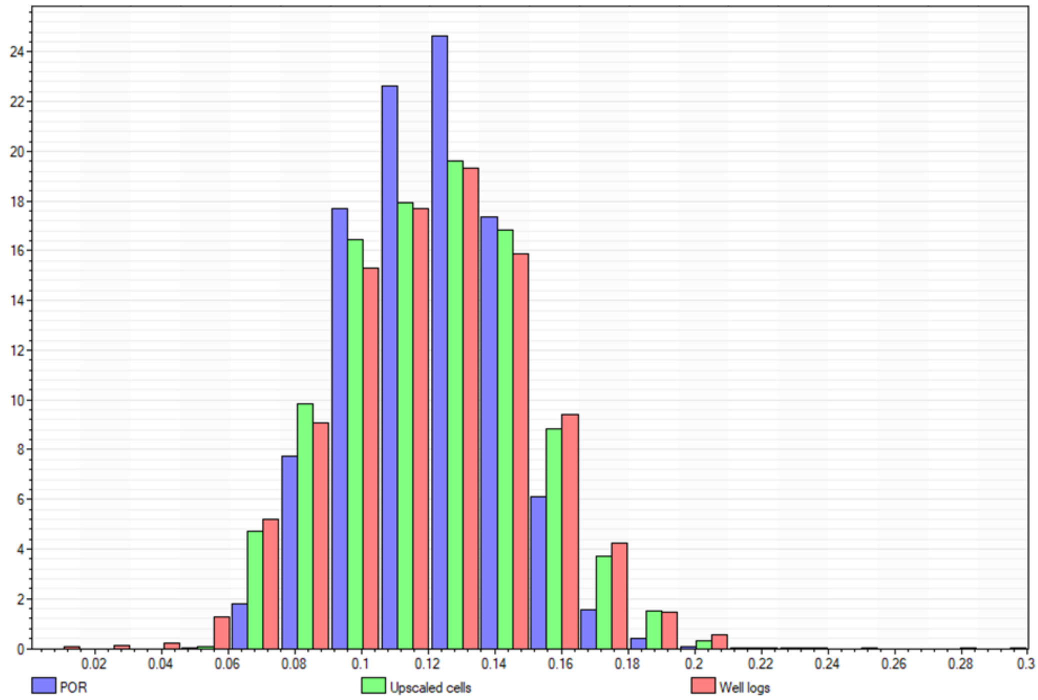

Figure 20 – Simulation model Lithology distribution with comparison to log data

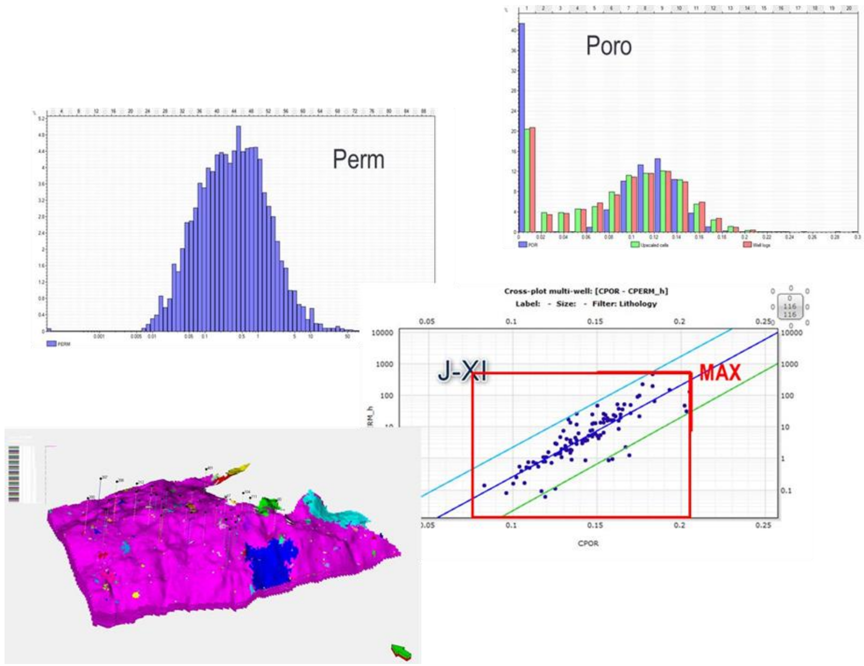

Figure 21 – Simulation model Porosity distribution with comparison to log data

Porosity and initial water saturation cut-off values were introduced to the simulation model in order to optimize simulation time and remove cells which do not contribute to simulation flow dynamic. Notes: Dynamic model cut-offs are different from petrophysical cut-off due to different definition and scale and applied on 50x50m grid block size. Property distribution diagram was reviewed as well as multiple simulation models were performed to select right cut-off values (figure 22) [8].

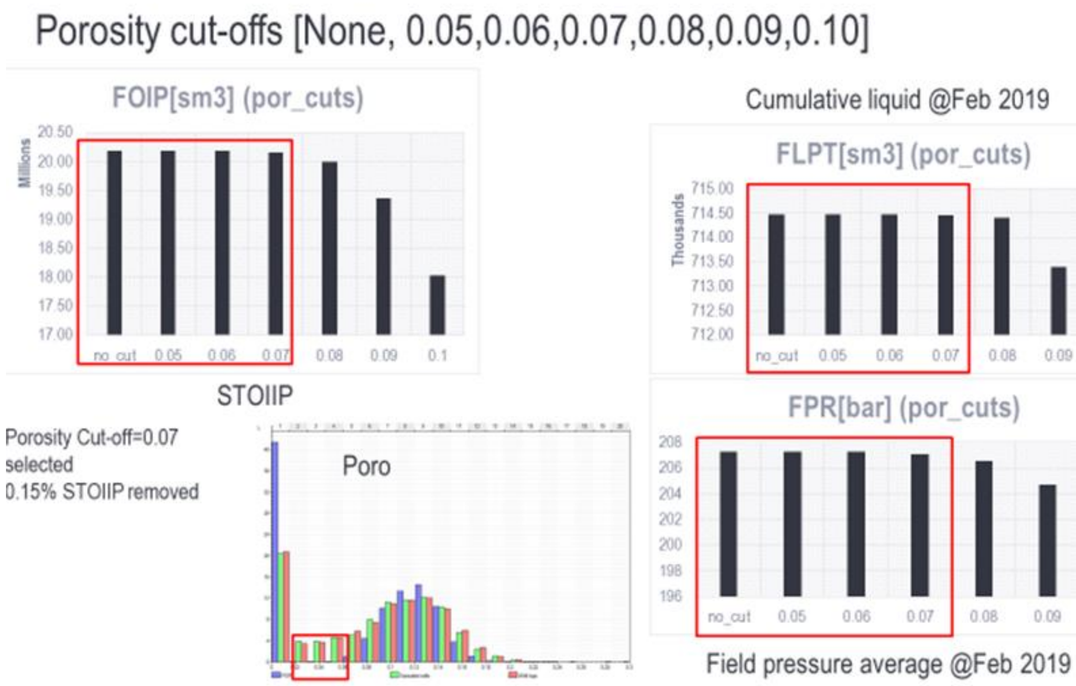

Figure 22 – Simulation model cut-off values selection approach

Run sensitivity on different cut-off values and choose value with minimum impact on STOIIP and dynamic data such as pressure, cumulative production. Several cut-off values were investigated and the best one was selected to use in further dynamic cases Porosity and Water saturation cut-off that were investigated are shown below on figure 23 and figure 24.

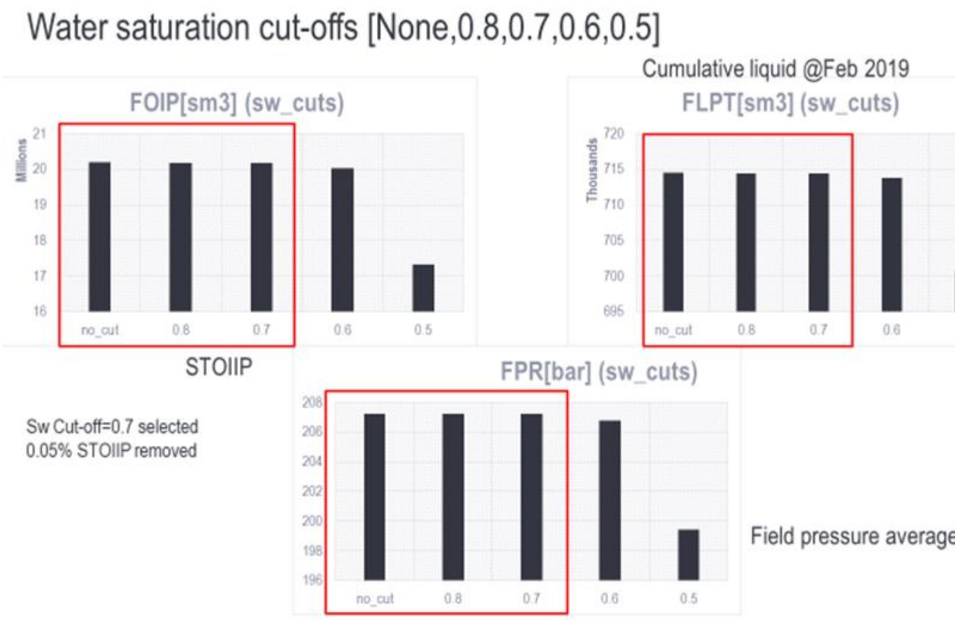

Figure 23 – Porosity cut-offs: None, 0.05,0.06,0.07,0.08,0.09,0.10

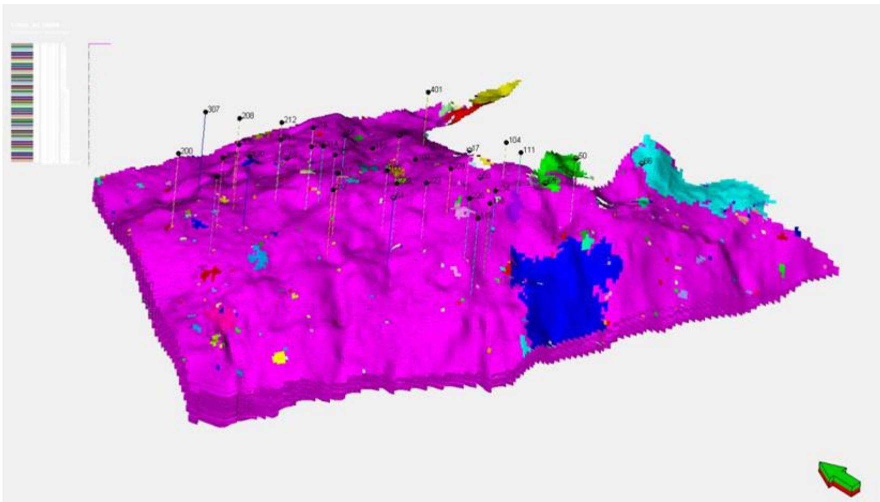

Figure 24 – Water saturation: None,0.8,0.7,0.6,0.5

0.07 (7%) Porosity Cut-off was selected. Applying porosity cut-off value to simulation model removes only 0.15% of initial oil in place.

0.7 (70%) Irreducible water saturation (SWL) Cut-off was selected. Applying SWL cut-off value to simulation model removes only 0.05% of initial oil in place:

1. Porosity cut-offs: if grid block's porosity is less than particular cut-off, we make this block inactive.

2. Water saturation cut-offs: if grid block's water saturation is more than particular cut-off, we make this block inactive.

2.3 Estimated PI Range

Well PIs were calculated from production data (where it was possible) and simulation data by using well Region average pressure as described chapter above. Model shows good consistency with observed data figure 25.

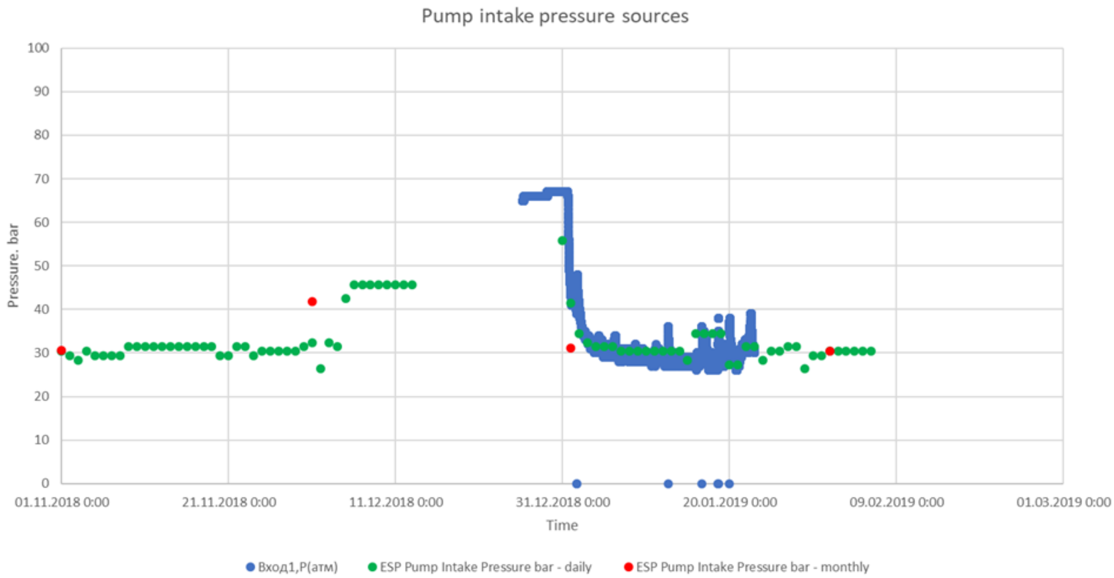

Figure 25 – Well PI calculation from observed and simulation data

Estimated PI range: Before HF 0.07 m3/bar/day; After HF: 0.2-1 m^3/bar/day

It depends on the well and area of location. Numbers above are shown to have feeling of reasonable range of PIs before and after frac.

PIs calculated from production data shows monotonic reduction with time with tendency to stabilize at some level. That indicates long transition period before well comes to stable production regime (SS, PSS)

Data uncertainty: Pump intake pressure averaging. Pressure on pump intake tube is measuring every 3 minutes and follows a long way and manipulations on each step from the sensor to be used in simulation model. Figure 26 shows pressure data averaging on different steps.

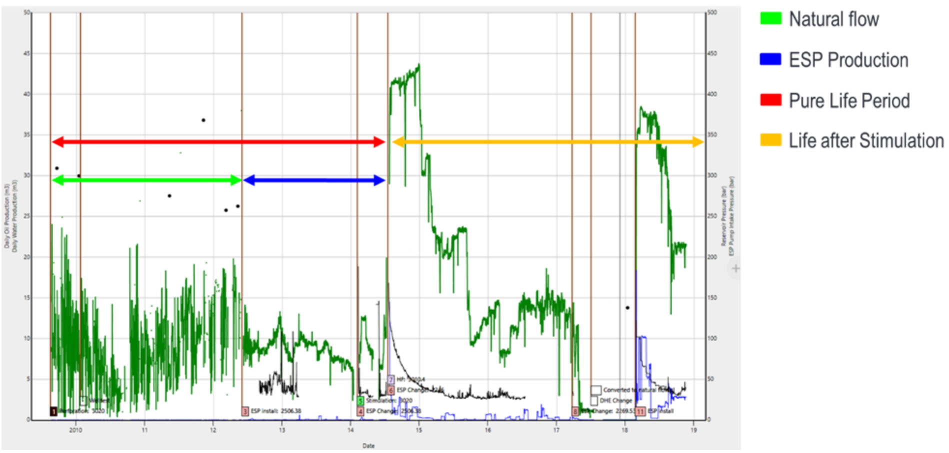

Figure 26 – PIP averaging and different sources

Observed PI calculation

In case of needs to estimate observed PI following approach was used:

1. BHP and PIP measurements was mapped to observed well reservoir pressure within 1 year search window, assuming no significant reservoir pressure drop in 1 year.

2. PIP measurements corrected to datum depth.

3. Pressure corrected data used to calculate pressure drawdown.

4. Liquid production rate divided to pressure drawdown.

Note: Such approach based on some approximations and can be used in case of estimate order of magnitudes of PI but not exact value.

2.4 History matching approach and process

History matching of simulation model was performed in order to calibrate model to observed production data and pressure measurement. Steps shown below were executed and described later:

– sensitivity analysis;

– select uncertain variable and range;

– optimization stage;

– select best case and fix global variables values;

– well by well analysis: local hm update.

Objective function: It is very important step to define objective function correctly to be able to differentiate bad/good cases in automated workflows. It was offered to split objective function into two time periods before and after frac for each well. Pressure dynamic before hydraulic fracture characterizes very well reservoir property such as permeability, and it is called Pure Life Period. Pressure dynamic after hydraulic fracture link to fracture property and modified well PI, it is called Life after Stimulation, figure 27.

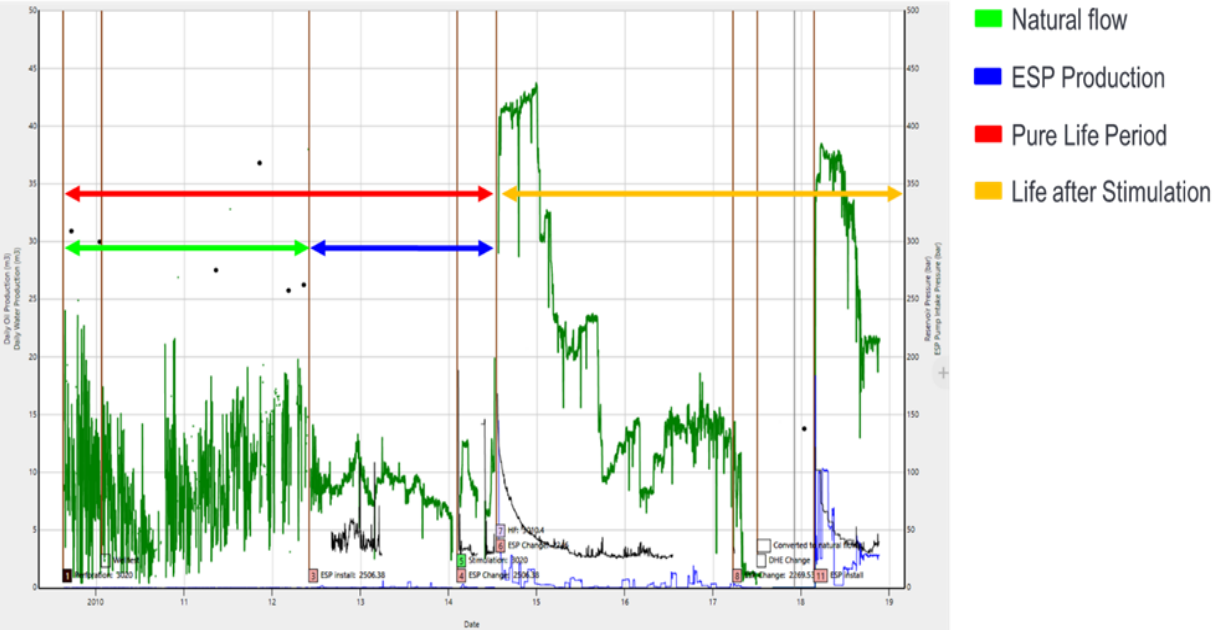

Figure 27 – Pure Life Period

	Observed quantity	Simulation quantity	Use
1	Bottom hole pressure	Bottom hole pressure	✓
2	Gas production cumulative	Gas production cumulative	
3	Gas production rate	Gas production rate	
4	Gas-liquid ratio		
5	Gas-oil ratio	Gas-oil ratio	
6	Instantaneous gas production rate		
7	Instantaneous liquid production rate		
8	Instantaneous oil production rate		
9	Instantaneous water injection rate		
10	Instantaneous water production rate		
11	Liquid production cumulative	Liquid production cumulative	
12	Liquid production rate	Liquid production rate	✓
13	Oil production cumulative	Oil production cumulative	
14	Oil production rate	Oil production rate	
15	Oil-gas ratio		
16	Tubing head pressure	Tubing head pressure	
17	Uptime fraction		
18	Water cut	Water cut	
19	Water injection cumulative	Water injection cumulative	
20	Water injection rate	Water injection rate	
21	Water injection uptime fraction		
22	Water production cumulative	Water production cumulative	
23	Water production rate	Water production rate	
24	Water-gas ratio	Water-gas ratio	

Figure 28 – Pure Life Period objective function setup

Pure Life Period objective function setup shown on figure 28. Time before stimulation selected by using introduced time weighted function as shown on figure 29.

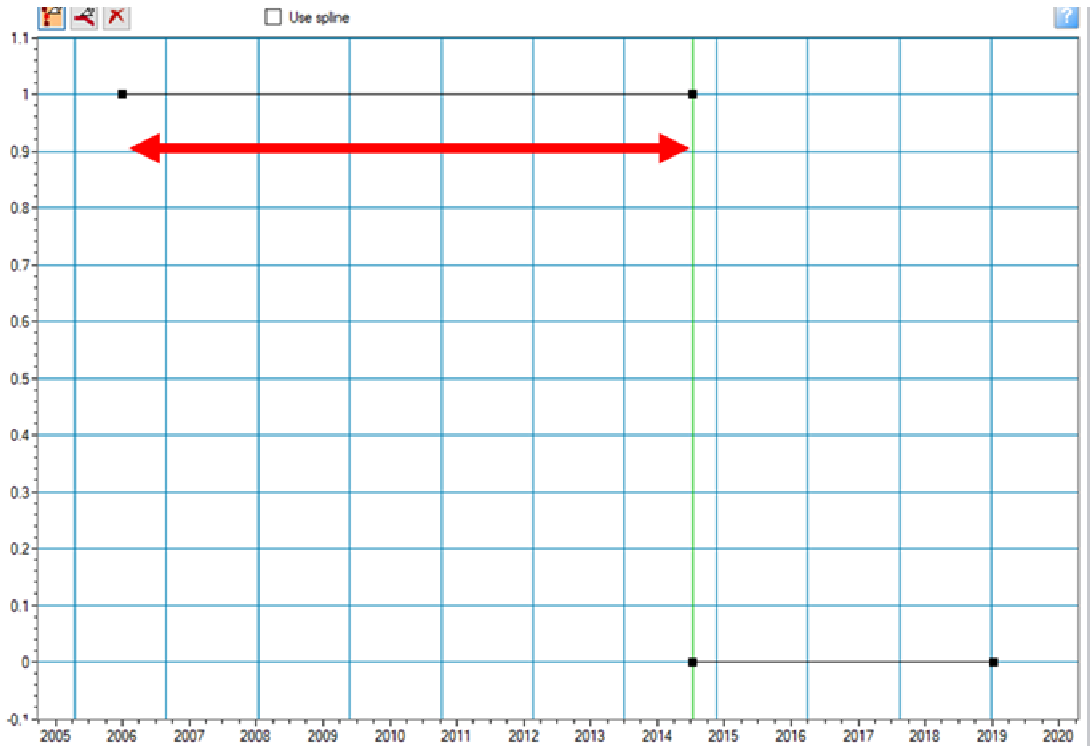

Figure 29 – Time weights setup

2.5 Sensitivity Analysis

Sensitivity analysis is important step which allows to understand influence strength of each parameter to reduce objective function and select most sensitive for further optimization stages.

Following parameters were selected for sensitivity analysis stage.

1. Structure uncertainty - Vshale ratio - Porosity.
2. Permeability - Rock Compressibility - Fault Transmissibility.
3. Kv/kh ratio - Frac Effect.

Min/max values range was assigned for each parameter according to the table below on figure 30, 31.

	Type	Pr	Int	Name	Base value	Distribution	Arguments			
1	SEED variable			$SEED_STR	6365					
2	Uncertain			$POR_LOG	0	Uniform	Min	-0.07	Max	0.07
3	Uncertain			$TM	0.5	Uniform	Min	0	Max	1
4	Uncertain			$ROCK	1.423E-05	Uniform	Min	1.4E-06	Max	0.00014
5	Uncertain			$KRWR	0.12	Uniform	Min	0.08	Max	0.6
6	Uncertain			$PERMA	29.0327	Uniform	Min	28.81624	Max	29.62352
7	Uncertain			$PERMB	3.478367	Uniform	Min	2.523059	Max	4.615148
8	Uncertain			$KVKH	0.5	Uniform	Min	0.3	Max	0.7
9	Uncertain			$KPR	0.5	Uniform	Min	0.01	Max	1
10	Uncertain			$YEARS	1	Uniform	Min	0.08	Max	3
11	Uncertain			$VSH	0.33	Uniform	Min	0.3	Max	0.45

Figure 30 – Sensitivity analysis setup

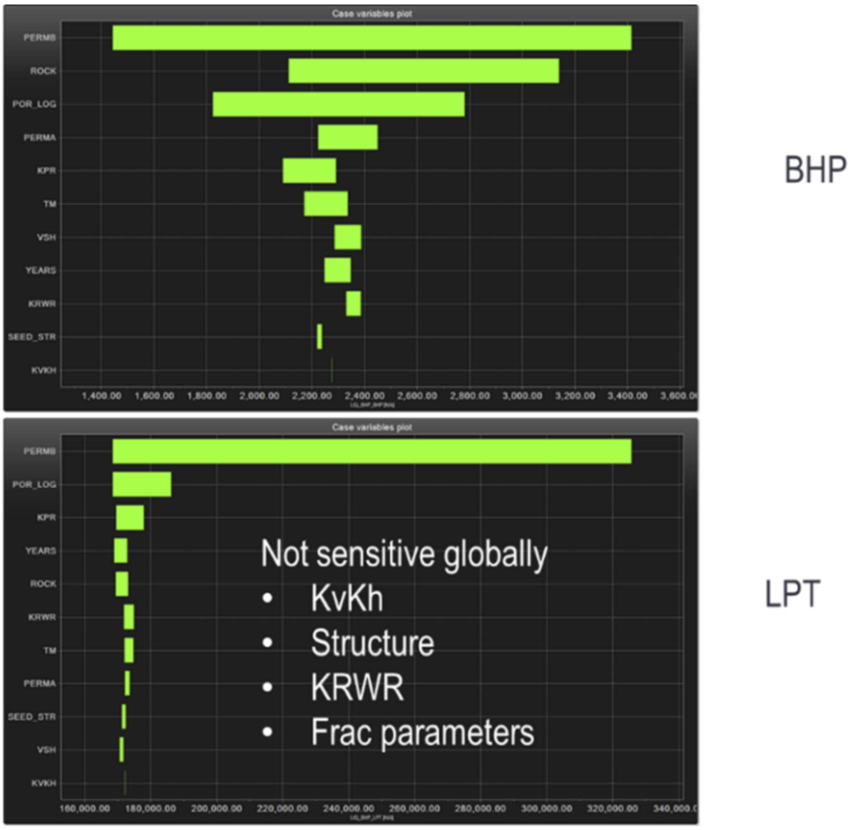

Figure 31 – Sensitivity to Life time objective function tornado plot

2.6 Base case scenario

Base scenario for this project has been described and provided by Customer company:

1. Prediction period for base scenario include 20 years.
2. Until 2023 year produced volume of water injected to 5 injectors: 106 (J-IX), 59 (J-XI), 118 (J-XI), 200 (J-XI+X), 300 (J-XI).
3. Completion strategies assume that the well produce from only one horizon.
4. Hydraulic Fracture planned on each well at the first day of production.
5. Refracture jobs planned 3 times during production period including first frac.
6. Fracture degradation: PI dropped on half for 3 years.
7. For new producers BHP limit 50 bar.
8. The last BHP pressure of existing wells used for prediction.
9. Maximum injection BHP 500 bar.
10. Maximum injection Rate 2000 m^3/day.
11. Maximum Field injection rate 1600 m^3/day allocated by PFM balancing algorithm.
12. Operation efficiency 90%.
13. Field liquid production limit – 3000 m^3/day.
14. Conversion producers to injection on the same horizon.

The schedule of drilling new producers provided by Customer company shown in table 2. The list of wells which were predetermined by drilling plan of 2022 year included wells: 419, 312, 238, 418, 412, 308, 706, 302, 415, 240. Starting from 2023 year the 30 of new producers were in the base case scenario plan of drilling on 10 wells each year.

Table 2 – New producers and conversion to injectors wells schedule

Horizon	J-V		J-VII		J-VIII		J-IX		J-X		J-XI		Total New Producers	Total Transfers to Inj
	new producer	transfer to inj	new producer	transfer to inj	new producer	transfer to inj	new producer	transfer to inj	new producer	transfer to inj	new producer	transfer to inj		
2022	0	0	0	0	0	0	3	0	1	0	6	0	10	0
2023	1	0	1	0	1	0	4	0	1	0	2	0	10	0
2024	0	2	2	2	1	1	4	5	1	4	2	5	10	19
2025	1	0	1	0	2	0	4	0	1	0	1	0	10	0
Total	2	2	4	2	4	1	15	5	4	4	11	5	40	19

New wells as the potential candidates for drilling producers were placed in undrilled areas with 300 m patten inside channel bodies where they exist and in undrilled areas of ARYSTAN and J-IX horizons. To find the optimum well location those wells used as a dynamic well list for INTERSECT automatic selection. Candidates for drilling with distance to open wells more than 200 m were choose with intention to find well with best potential production rate to improve field oil production rate. Conversion producer to injector conducted with conditions of oil rate

< 15 m^3/day and reservoir pressure less than 200 bar. The goal is to improve objective function (Oil Production Rate + Field water injection rate*0.5). Schematically the well's selection shown on the figure 32.

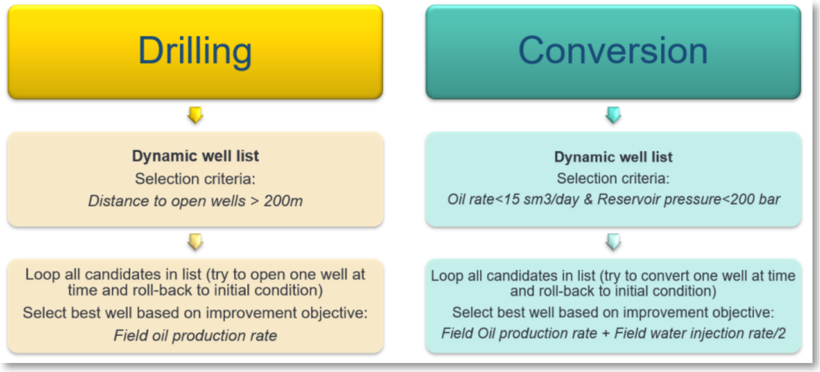

Figure 32 – Schematic of INTERSECT well selection

As example some snapshoots of well conversion to injection of horizon ARYSTAN have been taken from simulation process with adding explanations.

2.7 Sensitivity study of base case

The aim of sensitivity study was to determine uncertainty parameters which have more influence of quality of history matching and as result production forecast.

Uncertainty parameters have been identified during previous years reservoir properties study and when problems occurred with production history matching. The key factors of uncertainty are quality and completeness of available date for each horizon. Related to them are special core analysis of relative permeability, critical and irreducible water saturation, capillary pressure rock compressibility, faults transmissibility, OWCs which were limited representation or not available for each horizon.

	Type	Pr	Int	Name	Base value	Distribution	Arguments			
1	Disabled			$arg1	0					
2	Disabled			$wellname	0					
3	Uncertain			$Perm	0	Uniform	Min	-3	Max	3
4	Expression			$rad1	500		500			
5	Expression			$rad2	900		900			
6	Uncertain			$Poro	0	Uniform	Min	-0.03	Max	0.03
7	Uncertain			$DispEff	0	Uniform	Min	-0.1	Max	0.1
8	Uncertain			$Pc	0	Uniform	Min	-1	Max	1
9	Uncertain			$Krwr	0	Uniform	Min	-0.5	Max	1
10	Uncertain			$FltTr	0.5	Uniform	Min	0.25	Max	1
11	Uncertain			$RComp	1.423E-05	Uniform	Min	4.7E-06	Max	4.3E-05
12	Uncertain			$CoreyOW	2.8	Uniform	Min	2.2	Max	3.5
13	Uncertain			$CoreyW	2	Uniform	Min	1.5	Max	3.5
14	Expression			$CoreyW2	1.5		$CoreyW-0.5			
15	Uncertain			$OWC_XI	0	Uniform	Min	-1.5	Max	1.5
16	Uncertain			$OWC_X	0	Uniform	Min	-1.5	Max	1.5
17	Uncertain			$OWC_IX	0	Uniform	Min	-1.2	Max	1.2
18	Uncertain			$OWC_VIII	0	Uniform	Min	-2	Max	2
19	Uncertain			$OWC_VII	0	Uniform	Min	-1.5	Max	1.5
20	Uncertain			$OWC_V	0	Uniform	Min	-1.2	Max	1.2
21	[illegible]			[illegible]	[illegible]		[illegible]			

Figure 33 - Uncertainty parameters used in the sensitivity study of base case

In the figure 33 list of uncertainty parameters used during sensitivity study and their ranges. The explanations of parameters in the figure 34 additionally have comments where indicated how parameters were changed, for example: multiplying or adding some value. The modification of reservoir properties applied for undrilled area with some assumption that with distance to existing history well less than 500 m properties did not change, with distance between R1 (figure 35) and R2 modification of properties was made with linearly expression.

	Uncertain Parameter	Explanation	Comments
1	$Perm	Permeability multiplier	Multiplier
2	$rad1	Radius of no infuence	
3	$rad2	Radius of modification zone	
4	$Poro	Porosity	Addition (+- 3%)
5	$DispEff	Displacement efficiency	Addition (+- 10%)
6	$Pc	Max Capillary Pressure multiplier	Multiplier
7	$KRWR	Maximum Rel.Perm of Water	Multiplier
8	$FltTr	Fault Transmissibility	Value
9	$Rcomp	Compressibility	Multiplier
10	$CoreyOW	Oil-Water Corey	Value
11	$CoreyW	Water Corey	Value
15	$OWC_XI	Oil Water Contact	Addition
16	$OWC_X	Oil Water Contact	Addition
17	$OWC_IX	Oil Water Contact	Addition
18	$OWC_VIII	Oil Water Contact	Addition
19	$OWC_VII	Oil Water Contact	Addition
20	$OWC_V	Oil Water Contact	Addition

Figure 34 - Explanation of uncertainty parameters changes

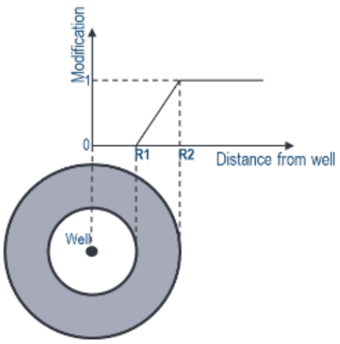

Figure 35 – Schematic of uncertainty properties modifications around existing well

Some attention has been paid on sensitivity study of water production depends on Low, Base and High OWCs by horizons. Water production has significant concern and OWC uncertainty critically reviewed during sensitivity study.

Dots show history water production and solid lines are results of simulation with OWC uncertainty. On the figure 36, 37, 38, 39, 40, 41 the plots demonstrate how much OWC uncertainty could be. The dots mostly located in the area between High and Low OWC lines except J-VIII where even with changes of OWC depths ±20 m historical water production more. Here are some notes should be made, the water cut produced from J-VIII mostly less than 15% and didn’t increase last 8 years. Most probably we are dealing with capillary pressure uncertainty.

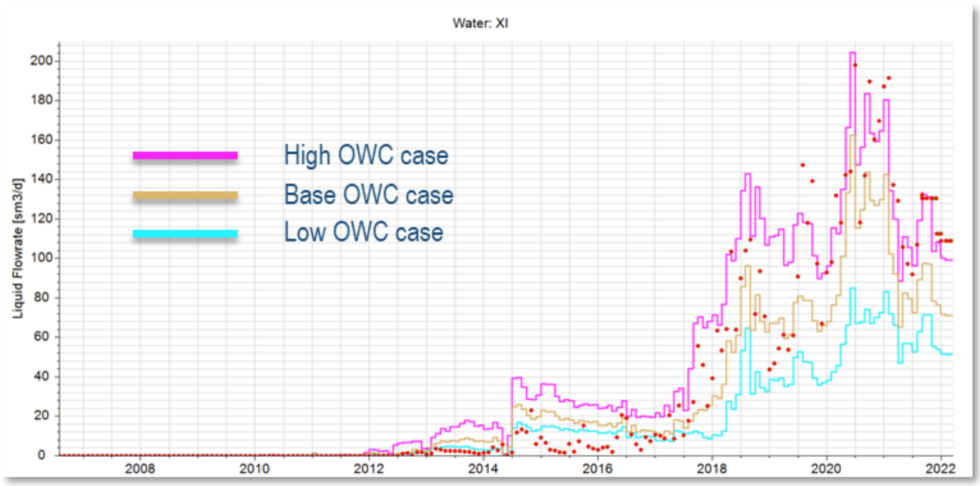

Figure 36 – Water production of Horizon ARYSTAN with uncertain OWCs

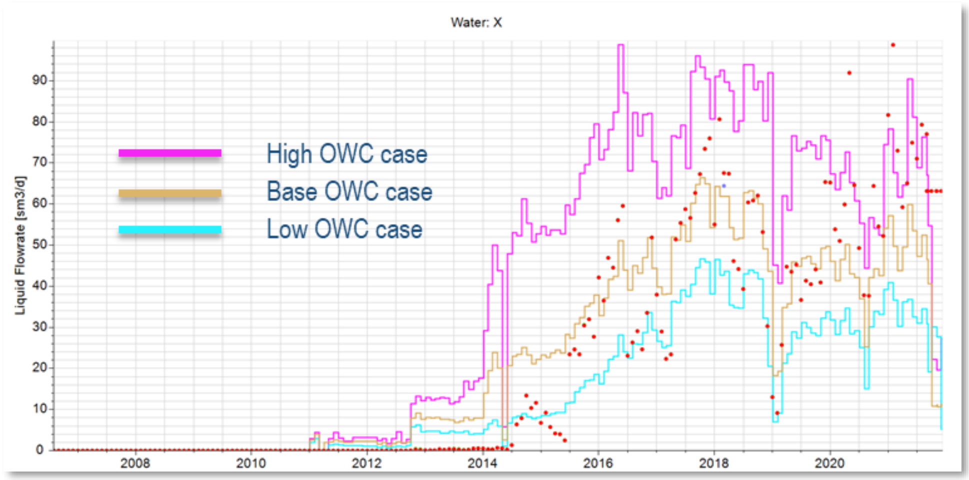

Figure 37 – Water production of Horizon J-X with uncertain OWCs

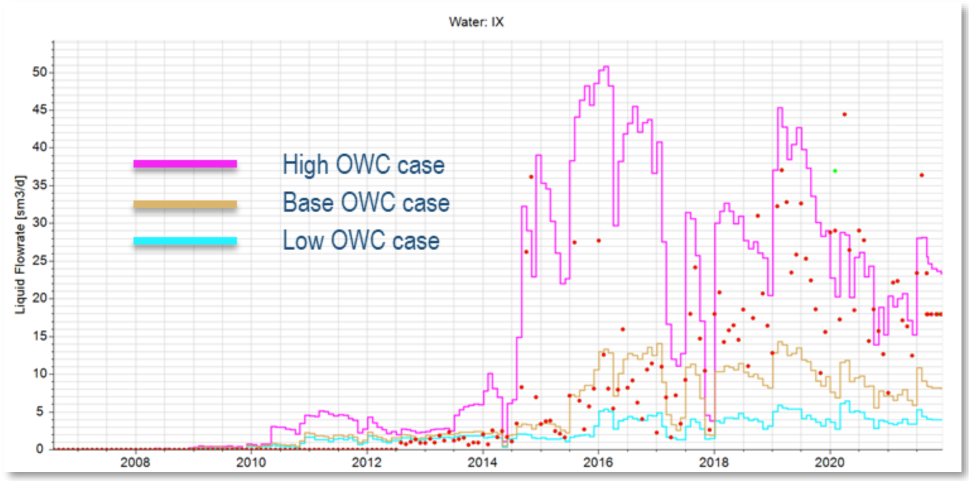

Figure 38 – Water production of Horizon J-IX with uncertain OWCs

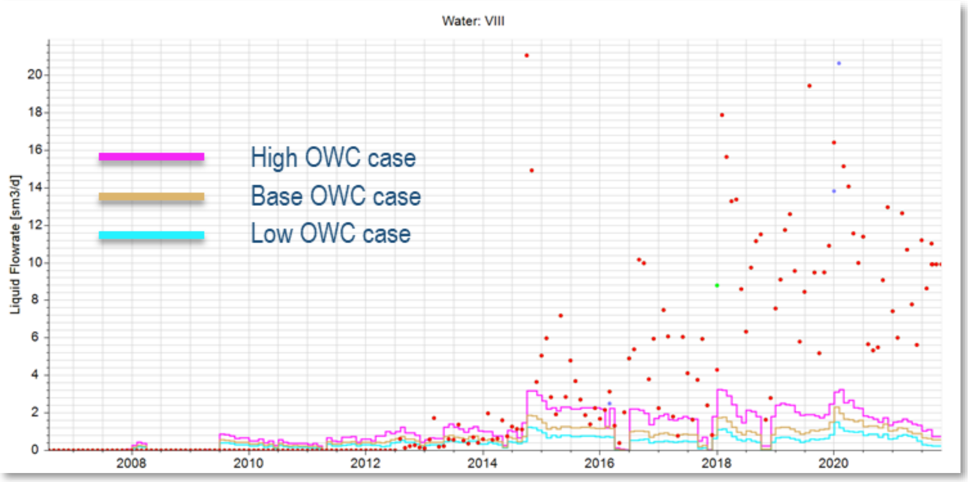

Figure 39 – Water production of Horizon J-VIII with uncertain OWCs

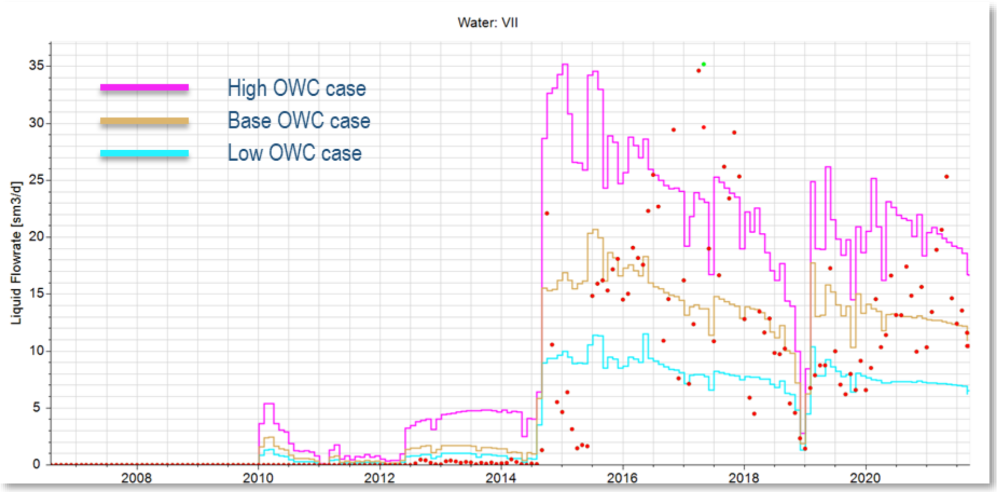

Figure 40 – Water production of Horizon J-VII with uncertain OWCs

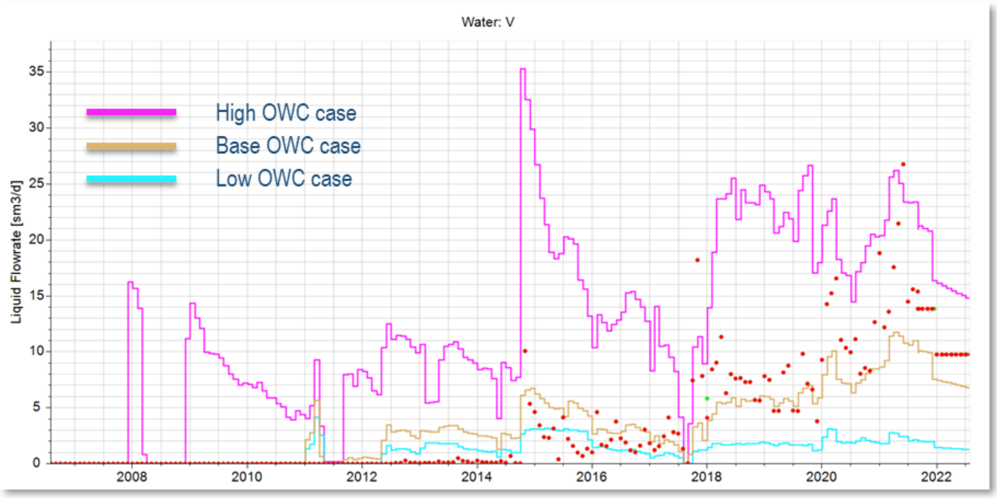

Figure 41 – Water production of Horizon J-V with uncertain OWCs

Sensitivity study of prediction period of production analyzed with Tornado Plot. On the figure 42 shown the parameters which have most influence on oil cumulative production in green color and less influence on red. The objective function of Tornado Plot on figure 43 is history match error. It shows how uncertainty parameters impact on quality of history matching. Right most values show worse HM result; left most values – better HM result.

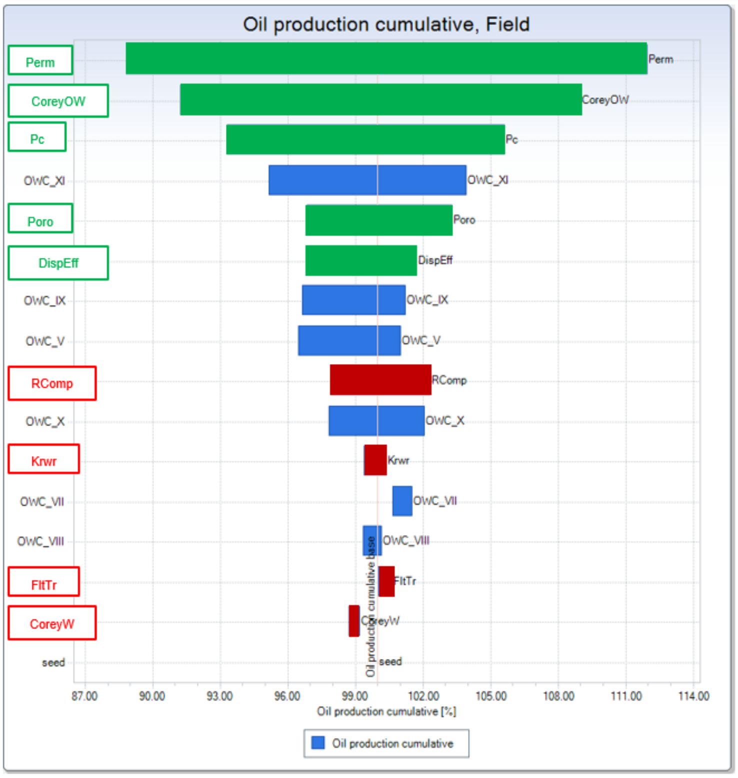

Figure 42 – Tornado Plot of field oil cumulative production

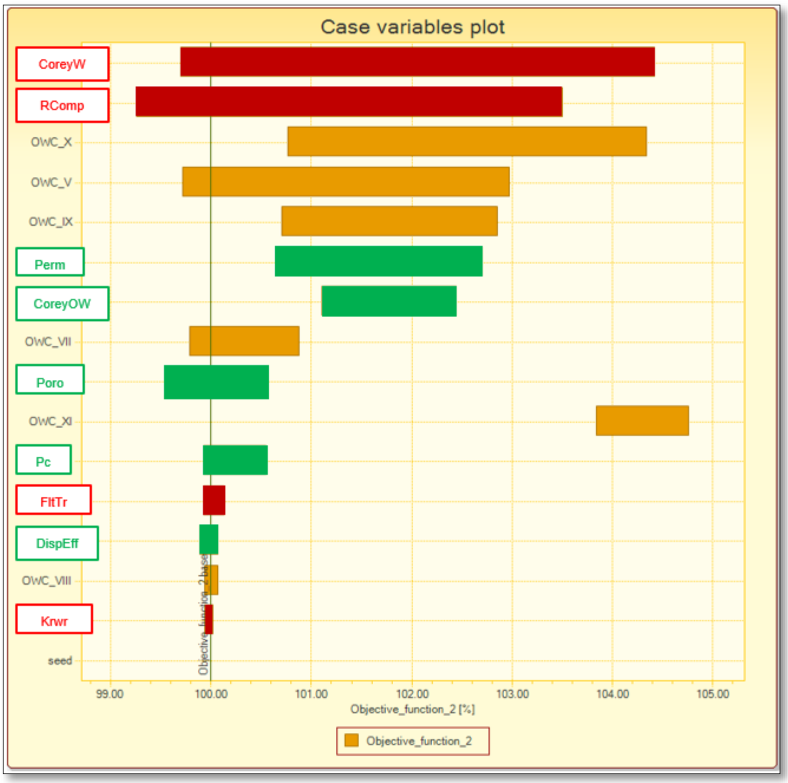

Figure 43 – Tornado Plot of History Match errors

Conclusions on the 2st section

Integrated full Arystan field dynamical model fine-tuned and updated with history production and new wells drilled up to 01/10/2021. Tuned simulation model validate the physical behavior of the reservoir by comparing the model output (such as production rates and pressure responses) to actual field data.

Sensitivity analyses: Determining of the impact of different input parameters on the model output. The most important parameters and the optimal values has been identified. Sensitivity analyses demonstrate that the most impact on forecast oil production have uncertainty of OWC, permeability, Corey OW, capillary pressure, porosity. After the model has bed tuned and sensitivity analyses has been run , the final model has been validated to ensure that it accurately represents the physical behavior of the reservoir and the hydraulic fracturing design.

The recommendation for further acquisition includes justification of upper horizons petrophysical properties, well integrity, production logging. As the result final tunned simulation model for hydraulic fracturing design using ECLIPSE/INTERSECT software quantified reservoir flow behaviors principles such as pressure boundary condition. As It is important to validate the model before making any changes, and to run sensitivity analyses to identify the most important parameters to tune

History matched simulation model of Arystan field will be used for hydraulic fracturing modeling which is described in Chapter 3. Further adjustment of the fracture parameters and validation of the simulation model will be conducted.

3 HYDRAULIC FRACTURING REVIEW AND APPROACH FOR MODELING

The methods of intensifying the inflow or intake of wells are well-known and widely used in the oil and gas industry. However, there are numerous methods and technologies available to intensify production, with hydraulic fracturing (or fracking) being the most effective for many fields both in Kazakhstan and abroad. This method has been developed through modern oil and gas science and has proven to be highly effective in enhancing production from reservoirs [9].

Hydrodynamic modeling technologies are actively used in popular industry simulators (ECLISPE, INTERSECT, Tnavi) to predict and evaluate the technological effect of hydraulic fracturing. It is generally accepted when modeling hydraulic fracturing to describe it as a change in the skin factor of the bottom-hole zone of the well. At the same time, an unwritten rule has been established (and for some companies this is the standard) that hydraulic fracturing is interpreted by setting the skin factor equal to -4.0. Hence, there are problems with the adaptation of hydrodynamic models to the development history and all the resulting problems with the low efficiency of subsequent forecasts [10].

At the same time, there are scientifically and practically sound approaches to hydraulic fracturing modeling, among which the most well-known and applicable are: Local Mesh Shredding (LGR) and creating virtual perforations

Local grid shredding (LGR)

It is important to know that this modeling method is used for the part of the model in which there is an accelerated change in any parameters (for example, pressure or rock property). The advantages of the considered technique are the ability to most accurately determine the direction of crack propagation, its geometry and filtration-capacitance properties in the selected local zone. The grinding of the grids can be carried out in a uniform and logarithmic form [11].

The position of the well in the section and in the plan when modeling hydraulic fracturing by the uniform LGR method. The color scale is specified for the permeability value. In the second type of grinding, the size of the grinding is higher near the well and falls exponentially within the half-length of the crack. Thus, the detail of the grid increases near the CCD, in which all filtration effects are most intensively manifested

Virtual perforations

The essence of the virtual perforation method is to create additional connections of the well with the formation. So the frac is described by a two-dimensional plane of unambiguous dimensions, revealing additional cells of the model. Thus, a connection for a well with a certain productivity index Kh appears in the fractured fracturing cells. The value of the Kh parameter depends on the geometry of the crack, the filtration-capacitance properties of a single cell of the model and the fracture of the hydraulic fracturing. At the same time, specific simulators calculate the values of the perforation productivity index in different ways, some examples can be found on the Internet.

To select the approach of hydraulic fracturing modeling in specific conditions and frac design, it should be remembered that local grid grinding (LGR) allows you to set a complex and individual design for each well. The virtual perforation method is applicable to a larger number of hydraulic fracturing wells. In turn, this method is inferior to LGR by a rather simple hydraulic fracturing design. However, the simulation of virtual perforations has an advantage in terms of the calculation time of a separate case and resistance to errors associated with errors in calculating the material balance when numerically solving filtration equations in grids with cells of different volumes. The inflow performance of a fracture-stimulated well is controlled by a number of factors, including the dimensionless Fracture Conductivity (Fcd). The Fracture Conductivity is a measure of the ability of the fractures created by the treatment to conduct fluid. It is calculated as the ratio [12] of the flow rate through the fractures to the pressure drop across the fractures.

The Fracture Conductivity is affected by a number of factors, including the width and length of the fractures, the permeability of the rock formation, and the viscosity of the fluid being injected. In general, wider and longer fractures with higher permeability and lower viscosity will have higher Fracture Conductivity, allowing for more efficient flow of fluid into the well.

The Fracture Conductivity (Fcd) of a hydraulic fracture treatment is defined as the ratio of the flow rate through the fractures to the pressure drop across the fractures. It is calculated using the following equation:

The Fracture Conductivity (Fcd) of a hydraulic fracture treatment is defined as the ratio of the flow rate through the fractures to the pressure drop across the fractures. It is calculated using the following equation.

Fcd = kfw / kLf   where:
*kf*w = fracture permeability (kf) * conductive fracture width (w)*
*k*Lf = formation permeability (k) * conductive fracture single wing length (Lf)*

The relationship between fracture conductivity, fracture length, and formation permeability on well inflow performance has been studied extensively. Cinco-Ley and Samaniego published a widely-used correlation in which the effective wellbore radius (r'w) divided by the conductive fracture length (Lf) is plotted against the dimensionless fracture conductivity (FCD). This allows the negative skin effect due to the propped hydraulic fracture (Sf) to be calculated from the dimensionless fracture conductivity. A FCD value of 15 is generally considered to be the threshold at which the well inflow is not limited by the fracture conductivity (figure 44).

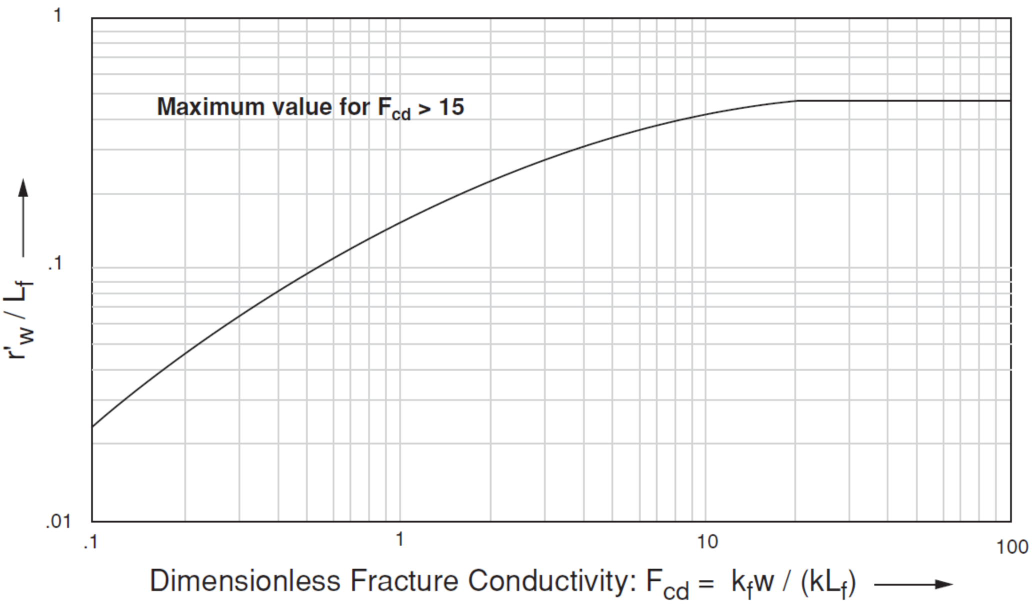

Figure 44 – Cinco-Ley and Samaniego's 1981 correlation between effective wellbore radius and fracture conductivity

Take into account widely used correlation of fracture conductivity and numerical methodology of simulation run, the sensitivity analyses showed that virtual perforations(Easy frac plug in) is the most suitable method for Arystan model. This solution is designed for mass application with a large number of wells in a full-scale models or multi-well sector model, in the case when the fracture half-length over the geometric size of the grid cell and modeling results of the fracture with the negative value of the skin factor isn't effective. The EasyFrac creates additional connection in the cells for wells with hydraulic fractures, through which the fracture passes. Calculation of the connection factor is based on fracture's geometrical parameters, rock and proppant permeability, also taking into account effects of "choke restriction" (happens when inflow to the fracture wings is much more than fracture's possibility of transportation).

In the case of "choke restriction" the outflow from central cell must be much larger than the outflow from the cells at the end of fracture's wings; this is defined in terms of uncovering ratio CF in each cell. In addition, the plug-in allows you to create and export ECLIPSE keywords, which are responsible for a reduction of the well productivity in course of time (reducing the impact of hydraulic fracturing) or for an increase intake capacity of injection wells in case of increase bottom hole pressure higher than the fracturing pressure (WINJMULT – automatic hydraulic fracturing in injection wells).

3.1 Hydraulic fracture modeling

In this project, hydraulic fractures are modelled using EasyFrac plugin since observed fracture half-length is found to be over the geometric size of the grid cell and modeling results of the fracture with the negative value of the skin factor isn't effective. Table 3 summarizes available well hydraulic fracturing data by horizons.

Table 3 – Summary of hydraulic fracture data

Parameter	Description	Units	Comments
Well name	Well name for which hydro fracturing will be modeled	Text	ALL_INJ – hydraulic fracturing on all pressure maintenance
Fdate	Date of hydro fracturing	Date	dd/mm/yyyy
MD top	Depth of top perforated interval	m (on the shaft)	Used interval center
MD bottom	Depth of bottom perforated interval	m (on the shaft)	
dw	Borehole diameter	m	
Xf	Fracture half-length	m	Xf <= Re * 0.75
w	Fracture width	m	0.001 < w < 0.1
Alpha	Fracture azimuth	degrees	-90<Alpha <90
dhTop	Fracture height upward from hydrofracturing interval center	m (vertical)	Up and down interval center – p.3-4
dhBottom	Fracture height downward from hydrofracturing interval center	m (vertical)	
Kprop	Conductivity for proppant	mD	
KfKprop	Correction for proppant destruction	part	10000<= Kprop*KfKprop<=5000000
Re	Drainage radius	m	Xf <= Re*0.75
SatNum	Number of phase curves table for connection to hydrofracturing: 7th parameter in COMPDAT keyword	integer	Opportunity to increase water mobility
Kmult	Common multiplier for history reproducing or model "correction"	real	Unload WPIMULT
Teff	Time of hydro fracturing effect reduction	monts	It provides WPI reduction through ACTION and WPIMULT
Kdown	Reduction factor for Teff period	part	
KntgUse	Effectiveness of filtration in fractures of low permeable layer (from 0.5 to 0.95). It affects only in case of long, thin fractures with low permeabilty.	part	Default = 0, if KntgUse>0 then there is need optimal value of parameters 9 and 10, if KntgUse= -1, it will be calcu lated by plug-in automatically
INJ	Indicator of injection well	part	Unload COMPINJK
Amult	WPI gradient factor – third parameter of WINJMULT keyword, auto-hydro fracturing for well with pressure maintenance	1/bar	Parameters of WINJMULT keyword, it is a model of auto-hydro fracturing for well with pressure maintenance
Pfinj	Hydraulic fracturing pressure on the well with pressure maintenance	bar	
Ro	Pirsman's radius for "layer of cells with hydro fracturing". It gives ability to correction of model for cells less than 10x10 meter	m	DEBUG parameter. Allows you to explicitly set the Pirsman's radius
Comment	Text string - comment	text	This field used as string identifier during the work with Ora2Petrel
Note – Compiled by the source [13]			

The EasyFrac (Easy Fracture) plug-in is used for accounting hydraulic fracturing results of the “Black Oil” simulation model. This solution is designed for mass application with a large number of wells in a full-scale models or multi-well sector model, in the case when the fracture half-length over the geometric size of the grid cell and modeling results of the fracture with the negative value of the skin factor isn’t effective. The EasyFrac creates additional connection in the cells for wells with hydraulic fractures, through which the fracture passes. Calculation of the connection factor is based on fracture’s geometrical parameters, rock and proppant permeability, also taking into account effects of “choke restriction” (happens when inflow to the fracture wings is much more than fracture’s possibility of transportation).

Mandatory parameters: The first and the second parameters (the well name and the hydraulic fracturing date) determine, respectively, the well and the event date. The plug-in can be used for monthly, quarterly, semi-annual and annual step modeling, however it is not recommended to solve the problems of well testing modeling (for daily and smaller steps) due to insufficient accuracy of the approach for such problems.

Parameters from 3rd to 10th inclusive describe the geometry of the fracture and include its half-length (6th), width (7th) and the direction of formation (8th). Two parameters are used to describe fracture height: 9th and 10th. They set the height in meters vertically above the "center of the formation" of fracture and the distance from the "center" to the lowest point, respectively. Fracture half-length also is set aside in the direction of “right” and “left” wings from the fracture “center of the formation”. The point on the well inclinometries, corresponding to the middle of the interval “perforation under hydraulic fracturing” specified parameters 3rd and 4th is taken as the central point. The calculation of the fracture location and determination of cells uncovered by fracture are based on the specified parameters (figure 45). If the area of cells uncovering is less than one-third of the diagonal section area, the cell is partially excavated, it is not sufficient to establish a separate connection [14].

WName	FracDate	MDTop	MDBottom	d	Xf	Wf	Alpha	dHTop	dHBtm	Kprop	Kf/Kprop	Re
W00	01/03/2000	2404.5	2407.5	0.2	100	0.004	-12	20	25	300000	1.00	315
W134	01/05/2006	2508.0	2510.5	0.2	70	0.004	-12	20	25	600000	0.35	450
W135	01/07/2007	2713.5	2715.0	0.2	50	0.003	-12	10	15	600000	0.35	300
IW334	01/05/2004	2835.0	2842.5	0.2	85	0.005	25	30	35	300000	1.00	550

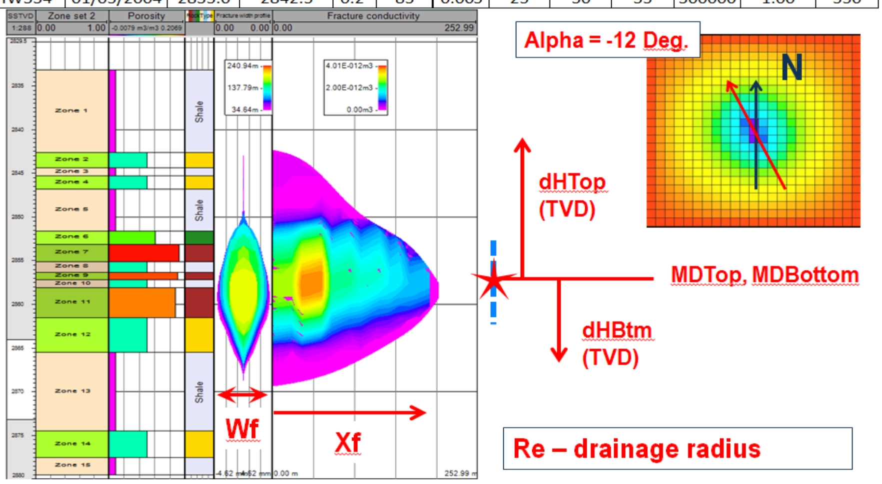

Figure 45 – Additional parameters

Hg Analytical and empirical methods are used to calculate the cell connection factor (CCF). On the first stage the value of the dimensionless productivity index for a well with given fracture and reservoir parameters (average among cells penetrated by fracture). The calculation is based on the modification of the M.Ekonomides formula and requires as input parameters, except for the geometrical parameters, the value of Re – drainage radius, which is the 13th parameter. As an effective permeability of the proppant is used multiplication of 11th and 12th parameters (proppant permeability and permeability multiplier - allowance for the gel or other conditions of proppant placing). The introduction of two parameters enables to recall to modeling engineers that effective permeability of the proppant in the fracture in reservoir conditions may be 30-40% of the “nominal” proppant permeability.

Using the analytical and empirical formula for calculating the dimensionless productivity index allows forecasting the index of productivity accurately depending on the fracture (Xf, wf, Kf) and stratum (K) parameters at steady state filtering. Using the Re value makes its limitations.

On the second stage there is the calculation from the dimensionless productivity index for the well with the hydraulic fracturing to opening coefficients of individual cells considering dimension of the grid and the sequence of cells and the “choke restriction” effect. The value is adjusted for Peaceman radius, number of uncovered cells and their size.

“Choke restriction” effect in each of the cells starting with the outer is calculated based on the assumption that the flow on the “output” of the crack generated from the flows to the plane of the crack and to the “input” flow into the crack. The flow ratio is directly proportional to cross-sectional area and permeability of the wings plane and the crack, respectively.

This proportion cannot describe the nonlinear effects that arise, including with the gas filtration or turbulent flow of liquid, and used as a “first approximation” for assessing the effect of “choke restriction” with laminar flow.

Among the additional options of models «EasyFrac» possibility of tasks which provide parameters from the 14th to the 22nd should make a point of the 18-th parameter (KntgUse). A non-zero value of this parameter means that the estimation of flow rate of the well with hydraulic fracturing and the "bandwidth" of cracks will be considered as a true height of crack which given by parameters 9 and 10 instead of the height of the active mesh as you receive from modeling effect of hydraulic fracturing with help of LGR. It means that bandwidth of crack is not only in "active" part of the stratum, which are described by active mesh but it is above or below the limits of grid modeling, as well as part of crack going through non-reservoir. Thus the thickness and conductivity of the crack is much less in the center than in upper or lower parts, the ratio defined by 18th parameter reduces “bandwidth" of crack outside of the active mesh of model. Geometric height is imperative for the "formation exposing" of water-saturated interlayers that are below or above the target interval, but bandwidth of top and bottom parts of crack should be reduced when we estimate the effect of "choke restriction" that provides by 18-th parameter (figure 46).

14th parameter (SatNum) is destined to indicate the numbers of phase permeability table for creation of new connection. We recommend you to use modified phase permeability with maximum increased relative permeability by water, but use it by original end points. It will considerably increase growth rate of watering connect with leading water penetration in the "body" of hydraulic fracturing crack (figure 46). Reproduction this effect without modification of phase permeability to compounds isn’t possible because capacity of the mesh modeling is better than size of crack.

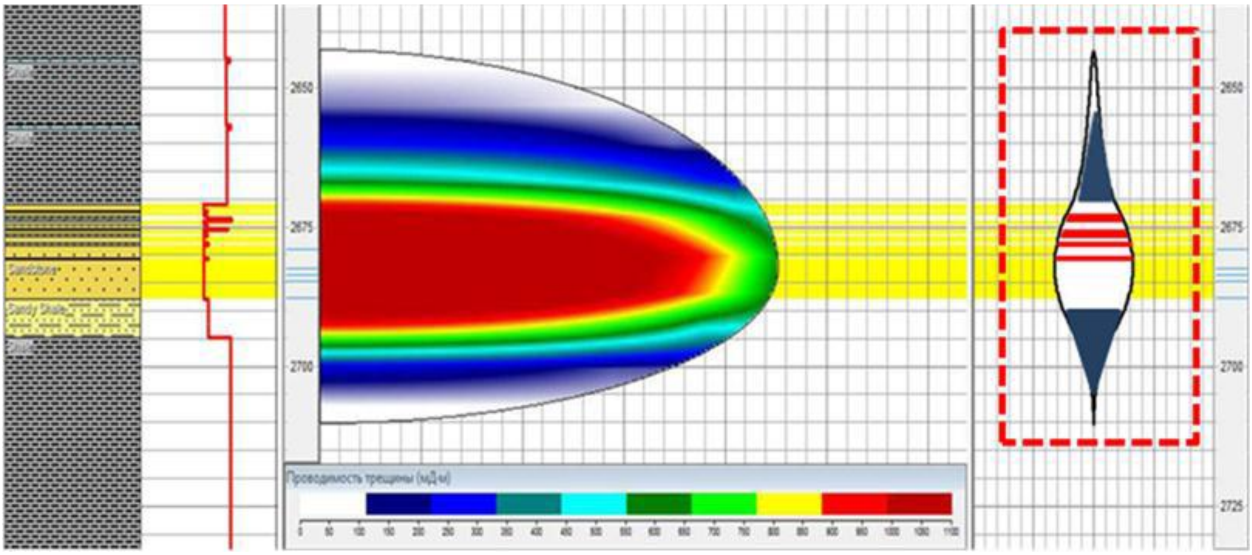

Figure 46 – Fracture zones which wasn’t taken into account when estimating filtration process from fracture wings to well, if 18th parameter (red) is equal to zero, and multiplier factor is less than one (blue) when the real fracture height is specified

The advantage of the module is the possibility to specify the fracture parameters of hydraulic fracturing in explicit form without modeling grid modifications and high speed calculation. The main disadvantage is the analytical and empirical approach to the definition of the dimensionless opening ratio, where the radius of drainage is one of the input calculation parameters. In addition, the correction of CCF values for each of the cells considering Peaceman radius and the number of exposed cells and their size cannot guarantee the accuracy of prediction better than + / - 15% (~ 10% on average) with account of crack rotation about the I and J axes of the mesh. The lack of consideration of the effects of nonlinear filtering in the fracture does not allow us to recommend this plug-in for hydraulic fracturing modeling in gas-condensate wells (E300) [15].

The plug-in can be used for playing a development history of a large number of wells with hydraulic fracturing within a single model, or to the sensitivity analysis of forecast production rates to the parameters of fracture (width, half-length, or proppant permeability). Using the plug-in for predicting the flow rates based on the results of specific hydraulic fracturing work on a new well may introduce additional error of ~ 10% at the direction of the crack at a diagonal to the grid. It is more appropriate to use the fracture modeling in explicit form (NWM, Tartan, LGR) at the hydraulic fracturing modeling for single well [16].

EasyFrac is a software tool designed to help engineers and geoscientists analyze and design hydraulic fracturing operations. Some of the main features of EasyFrac include:

3.1.1 Fracture design

Current approach enables to design and optimize hydraulic fracturing treatments, taking into account factors such as rock properties, fluid properties, and wellbore geometry.

Rock properties: The physical properties of the rock, such as its strength, stiffness, and fracture toughness, can affect the geometry of fractures. For example, weaker rocks may be more prone to developing wider, shallower fractures, while stronger rocks may develop narrower, deeper fractures [17].

Fluid properties: The properties of the fluid used in the hydraulic fracturing operation, such as its viscosity, density, and flow rate, can affect the geometry of fractures. For example, using a more viscous fluid may result in narrower, deeper fractures, while using a less viscous fluid may result in wider, shallower fractures.

Injection rate: The rate at which the fluid is injected into the wellbore can also affect the geometry of fractures. Higher injection rates may result in wider, shallower fractures, while lower injection rates may result in narrower, deeper fractures.

Stress and strain: The stress and strain on the rock can also influence the geometry of fractures. Higher stress and strain may result in deeper, narrower fractures, while lower stress and strain may result in shallower, wider fractures.

Wellbore geometry: The geometry of the wellbore, including its depth, inclination, and orientation, can also affect the geometry of fractures. For example, fractures may be more likely to develop perpendicular to the wellbore in horizontal wellbores, while they may be more likely to develop at an angle in inclined or vertical wellbores.

There are several formulas and calculations that can be used to model and predict fluid flow and proppant transport during hydraulic fracturing operations. Some examples include:

Darcy equation: The Darcy equation is a mathematical formula used to calculate the flow of fluids through porous media, such as rocks. It is often used in the oil and gas industry to predict fluid flow through fractures and wellbores. The general form of the Darcy equation is: $Q = (k * A * \Delta p)/(\mu * L)$ where Q is the volumetric flow rate, k is the permeability of the porous medium, A is the cross-sectional area of the flow path, Δp is the pressure drop across the porous medium, μ is the viscosity of the fluid, and L is the length of the flow path.

Hagen-Poiseuille equation: The Hagen-Poiseuille equation is a mathematical formula used to calculate the flow of fluids through a circular pipe. It can be used to predict the flow of fluids through wellbores during hydraulic fracturing operations. The general form of the Hagen-Poiseuille equation is: $Q = (\pi * r^4 * \Delta p)/(8 * \mu * L)$ where Q is the volumetric flow rate, r is the radius of the pipe, Δp is the pressure drop across the pipe, μ is the viscosity of the fluid, and L is the length of the pipe.

Carman-Kozeny equation: The Carman-Kozeny equation is a mathematical formula used to predict the flow of particles through a porous medium. It is often used in the oil and gas industry to calculate the transport of proppant during hydraulic fracturing operations. The general form of the Carman-Kozeny equation is:

$V = (C * K^2)/(150 * \mu * \Delta p)$ where V is the volumetric flow rate of the particles, C is a constant, K is the permeability of the porous medium, μ is the viscosity of the fluid, and Δp is the pressure drop across the porous medium [18].

3.1.2 Fracture analysis

Applied methodology provides tools for analyzing and interpreting the results of hydraulic fracturing operations, including fracture geometry, fluid flow, and proppant transport.

Fracture mapping: Fracture mapping involves analyzing data such as pressure, temperature, and fluid flow to create a visual representation of the fractures that were created during the hydraulic fracturing operation. This can help engineers and geoscientists understand the geometry and extent of the fractures and how they intersect with the wellbore [19].

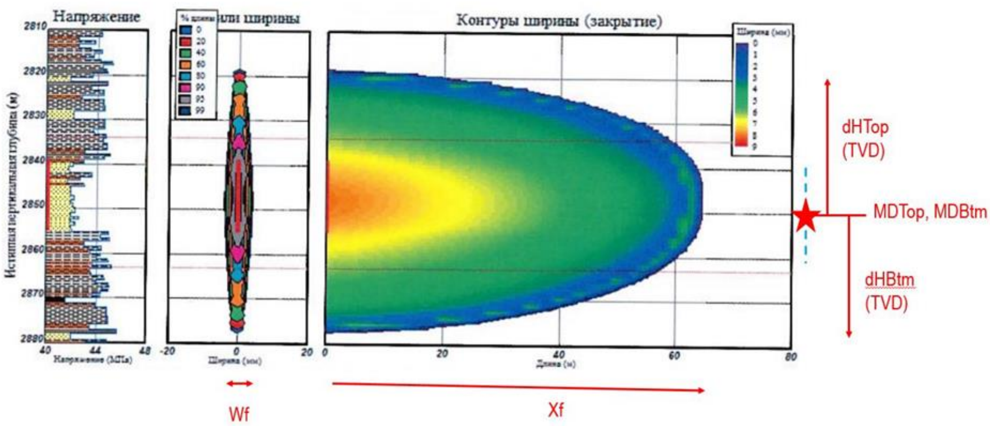

Figure 47 – Example of the EasyFrac based model

Borehole data, in particular breakouts, can indicate present day stress directions. Borehole breakouts form in the direction of the minimum horizontal stress. Drilling-induced fractures form normal to borehole breakouts and strike that are parallel to hydraulic fractures induced during the well stimulation process (figure 47). According to breakout interpretation at well 125, the direction of the minimum horizontal stress is at around 50deg NE which is perpendicular to the fault directions implying fracture azimuth of -50deg NW. Fracture orientation for the base case is set to -50deg NW, however, for waterflooding studies a separate scenario with fracture azimuth of 45deg NE (parallel to faults) should be tested [20].

3.1.3 Local update of hydraulic fractures parameters

Most of the wells have hydraulic fractures stimulation events in order to allow wells to produce. Some of the wells has more than one HF event. In order to match well BHP pressure dynamic, HF parameters were adjusted for each well individually (figure48).

Main parameter to match:

1. Fracture Xf.
2. Fracture degradation if observed

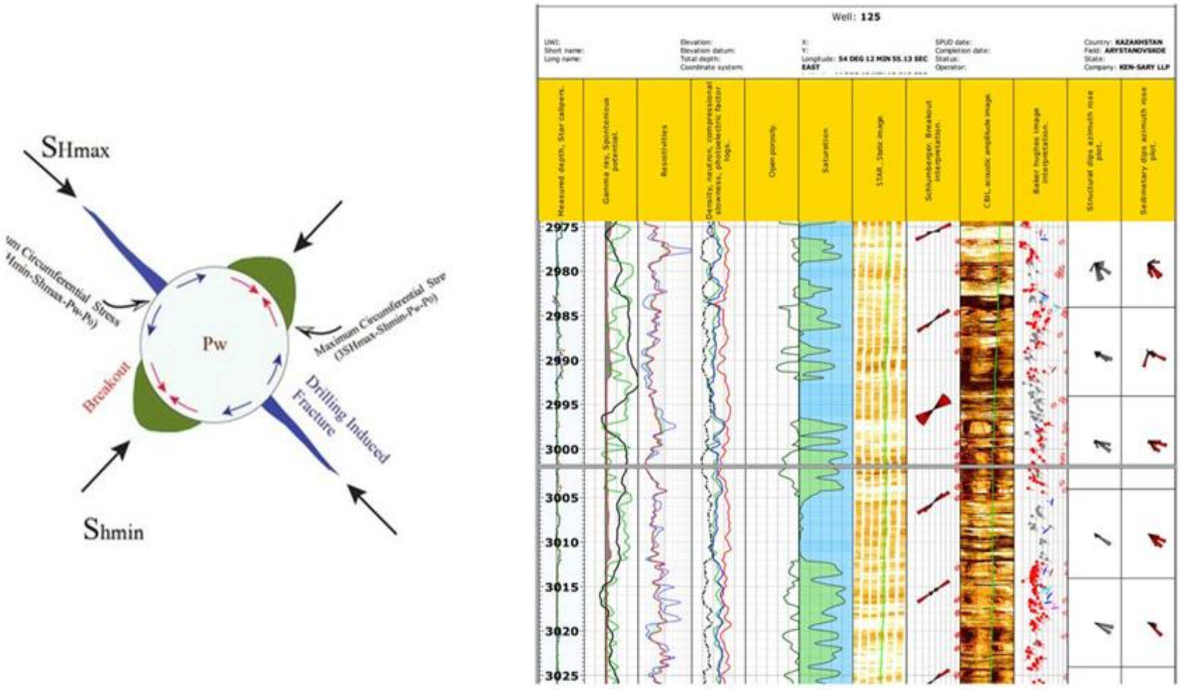

Figure 48 – Minimum horizontal stress direction identification based on borehole breakouts, well 125 (Sh max-Max horizontal stress, Sh min- Min horizontal stress

Matched Hydraulic fractures parameters for each well were defined using EasyFrac plugin shown on figure 49 [21].

Show	Well name	Fdate	MD top [m]	MD bottom	dw [m]	Xf [m]	w [m]	Alpha [deg]	dhTop [m]	dhBottor [m]	Kprop [mD]	KfKprop [part]	Re [m]
☑	102	12/12/2009	2993	3007	0.177	50	0.0059	-50	50	17.5	327000	1	201.3...
☐	102	01/01/2016	2993	3007	0.177	100	0.0059	-50	50	17.5	327000	1	201.3
☑	107	16/07/2014	3020	3043	0.177	50	0.0053	-50	29.4	10.7	396000	1	152.55
☐	107	01/01/2018	3020	3043	0.177	50	0.0053	-50	29.4	10.7	396000	1	152.55
☑	108	23/11/2012	3025	3039.5	0.177	20	0.00259	-50	42	39.1	167681.75	1	107.1
☐	108	01/10/2018	3025	3039.5	0.177	90	0.00259	-50	42	39.1	167681.75	1	120
☑	109	28/12/2011	2998	3010.5	0.177	50	0.0083	-50	19.2	7.5	408250	1	123
☑	109	08/08/2014	2998	3010.5	0.177	100	0.0078	-50	17.8	16.2	232000	1	153.3...

Figure 49 – Hydraulic fractures parameters for each well-defined using EasyFrac

Average HF length was significantly reduced after local adjustment from 115 to 60m in average. Xf histogram can be observed below on figure 50.

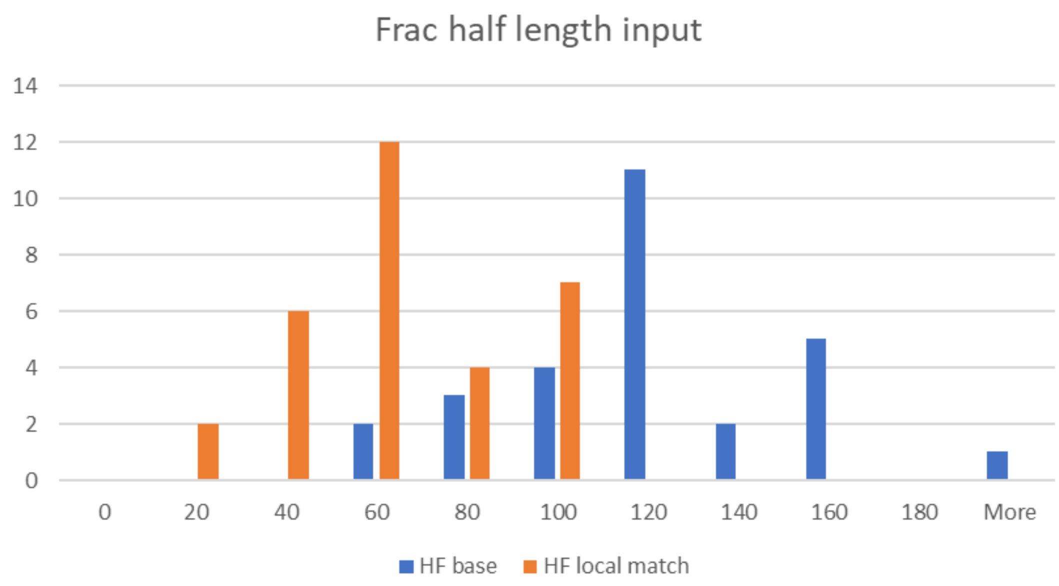

Figure 50 – Average HF length before and after local adjustment

3.1.4 Fracture degradation modelling

It was observed anomalous simulated BHP behavior for some wells. Attempts to match such response with local well permeability and HF properties was unsuccessful. Various hypothesis was tested and the best fit of simulated BHP compare to observed showed fracture degradation hypothesis.

UDQ and ACTIONX keywords was using to mimic fracture degradation impact. Figure 51 shows example of implementation fracture degradation for well 108. Please refer to Petrel project and DK_ECL_MONTHLY_Jan 2019_R300_TRACER_UDQ development strategy to find more details of fracture degradation definition.

```
UDQ                                    -- Generated : Petrel
ASSIGN FUPIM108 1   /
/

ACTIONX                                -- Generated : Petrel
PI108HI  10000 10   /
WLPR '108' > 0 AND  /
WBHP '108' > 65 AND /
WUBHERR1 '108' > 0.2 /
/

WPIMULT                                -- Generated : Petrel
'108'  0.8 /
/

UDQ                                    -- Generated : Petrel
DEFINE FUPIM108 FUPIM108*0.8     /
UPDATE FUPIM108 NEXT /
/

ENDACTIO                               -- Generated : Petrel
```

Figure 51 – UDQ and ACTIONX keywords using to mimic fracture degradation

Noted: this hypothesis was discussed during workshop in April 2019. It was decided to have both versions of HM model together: without and with fracture degradation modelling (DK_BEST_HMU_APR19B and DK_BEST_HMU_APR19 C accordingly) to be able to test any impact on forecast from both approaches.

3.2 Well candidate selection criteria

There are a number of factors to consider when selecting a hydraulic fracture treatment, including the type of reservoir being stimulated, the type of fluid to be injected, and the design of the treatment. In general, the goal of the treatment is to create a highly conductive fracture or channel that will allow for the efficient flow of hydrocarbons into the well [22-24].

Propped hydraulic fracture well stimulation should only be considered when certain minimum criteria are met. These criteria include the presence of adequate producible reserves, sufficient reservoir pressure to maintain flow when producing these reserves, and a production system that can process the extra production. In addition, it is important to have professional, experienced personnel available for treatment design, execution, and supervision, as well as high-quality pumping, mixing, and blending equipment.

The minimum criteria that can be used to screen wells for treatment (table 4).

Table 4 – Screening criteria

Parameter	Oil Reservoir	Gas Reservoir
Hydrocarbon Saturation	>40%	>50%
Water Cut	<30%	<200 bbls/MM scf
Permeability	1-50 mD	0,01-10 mD
Reservoir Pressure	<70% depleted	twice abandonment pressure
Gross Reservoir Height	>10 m	>10 m
Production System	20% spare capacity	

With the advent of powerful computing technology, the role of a Easy frac module has significantly increased, namely, as a working tool that allows describing processes and phenomena in the language of numerical concepts as well as analytical approach. The created model for hydraulic fracturing simulation enables numerically describe object and makes it possible to study in detail the necessary processes, conduct a quantitative analysis of well stimulation to be incorporated to simulation model outcomes such as time grid and resulted Isobar and net pay map .The process of numerical modeling mainly includes several stages. The first stage is to identify the relationships between the main parameters of the frac design and numerical model itself . First of all, at this stage there is a qualitative analysis of the phenomena under study and the formation of patterns that link the main objects of research. Objects that allow quantitative description are identified. Thus, the end of the first stage is considered to be the construction of a hypothetical model, which includes the recording in mathematical language of concepts of qualitative representations about the relationships between the main objects of the model, which can be quantitatively characterized. Take into it account Reservoir pressure > 50-70% (ability to flow back gel products), figure 52, 53, 54, 55, 56, 57, 58, 59 is presented as follow.

For adequate producible reserves and as a result of sensitivity study presented in Chapter 1 for J-XI net pay above OWC >10 is considered The well should be connected to a reservoir with sufficient reserves of hydrocarbons to justify the cost of the treatment.

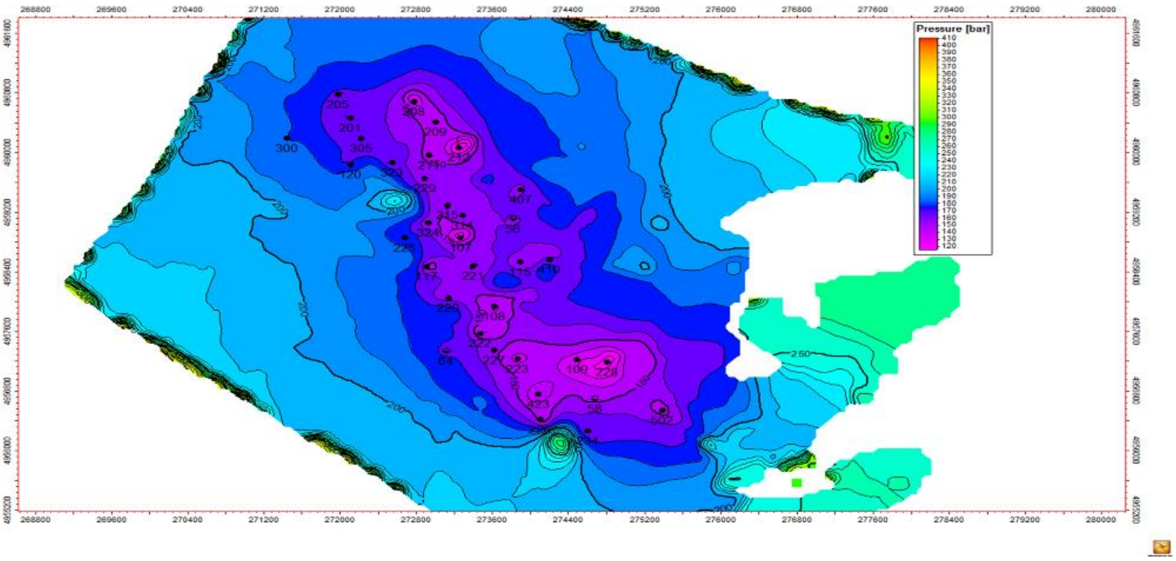

Figure 52 – No applied pressure filter

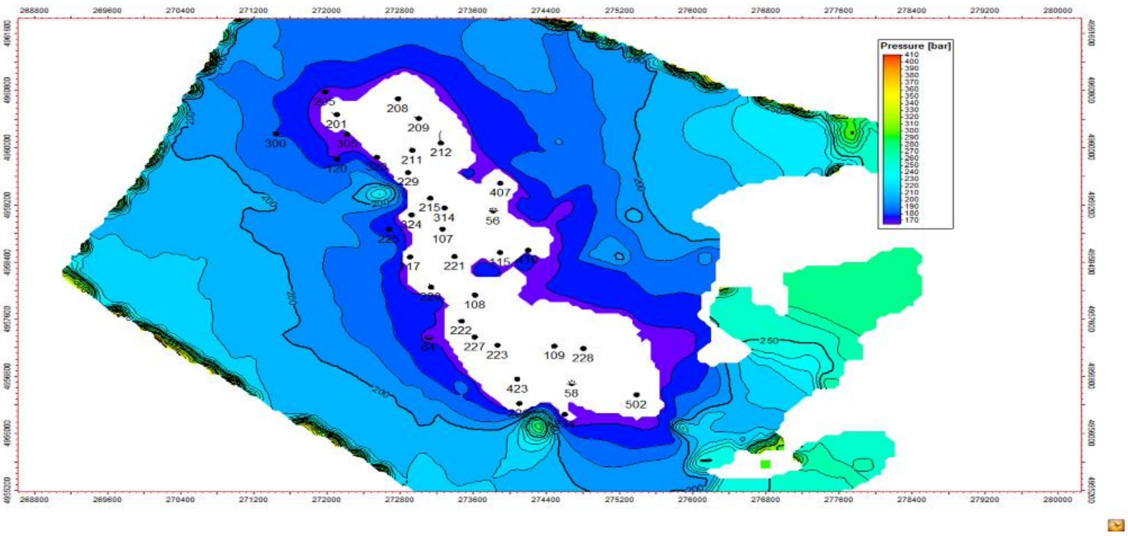

Figure 53 – No applied pressure filter = 165(70% from initial Pressure)

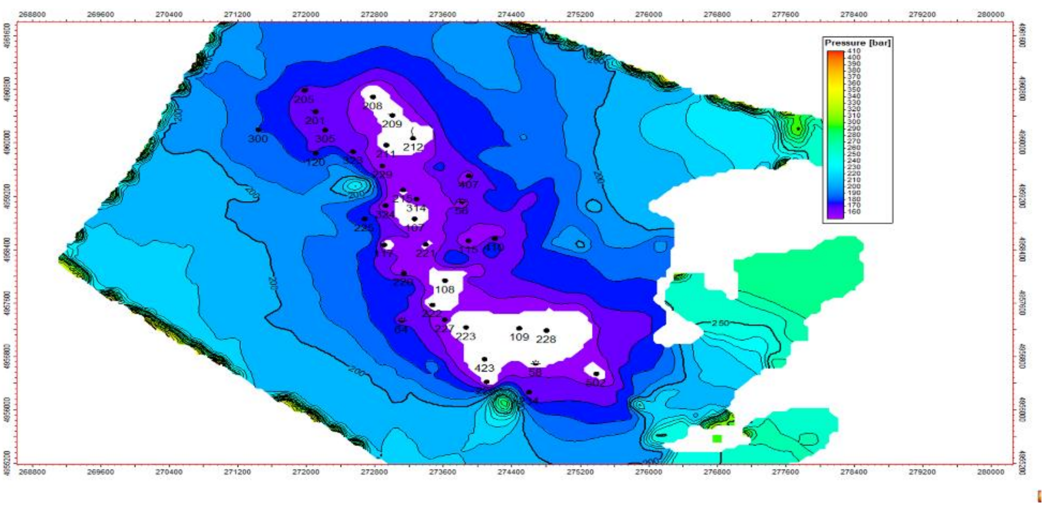

Figure 54 – No applied pressure filter = 150 (60% from initial Pressure)

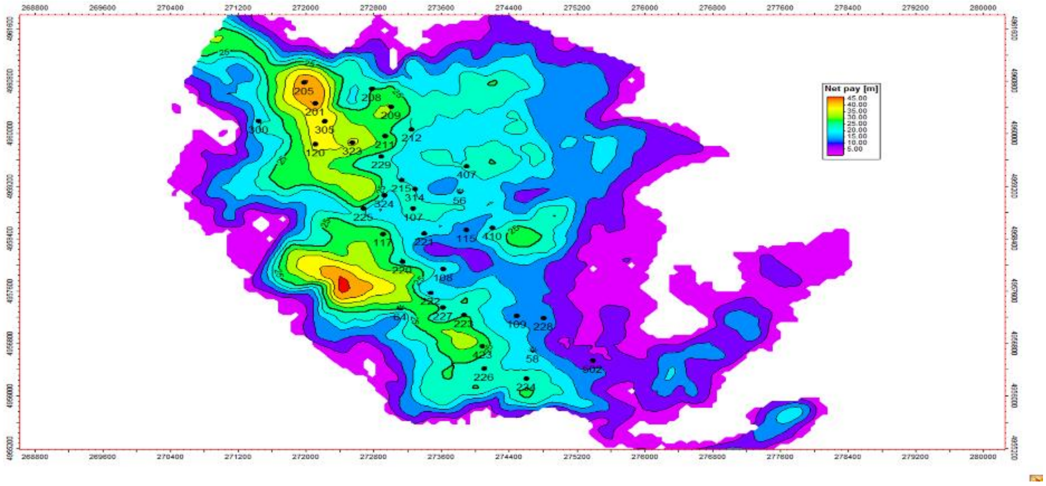

Figure 55 – No applied net pay filter

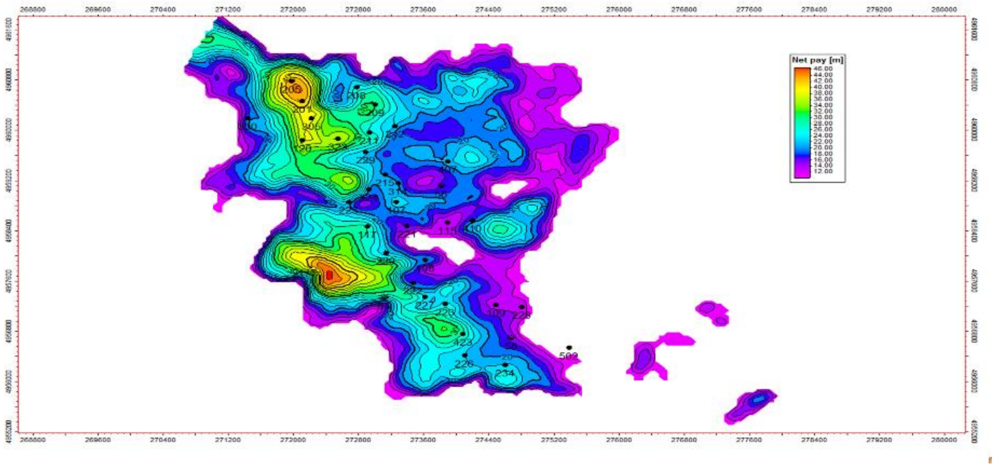

Figure 56– Net pay > 10 m filter applied

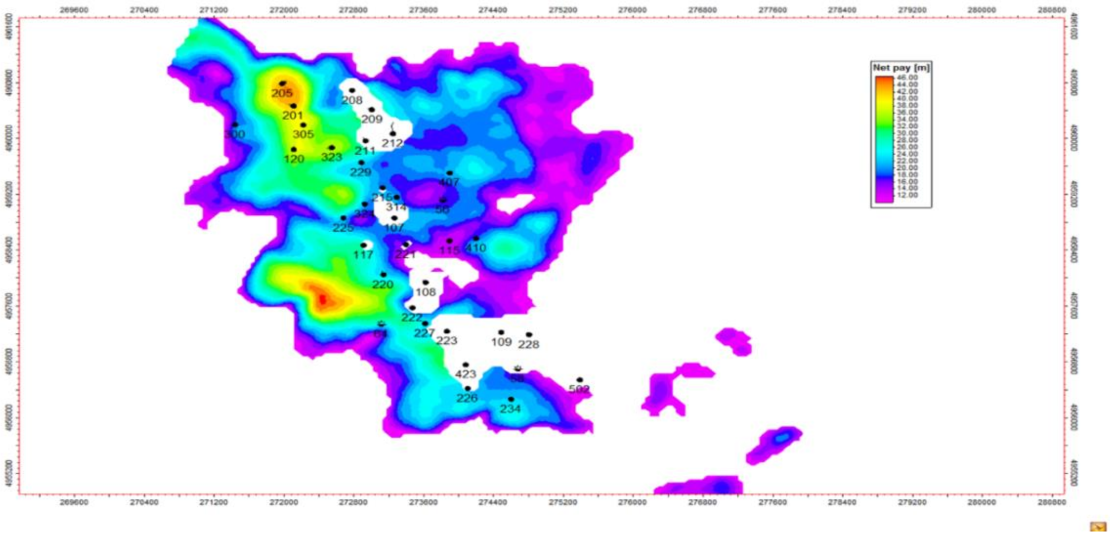

Figure 57 – Net pay > 10 m and pressure > 165 bar filter applied

Based history matched Petrel project combined map view that displays the relevant data map for the pressure and net pay. The combined filter applied based on (Net pay >10 and Pressure > 165/150).

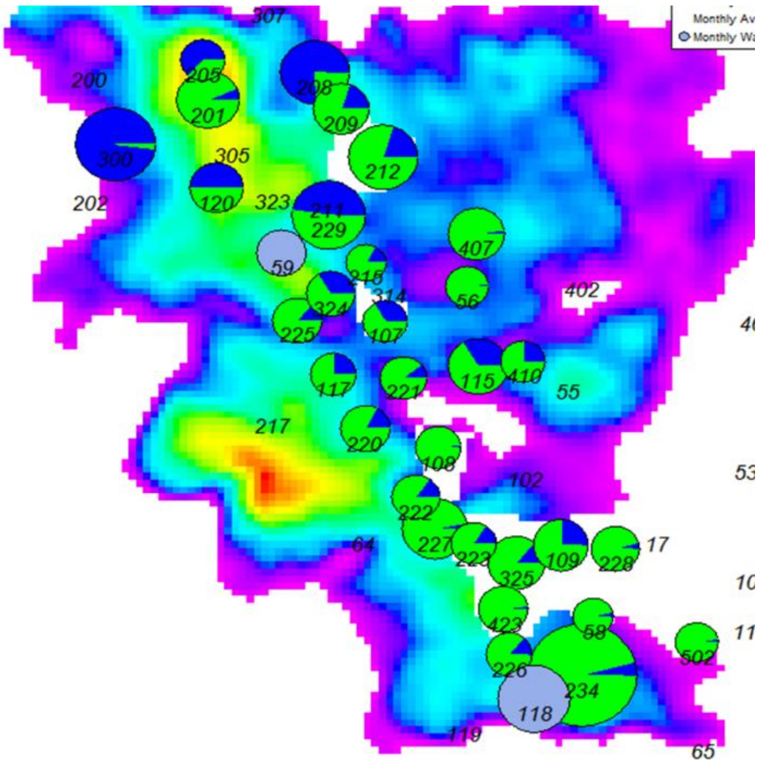

Figure 58 – net pay > 10 m and pressure > 150 bar filter applied

In order to select proper well candidate combined map was analyzed with the production bubble map that allows for the visualization of complex production data in a clear and concise manner. This enables to track performance over time, and to make informed decisions about production strategies.

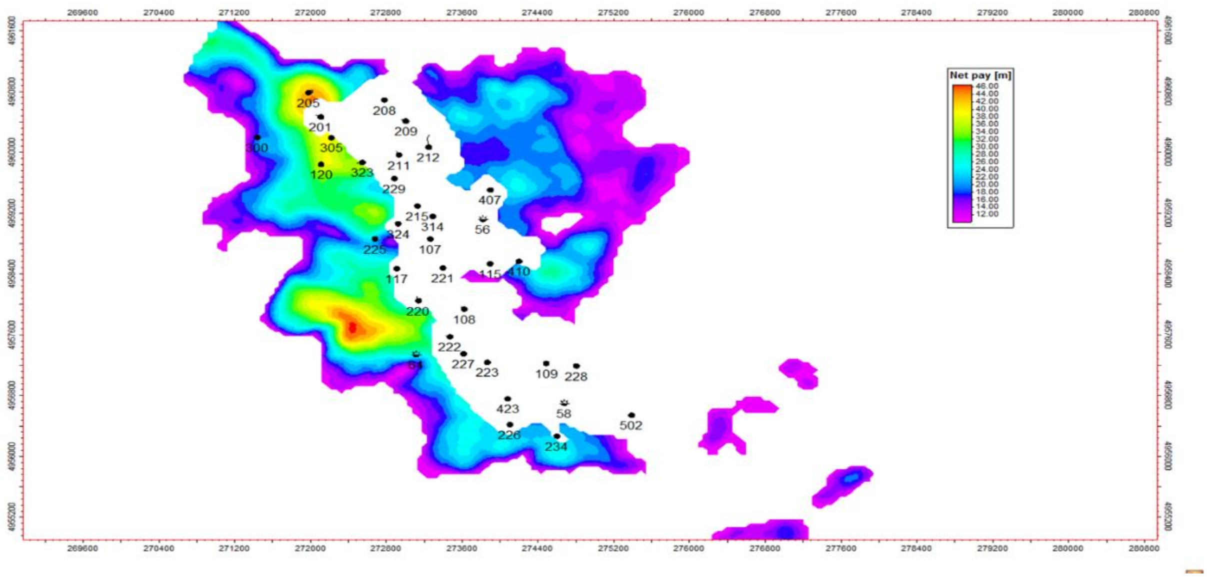

Figure 59 – Bubble map view without WCUT filtered values

The size of the bubbles (figure 60) corresponds to the amount of production from each well and the color of the bubbles indicates the type of production (oil, water).

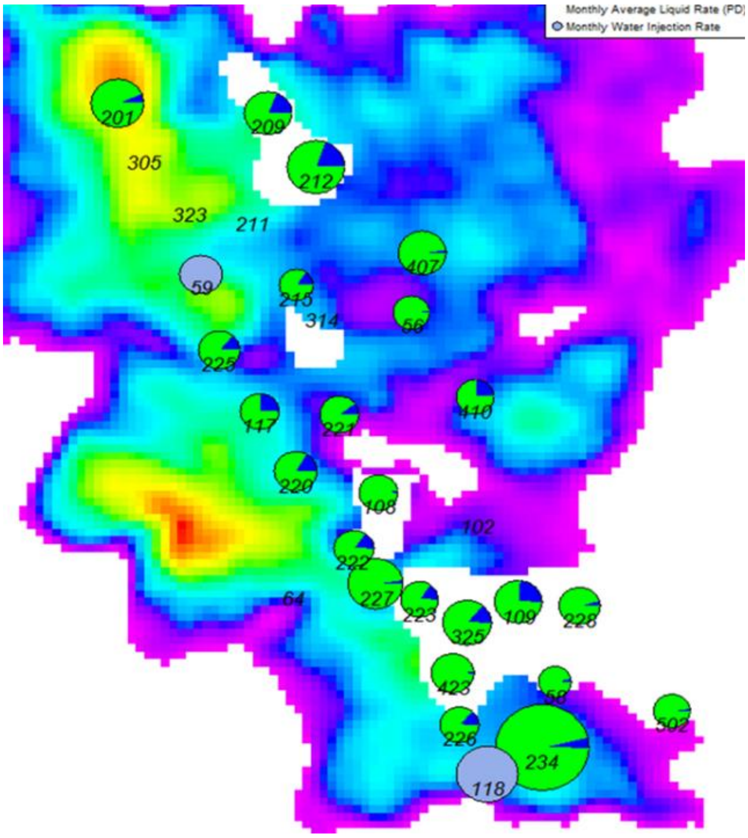

Figure 60 – Bubble map view without WCUT filtered values>30%

Finally applying a water cut filter to a bubble map, it is possible to display only the wells or fields that meet a certain water cut threshold (30% based on sensitivity study). This is useful for identifying areas with low water production, which may indicate that the reservoir is producing primarily hydrocarbons and is therefore more productive.

Conclusions on the 3st section

Physical limits identified such as the maximum allowable treating pressure, which can limit the injection rate and the type of treating fluids that can be used. The ability to isolate the treatment zone from other intervals through perforating and/or the integrity of the tubulars is also an important consideration.

In addition to these physical limits, reservoir constraints such as production failures (e.g. water or gas coning or influx, formation sanding) and the physical location and thickness of the zones being treated can also impact the effectiveness of the hydraulic fracturing treatment. It is important to consider these factors when designing a hydraulic fracturing treatment in order to optimize the treatment for the specific well and reservoir conditions [25-27].

As the result we have following outcomes:

1. Obtained adequate material balance of reserves to justify the cost of the hydraulic frac treatment.

2. Obtained reservoir pressure limits to maintain flow when producing the reserves economically justifiable to install artificial lift to maintain flow [28-31].

3. Obtained production system limit that should be able to handle the

increased production resulting from the treatment.

4. Obtained quantification of the rock formation that should be suitable for hydraulic fracturing, with the presence of shale or other tight rock formations that are likely to contain hydrocarbons.

Come up with sensitivity result HF constraint:

– water cut > 30% (based logging results) Connate and movable water in reservoir not exceeded 30%, if well produce more 30% water it is highly probable due to water breakthrough. As an example Jurassic XI (main object) is presented with Initial pressure equal to 280 bar bdu;

– reservoir pressure > 50-70% (ability to flow back gel products);

– net pay above OWC >10 (tight formation will resulted in ESP failure).

4 INTEGRATED LABORATORY AND SIMULATION METHODS FOR SCALE ANALYSIS

In the previous sections, the author carried out a detailed analysis of the material balance of research objects based numerical simulation and modeling isue of hydraulic fracturing . We have seen that with the help of modeling tools it was possible to analyze well productivity decline based on pressure and possible frac degradation effect. Among these tasks, monitoring the bottomhole well condition and study scale precipitation impact on well productivity is one of the priorities that should be studied in details [32, 33].

As a result of the analysis, the tasks of the dissertation work were substantiated and the basic of research were to differentiate 3 main effect on production decline (pressure depletion , hydraulic frac degradation and quantification of scale effect) , the thermobaric condition and behavior of which significantly depends on the bottomhole and reservoir condition.

At the same time, in accordance with the results of the review of the literature data on the topic of the dissertation (Chapter II), the author identified two areas of well research for analysis.

First as it was written estimated PI range(before HF 0.07 m^3/bar/day and after HF: 0.2-1 m^3/bar/day).It depends on the well and area of location. Numbers above are shown to have feeling of reasonable range of PIs before and after frac. PIs calculated from production data shows monotonic reduction with time with tendency to stabilize at some level. That indicates long transition period before well comes to stable production regime.

Secondly it is curial to investigate the effect of scale precipitation as far as it is main reason for well workovers and productivity decline.

Passive monitoring of the development object (well, reservoir, deposit), as a rule, does not allow solving numerous problems related to monitoring its current state and justification of measures for its more effective development. In this connection, it is proposed to study scaling mechanism and effect on permeability decline. Even with a good knowledge of the parameters of the behavior of the fields, the task remains to assess the unambiguity of the interpretation of the data, since it is necessary to distinguish some processes from others.

In this connection, the author pays special attention to scale laboratory study with novel thermobaric simulation . For the successful application of these methods, the problems of data informativeness analysis are more important than ever. Let's take a closer look at the principle and possibilities of this approach [34].

Objective

Integrated laboratory and simulation studies of the scaling issue is the main part of the dissertation that quantify the impact on hydarulic fractured well post production decline and effect on well productivity

Scaling issues study has the following objectives: to define type of scales (within the frame and using resources available for the study), to run simulations in order to understand long-term scaling tendencies (during water injection projects) or short-term scale tendencies (during fracturing or workover operations), and to give recommendations based on tests and Schlumberger database.

The Research and Scientific nature of this work is supported by the fact that

Scale analysis scientific software which is new to Kazakhstan hydrocarbon production stimulation industry, was used.

The objective of the scaling issues study is to understand the type of scales that can occur in Arystan reservoirs and production wells and to provide recommendations to mitigate or prevent scaling. The study aims to achieve this by defining the types of scales that can occur within the system and using the available resources to run simulations that can help understand the long-term or short-term scaling tendencies.

In the case of water injection projects, the study will focus on understanding the long-term scaling tendencies that can occur due to the injection of water into the reservoir. This can include understanding the chemical composition of the injected water, the temperature and pressure conditions, and the potential for mineral precipitation over time. By running simulations, the study can provide insights into the potential scaling issues that can occur in the reservoir and provide recommendations for mitigation or prevention [35, 36].

In the case of fracturing or workover operations, the study will focus on understanding the short-term scaling tendencies that can occur during these operations. This can include understanding the types of scales that can form due to the fracturing or workover operations, the chemical composition of the fluids used, and the temperature and pressure conditions. By running simulations, the study can provide insights into the potential scaling issues that can occur during these operations and provide recommendations for mitigation or prevention.

Ultimately, the study aims to provide recommendations based on tests and the Schlumberger database to help prevent or mitigate scaling issues in oil and gas reservoirs and production wells. The recommendations may include changes to the injection or production fluids, changes to the operating conditions, or other measures to prevent or mitigate scaling issues. Overall, the scaling issues study is an important component of oil and gas production optimization as it can help prevent costly and damaging scaling issues that can impact production and profitability [37-39].

4.1 Scales Laboratory Testing

Schlumberger RPS Laboratory performed solubility test of samples taken from the Arystan field from wells A-234, A-509 and A-65.

The tests procedure was:

1. Prepare 6 samples approximately 3 grams from each well.
2. Prepare the following systems:
   a) xylene;
   b) methanol;
   c) hydrochloric acid 20%;
   d) mutual solvent;
   e) 10% Mutual Solvent/80% Xylene/10% Organic acid;
   f) diesel.
3. All samples to be tested at 95 degC:
   a) place Bottles into Hot Water Bath for 1 hour;
   b) filter the solvent, wash and dry them;
   c) calculate the weight % dissolved.

Below are the laboratory pictures of scales after filtration is over (figures 61, 62). For each fluid, the left picture is sample from well A-234, picture in the centre is sample from well A-509, and right picture is sample from well A-65.

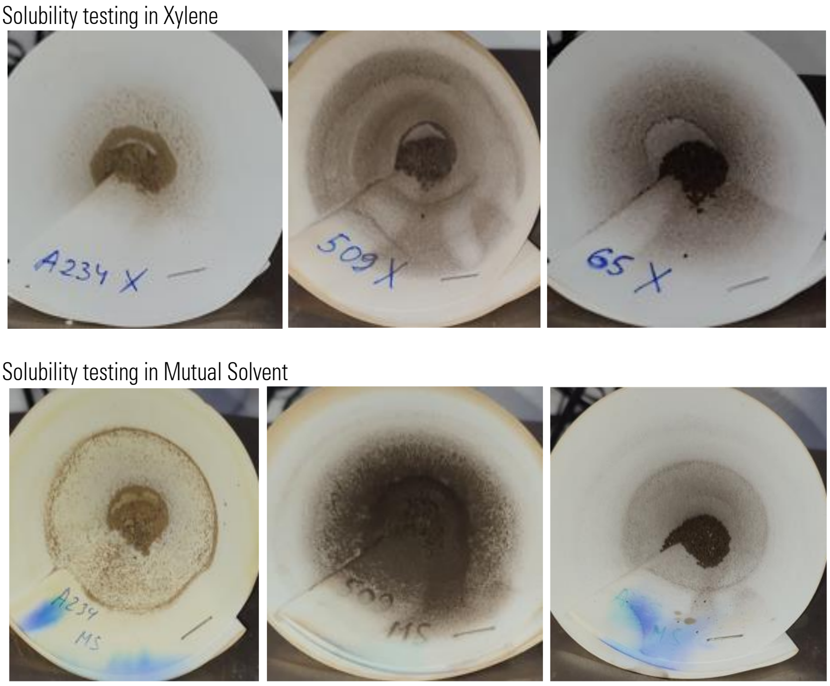

Figure 61 – Scales after filtration

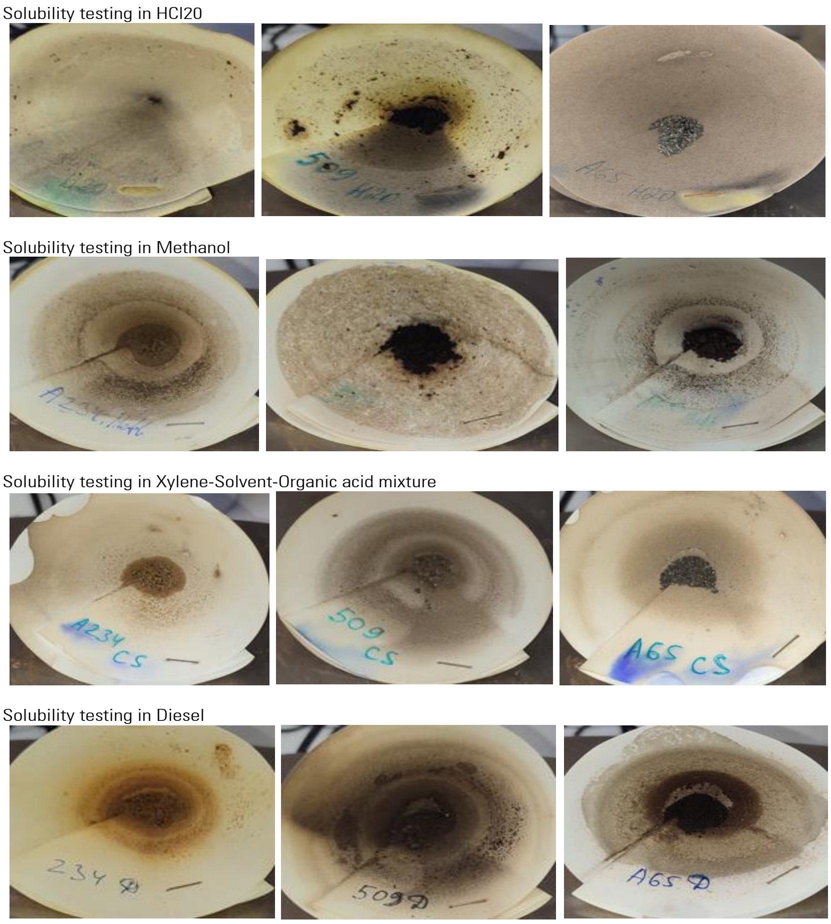

Figure 62 – Scales after filtration

Dissolution summary is shown in the following figure 63 In bold, we highlighted the fluids which dissolved the most of the scale mass.

Fluid system	Well No	Sample weight (g)	Residue weight (g)	% Dissolved
HCl20	**A-234**	**3.00**	**0.28**	**91%**
Mutual Solvent	**A-234**	**3.00**	**2.60**	**13%**
Xylene	A-234	3.00	2.90	3%
Methanol	**A-234**	**3.00**	**2.60**	**13%**
Xylene-Solvent-Organic acid	A-234	3.00	2.90	3%
Diesel	A-234	3.00	2.99	0%
HCl20	**A-509**	**3.00**	**1.50**	**50%**
Mutual Solvent	A-509	3.00	2.70	10%
Xylene	**A-509**	**3.00**	**2.56**	**15%**
Methanol	A-509	3.00	2.79	7%
Xylene-Solvent-Organic acid	**A-509**	**3.00**	**2.58**	**14%**
Diesel	A-509	3.00	2.85	5%
HCl20	A-65	3.00	2.79	7%
Mutual Solvent	A-65	3.00	2.94	2%
Xylene	A-65	3.00	2.94	2%
Methanol	A-65	3.00	2.97	1%
Xylene-Solvent-Organic acid	A-65	3.00	2.95	2%
Diesel	A-65	3.00	2.98	1%

Figure 63 – Dissolution summary

Conclusions on laboratory analysis of scales:

1. Samples from the well A-234 are represented by at least 85-90% of carbonate, which can be a formation carbonate or carbonate scale. Most probably, majority of this sample is a Calcium Carbonate, though possibility of some Magnesium carbonate or traces of sulphates exists (this can not be distinguished without more detailed methods of scale analysis). The rest 10-15% can be a residue of paraffinic or waxes components of oil.
2. Samples from the well A-509 are represented by at least 50-55% of carbonate, which can be a formation carbonate or carbonate scale. Most probably, majority of this carbonate is a Calcium Carbonate, though possibility of some Magnesium carbonate or traces of sulphates exists (this can not be distinguished without more detailed methods of scale analysis). 10-15% can be a residue of paraffinic or waxes components of oil, including possibility of not more than 10% of asphaltenic component (solubility in Xylene). The rest 30-40% of the sample is represented by non-soluble component, which is, most probably, either Quartz, Clay, Iron compounds (Iron oxides, Pyrite) or any other Clastic rock component from the target interval.
3. Samples from the well A-65 are represented by at least 95% of one of the following (or mixture of the following): Quartz, Clay, Ceramic Proppant, Iron compounds (Iron oxides, Pyrite) or any other Clastic rock component from the target interval.
4. The sample from the well A-234 is similar to samples from wells A-52 and A-401 (which SUBSOIL USER tested in Novomet lab in July 2020).

5. The samples from the wells A-234 and A-509 are similar to samples from wells A-236 and A-234 (which SUBSOIL USER tested in NIPI in 2018).

6. In terms of solubility, the sample from the well A-65 is similar to sample from well A-502, which SUBSOIL USER tested in Novomet lab in July 2020.

Conclusions on laboratory analysis of scales:

1. Samples from the well A-234 are represented by at least 85-90% of carbonate, which can be a formation carbonate or carbonate scale. Most probably, majority of this sample is a Calcium Carbonate, though possibility of some Magnesium carbonate or traces of sulphates exists (this can not be distinguished without more detailed methods of scale analysis). The rest 10-15% can be a residue of paraffinic or waxes components of oil.

2. Samples from the well A-509 are represented by at least 50-55% of carbonate, which can be a formation carbonate or carbonate scale. Most probably, majority of this carbonate is a Calcium Carbonate, though possibility of some Magnesium carbonate or traces of sulphates exists (this can not be distinguished without more detailed methods of scale analysis). 10-15% can be a residue of paraffinic or waxes components of oil, including possibility of not more than 10% of asphaltenic component (solubility in Xylene). The rest 30-40% of the sample is represented by non-soluble component, which is, most probably, either Quartz, Clay, Iron compounds (Iron oxides, Pyrite) or any other Clastic rock component from the target interval.

3. Samples from the well A-65 are represented by at least 95% of one of the following (or mixture of the following): Quartz, Clay, Ceramic Proppant, Iron compounds (Iron oxides, Pyrite) or any other Clastic rock component from the target interval.

4. The sample from the well A-234 is similar to samples from wells A-52 and A-401 (which SUBSOIL USER tested in Novomet lab in July 2020).

5. The samples from the wells A-234 and A-509 are similar to samples from wells A-236 and A-234 (which SUBSOIL USER tested in NIPI in 2018).

6. In terms of solubility, the sample from the well A-65 is similar to sample from well A-502, which SUBSOIL USER tested in Novomet lab in July 2020.

4.2 Water Laboratory Testing

Tests of water samples in Schlumberger Laboratory

Schlumberger RPS Laboratory performed analysis of water samples, in order to use it for the Scales simulation and for the Fracturing fluid rheology analysis.

The following samples were received by the lab:

Injection Water from well A-59 – 5 L.

Fracturing Water from well A-411 – 10 L.

Water from wells A-121, A-107, A-57, A-229 – 1.5 litres.

Results of the ion analysis is shown below:

Fracturing Water (well A-411) Analysis:

SG – 1.00

pH – 7.26

Injection Water (well A-59) Analysis:

SG – 1.10

pH – 5.38

Cl – 48 000 mg/L

Cl – 60 mg/L
Sulphate – 120 mg/L
Ca – 140 mg/L
Mg – 120 mg/L
Fe – 0.7 mg/L
Carbonates – 0 mg/L
Bicarbonates – 140 mg/L
Hydroxides – 0 mg/L

Water from well A-57:
SG – 1.1020
pH – 5.89
Cl – 94000 mg/L
Sulphate – 200 mg/L
Ca – 48000 mg/L
Mg – 1000 mg/L
Fe – 300 mg/L
Carbonates – 0 mg/L
Bicarbonates – 180 mg/L
Hydroxides – 0 mg/L

Water from well A-229:
SG – 1.0970
pH – 6.04
Cl – 92000 mg/L
Sulphate – 200 mg/L
Ca – 48000 mg/L
Mg – 1000 mg/L
Fe – 300 mg/L
Carbonates – 0 mg/L
Bicarbonates – 180 mg/L
Hydroxides – 0 mg/L

Sulphate – 100 mg/L
Ca – 33 000 mg/L
Mg – 0 mg/L
Fe – 10 mg/L
Carbonates – 0 mg/L
Bicarbonates – 980 mg/L
Hydroxides – 0 mg/L

Water from well A-121:
SG – 1.0980
pH – 5.97
Cl – 93000 mg/L
Sulphate – 200 mg/L
Ca – 49000 mg/L
Mg – 2000 mg/L
Fe – 320 mg/L
Carbonates – 0 mg/L
Bicarbonates – 160 mg/L
Hydroxides – 0 mg/L

Water from well A-107:
SG – 1.0890
pH – 5.92
Cl – 90000 mg/L
Sulphate – 200 mg/L
Ca – 47000 mg/L
Mg – 2000 mg/L
Fe – 280 mg/L
Carbonates – 0 mg/L
Bicarbonates – 140 mg/L
Hydroxides – 0 mg/L

Review of water analysis results provided by subsoil user. The following water analysis results were provided by subsoil user (figure 64).

Содержание ионов, моль/м^3 и примесей, г/м^3	Горизонт Ю-I, блок IV				Горизонт Ю-VIa, блок IV				Горизонт Ю-VIв, блок XI				Горизонт Ю-VIIa, блок IV			
	Количество исследо-ванных		Диапазон изменения	Среднее значение	Количество исследо-ванных		Диапазон изменения	Среднее значение	Количество исследо-ванных		Диапазон изменения	Среднее значение	Количество исследо-ванных		Диапазон изменения	Среднее значение
	скв-н	проб			скв-н	проб			скв-н	проб			скв-н	проб		
Cl^-	1	1	-	3135,02	1	1	-	3330,2	1	1	-	3098,42	1	1	-	3232,61
SO_4^-	1	1	-	0,12	1	1	-	0,07	1	1	-	0,05	1	1	-	0,03
HCO_3^-	1	1	-	3,00	1	1	-	1,80	1	1	-	2,00	1	1	-	1,60
Ca^{2+}	1	1	-	403,44	1	1	-	419,56	1	1	-	41,49	1	1	-	447,16
Mg^{2+}	1	1	-	70,77	1	1	-	71,00	1	1	-	62,28	1	1	-	73,74
Na^+K^+	1	1	-	2206,41	1	1	-	2373,56	1	1	-	2910,95	1	1	-	2214,42
Примеси	-	-	-	-	-	-	-	-	-	-	-	-	-	-	-	-
pH	-	-	-	-	-	-	-	-	-	-	-	-	-	-	-	-

Содержание ионов, моль/м^3 и примесей, г/м^3	Горизонт Ю-VIIa, блок VIII				Горизонт Ю-VIIIб, блок IV				Горизонт Ю-Xa+б, блок I				Горизонт Ю-Xб, блок IX			
	Количество исследо-ванных		Диапазон изменения	Среднее значение	Количество исследо-ванных		Диапазон изменения	Среднее значение	Количество исследо-ванных		Диапазон изменения	Среднее значение	Количество исследо-ванных		Диапазон изменения	Средне значени
	скв-н	проб			скв-н	проб			скв-н	проб			скв-н	проб		
Cl^-	1	1	-	2655,12	1	1	-	3244,81	1	1	-	2829,52	1	1	-	2448,15
SO_4^-	1	1	-	0,62	1	1	-	0,05	1	1	-	0,17	1	1	-	0,31
HCO_3^-	1	1	-	1,36	1	1	-	отс.	1	1	-	1,28	1	1	-	0,65
Ca^{2+}	1	1	-	251,17	1	1	-	449,92	1	1	-	262,50	1	1	-	281,10
Mg^{2+}	1	1	-	170,54	1	1	-	71,00	1	1	-	200,33	1	1	-	163,31
Na^+K^+	1	1	-	1813,73	1	1	-	2224,98	1	1	-	1851,58	1	1	-	1560,15
Примеси	-	-	-	-	-	-	-	-	-	-	-	-	-	-	-	-
pH	1	1	-	6,2	-	-	-	-	1	1	-	5,6	1	1	-	5,2

Содержание ионов, моль/м^3 и примесей, г/м^3	Горизонт Ю-Xб, блок XI				Горизонт Ю-XI, блок II				Горизонт Ю-XI, блок V			
	Количество исследо-ванных		Диапазон изменения	Среднее значение	Количество исследо-ванных		Диапазон изменения	Среднее значение	Количество исследо-ванных		Диапазон изменения	Среднее значение
	скв-н	проб			скв-н	проб			скв-н	проб		
Cl^-	1	1	-	2805,66	1	1	-	2357,14	1	1	-	2447,85
SO_4^-	1	1	-	0,33	1	1	-	отс.	1	1	-	0,14
HCO_3^-	1	1	-	1,60	1	1	-	отс.	1	1	-	1,23
Ca^{2+}	1	1	-	363,38	1	1	-	409,2	1	1	-	285,60
Mg^{2+}	1	1	-	53,79	1	1	-	12,34	1	1	-	163,29
Na^+K^+	1	1	-	1988,99	1	1	-	1516,24	1	1	-	1551,14
Примеси	-	-	-	-	-	-	-	-	-	-	-	-
pH	-	-	-	-	-	-	-	5,56	1	1	-	6,2

Figure 64 – Water analysis results

Example of conversion from SUBSOIL USER -provided test values to the SLB laboratory values

– M (HCO3-) = 3 Mol/m^3 = 0.003 Mol/l;
– c (HCO3-) = 61 g/mol;
– m/v (HCO3-) = M*c = 0,183 g/l = 183 mg/l.

4.3 Analytical Study

A Stiff diagram is a graphical representation of chemical analyses. It is widely used by hydrogeologists and geochemists to display the major ion composition of a water sample. A polygonal shape is created from four parallel horizontal axes extending on either side of a vertical zero axis. Cations are plotted in milliequivalents per liter on the left side of the zero axis, one to each horizontal axis, and anions are plotted on the right side. Stiff patterns are useful in making a rapid visual comparison between water from different sources.

Stiff diagrams can be used:

1) to help visualize ionically related waters from which a flow path can be determined, or;

2) if the flow path is known, to show how the ionic composition of a water body changes over space and/or time.

The Langelier Saturation index (LSI) is an equilibrium model derived from the theoretical concept of saturation and provides an indicator of the degree of saturation of water with respect to calcium carbonate. It can be shown that the Langelier saturation index (LSI) approximates the base 10 logarithm of the calcite saturation level. The Langelier saturation level approaches the concept of saturation using pH as a main variable.

LSI<0 Water is undersaturated with respect to calcium carbonate. Undersaturated water has a tendency to remove existing calcium carbonate protective coatings in pipelines and equipment.

LSI-0 Water is considered to be neutral. Neither scale-forming nor scale removing.

LSI>0 Water is supersaturated with respect to calcium carbonate ($CaCO_3$) and scale forming may occur.

The Ryznar Stability Index (RSI) is an empirical method for predicting scaling tendencies of water based on a study of operating results with water of various saturation index. This index is often used in combination with the Langelier index to improve the accuracy of predicting the scaling tendencies of a water. The criteria used for the RSI is:

RSI <5.5 Heavy Scale Tendency.

RSI 5.5-6.2 Scale Tendency.

RSI 6.2-6.8 Equilibrium.

RSI 6.8-8.5 Significantly Agresive Tendency.

RSI 8.5-9 Strongly Agresive Tendency.

RSI >9 Very Strongly Agresive Tendency.

Puckorius Scaling Index (PSI) Other indices do not account for two other critical parameters: the buffering capacity of the water, and the maximum quantity of precipitate that can form in bringing water to equilibrium. The PSI attempts to quantify the relationship between saturation state and scale formation by incorporating an estimate of buffering capacity of the water into the index. The PSI index is calculated in a manner similar to the Ryznar Stability Index. Puckorius uses an equilibrium pH rather than the actual system pH to account for the buffering effects:

PSI 6.5 Corrosive Tendency.

PSI 4.5-6.5 Optimum Range.

PSI <4.5 Scaling Tendency.

Research methods

Scaling Tendency for Fracturing Water (well A-411), pH sensitivity

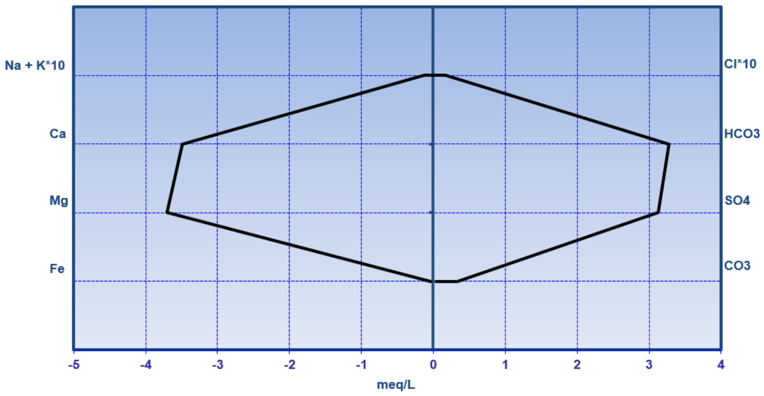

Figure 65 – Stiff diagram

Figures 65, 66 comparison of Fracturing water as per lab test (pH= 7.26, Conductivity=10000 mcS/sm) versus Hypothetical Fracturing Water (pH=8, Conductivity = 1000 mcS/sm), both waters are given ion concentrations as per lab test.

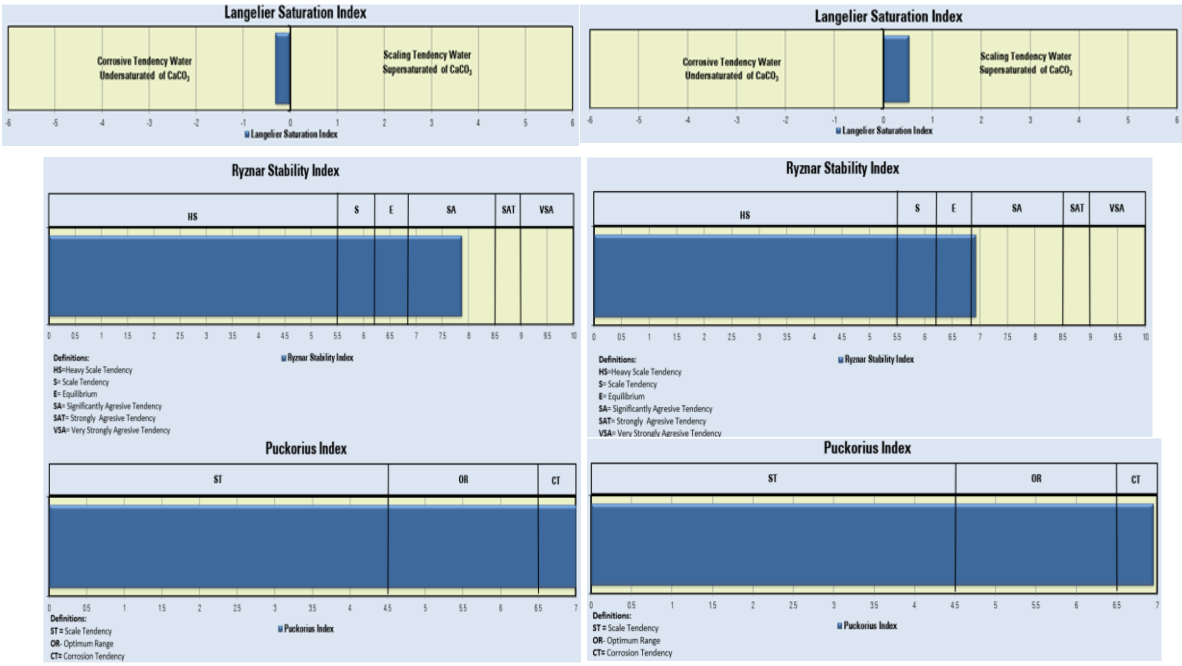

Figure 66 – Scaling Tendency for Injection Water (well A-59), pH sensitivity

Comparison of Injection water as per lab test (pH= 5.38, Conductivity = 70000 mcS/sm) versus Hypothetical Injection Water (pH=6, Conductivity = 70000 mcS/sm), both waters are given ion concentrations as per lab test (figure 67) (refer to 3.1).

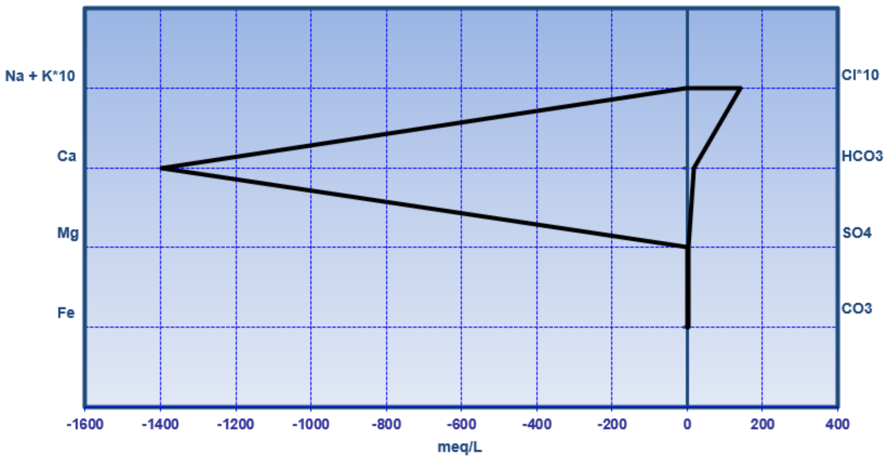

Figure 67 – Stiff diagram

Note – the plot above doesn't illustrate Na+K ions, because these ions are not quantified by the water analysis kits used in this study. However, Na+K ions were taken into account during simulation of scaling tendency (P-T thermobaric diagrams below) using the SUBSOIL USER water analysis data, and simulator's equilibrium concentration calculations.

Puckorius Index for both cases is minus 0.4 (Scaling Tendency), (figure 68).

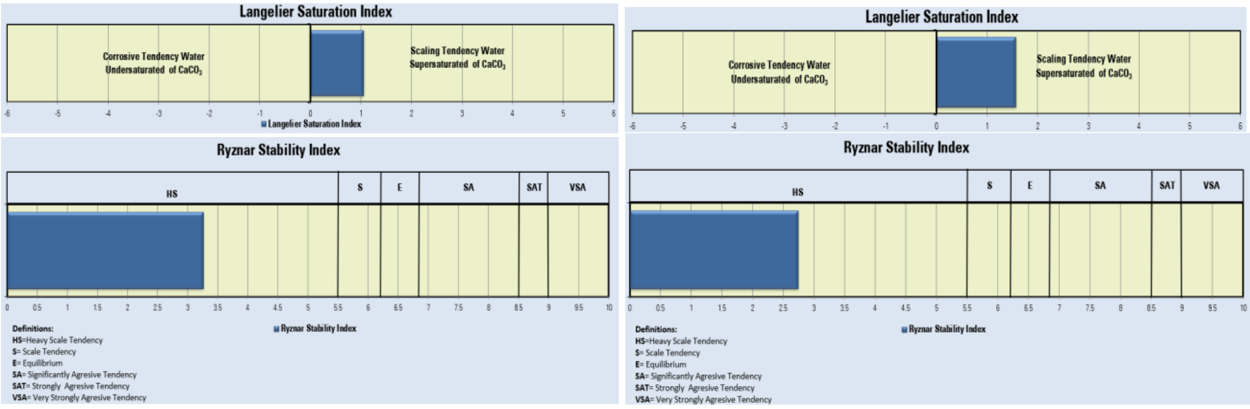

Figure 68 – Scaling Tendency for Reservoir Water (wells 57, 121, 107, 229 and previous tests), Temperature sensitivity

Note – the plot above doesn't illustrate Na+K ions, because these ions are not quantified by the water analysis kits used in this study. However, Na+K ions were taken into account during simulation of scaling tendency (P-T thermobaric diagrams below) using the SUBSOIL USER water analysis data, and simulator's equilibrium concentration calculations

Sensitivity of the averaged Reservoir water composed from lab tests in wells 57, 121, 107, 229 (pH= 5.95, Conductivity = 70000 mcS/sm) and previous tests to the temperature: 25ºC versus 80ºC. The worst cases for each ions were taken, from the pool of lab tests (wells 57, 121, 107, 229) and existing lab tests (figures 69, 70).

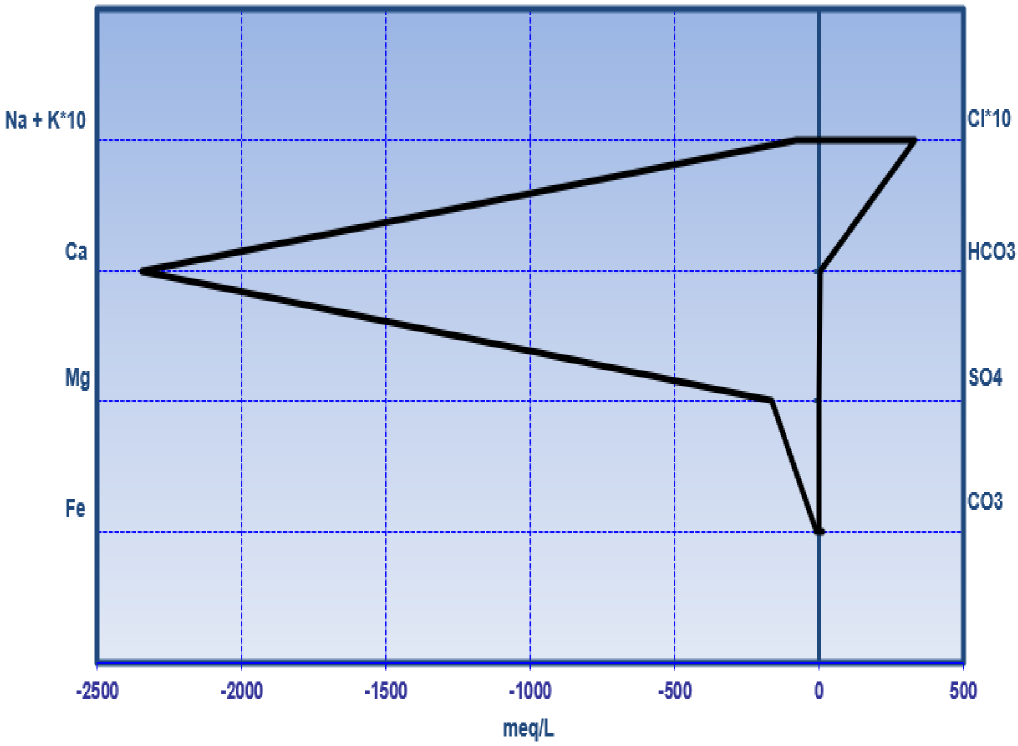

Figure 69 – Stiff diagram

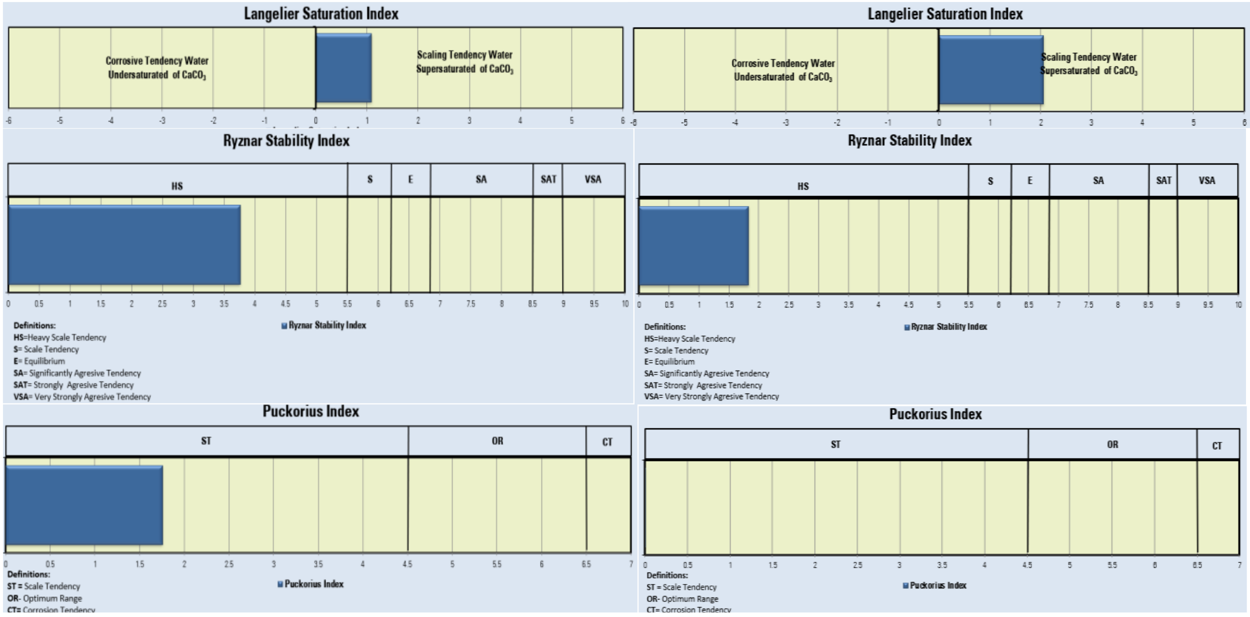

Figure 70 – Scaling Tendency

Puckorius Index for heated case is minus 0.2 (Scaling Tendency)

Important Note: Presence of CO_2 as a factor favouring corrosion

The analysis above deals with surface water.

However, it is known that CO_2 present in product from the given reservoir. The information below provides a view on how CO2 may affect the water corrosion properties.

When CO2 is dissolved in water it is partly hydrated and forms carbonic acid. When the steel corrodes in carbonic acid, Fe2+ and an equivalent amount of alkalinity are released in the corrosion process, forming an iron carbonate. When solid $FeCO_3$ is formed at the same rate as the steel corrodes, the pH becomes constant in the corroding system. Once the film is formed, it will remain protective at a much lower supersaturation.

The temperature strongly influences the CO_2 corrosion due to its effect on the rate of iron carbonate formation (figure 71). At low temperatures, corrosion rates increase because of high solubility of the $FeCO_3$ film. As temperatures increase (around 60-80°C) the iron carbonate layer becomes more adherent to the metal surface and more protective in nature resulting in a decrease of the corrosion rate. It is illustrated on the plot below: Calculated corrosion rates as a function of temperature at 0.5, 2 and 5 bar CO_2 partial pressure and pH 4 and 5.5 respectively (after Dugstad, Schmitt). Conclusion from this plot is that maximum corrosion rate is expected at the depths where the CO_2 – enriched fluid has temperature 40-90°C; and at the bottomhole, where temperature is above 100°C, the corrosion may be less severe due to stronger affinity of the iron carbonate film to the steel surface [40-42].

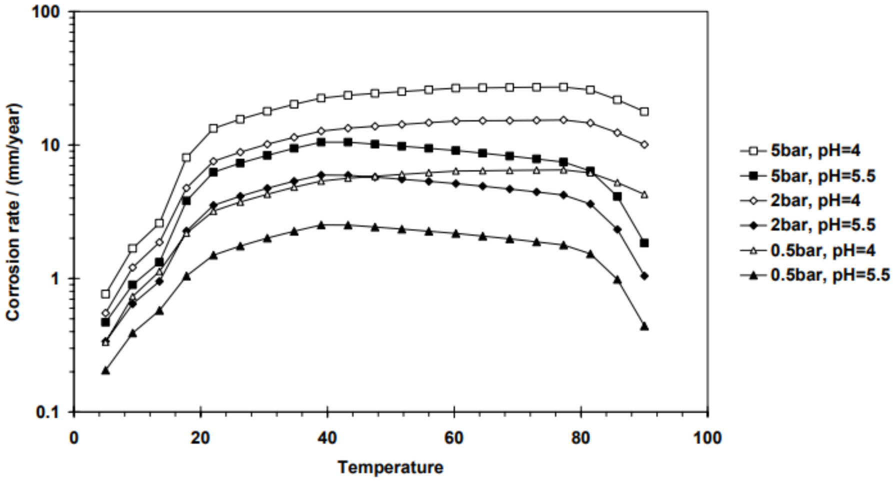

Figure 71 – Stronger affinity of the iron

Furthermore, in flow systems corrosion films obviously can grow for months without giving protection unless the steel is exposed to stagnant or "wet" conditions. During a few days stagnation, corrosion products can accumulate on the steel surface and form protective films. Thus, the kinetics of $FeCO_3$ precipitation seems to be a controlling factor for the protectiveness of the corrosion product layer. Above the critical flow intensity the interaction between the fluid and the wall becomes so intense that protective films or scales are destructed by near-wall turbulence elements which also prevent re-formation of the protective film (Schmitt et al.). On the other hand, Cations such as Ca2+ and Mg2+ react with carbonic acid and deposit calcium and magnesium carbonates. This codeposition of earth alkali and iron carbonates enhances the scale formation and, hence, reduces the corrosion rates. However, this additional inhibition may not be sufficient for the flowing conditions in the corrosion-prone temperatures.

To conclude, the presence of CO_2 significantly affects the corrosion risks for the given water, provided that the following parameters are met:

– partial pressure of CO_2 in the fluid is above 0.5 bar. Note that in certain conditions, there may be an upper threshold for partial pressure of CO_2, above which the corrosion tendency decreases;

– temperature range 40-90°C;

– flowing conditions, i.e. there was no static period for the fluid containing CO_2.

For the following plots and analysis, the P-T (Pressure-Temperature, or Thermobaric) diagrams are used, with changing concentration of scales shown in colour (figure 72). The P-T diagrams are effective tools for analysis of the scaling mechanisms, because the scaling process is not always directly dependant on pressure and temperatures. Moreover, some scale may exhibit the change of dependency after certain temperatures from direct to reverse. The software used for analysis of these complex processes is the OLI studio plug-in responsible for the scale analysis for oil/gas, and water wells.

Pressure and Temperature influence on the $FeCO_3$ Scales for Reservoir Water (well 59) (figure 73).

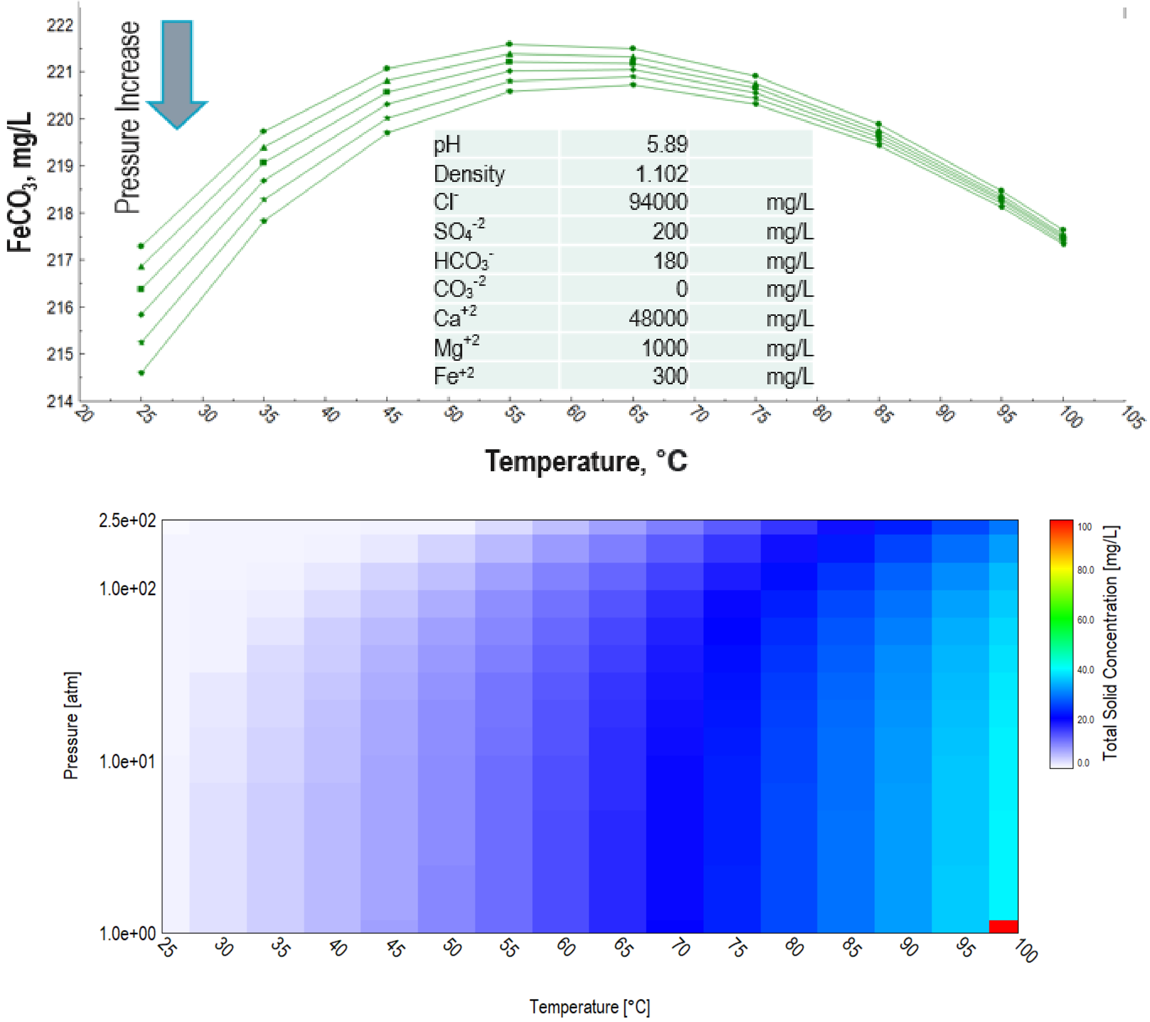

Figure 72 – Thermobaric Diagram of Scaling Tendency for Fracturing Water (well A-411)

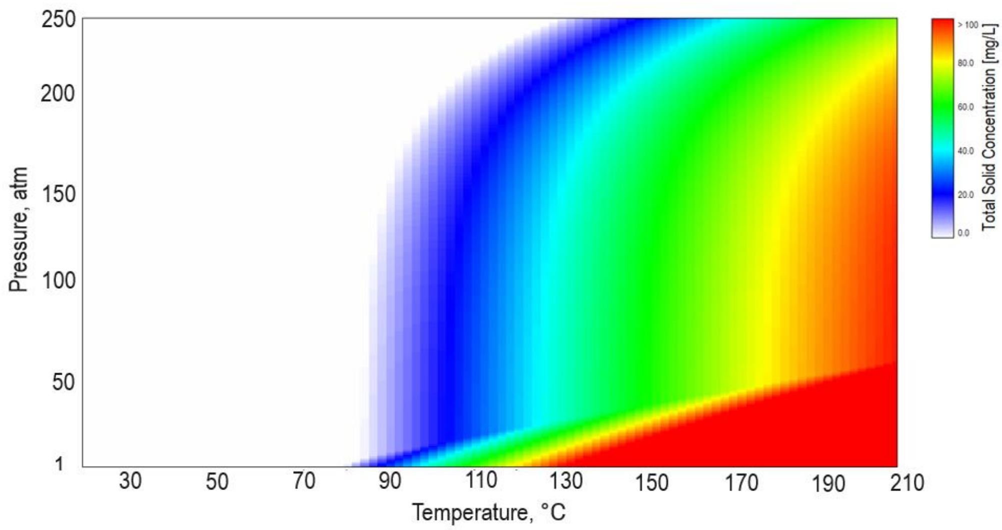

Figure 73 – Thermobaric Diagram of Scaling Tendency for Injection Water (well A-59)

If different types of salty water re mixed, scaling behavior may significantly change (figure 74). This change depends on the ratio of the fluids in the mixture. On the figures 75, 76, 77, 78, 79 below the influence of such mixtures is analyzed.

Injection (A-59) to Reservoir (A-57) water ratio sensitivity

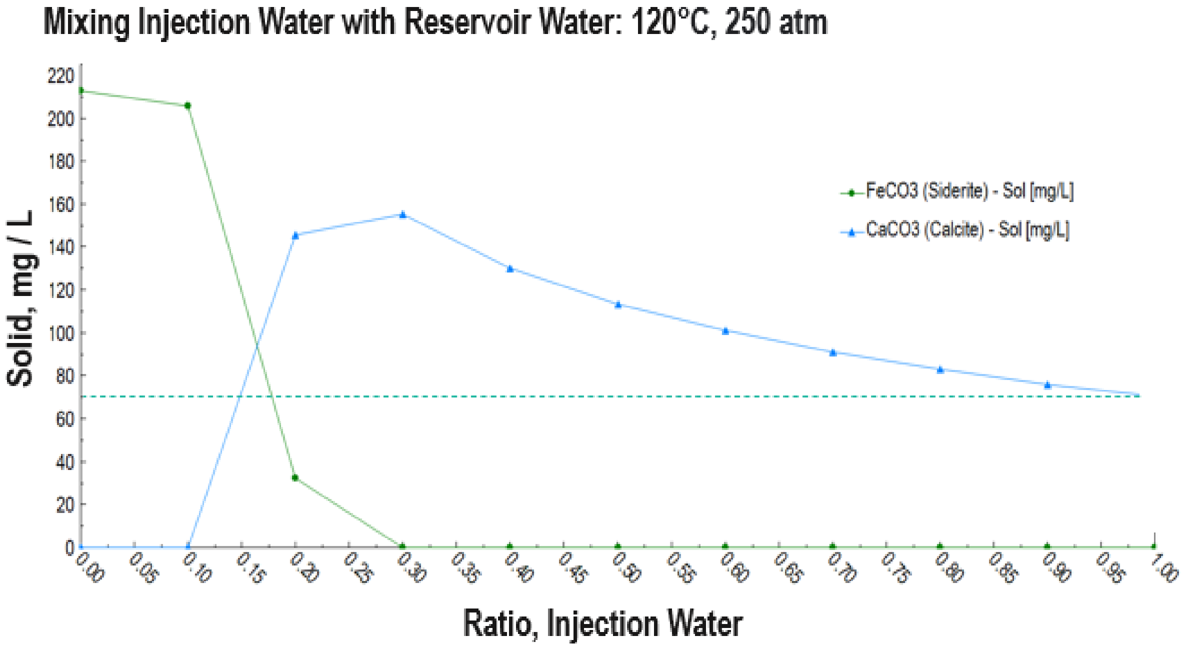

Figure 74 – Mixed Water Conditions

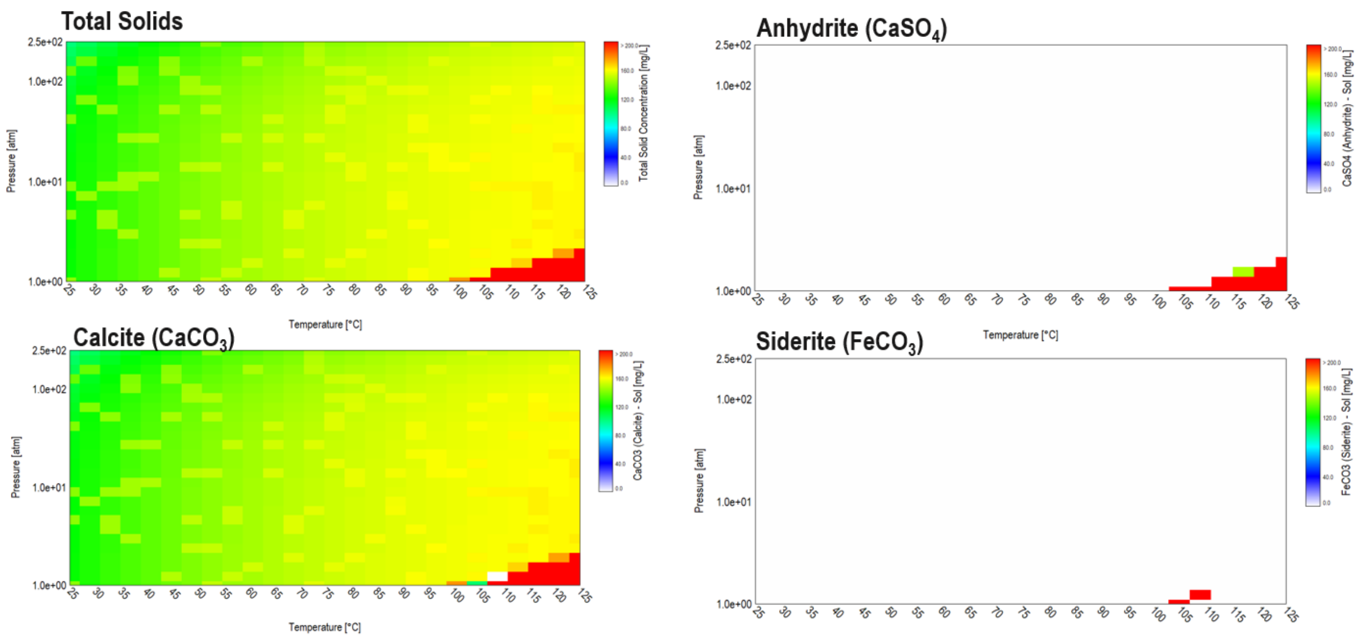

Figure 75 – 30% Injection (A-59) + 70% Reservoir (A-57)

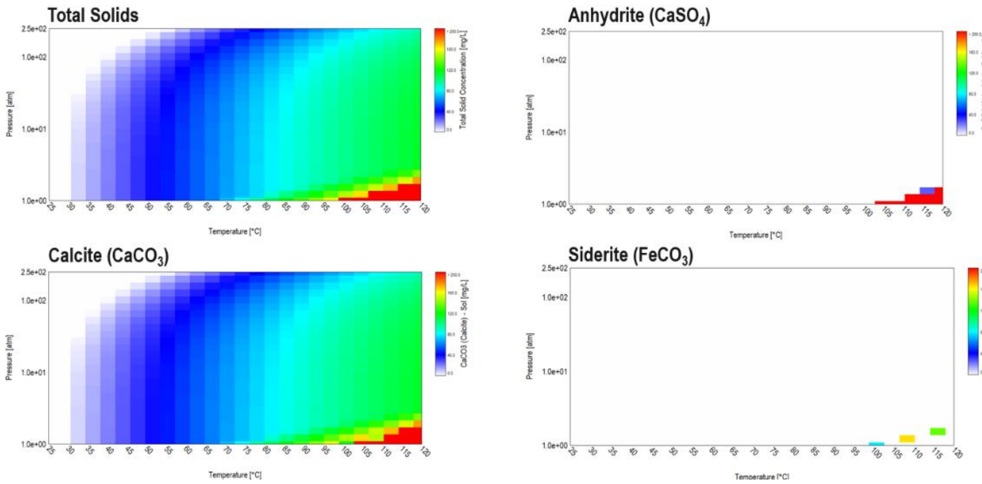

Figure 76 – 50% Injection (A-59) + 50% Reservoir (A-57)

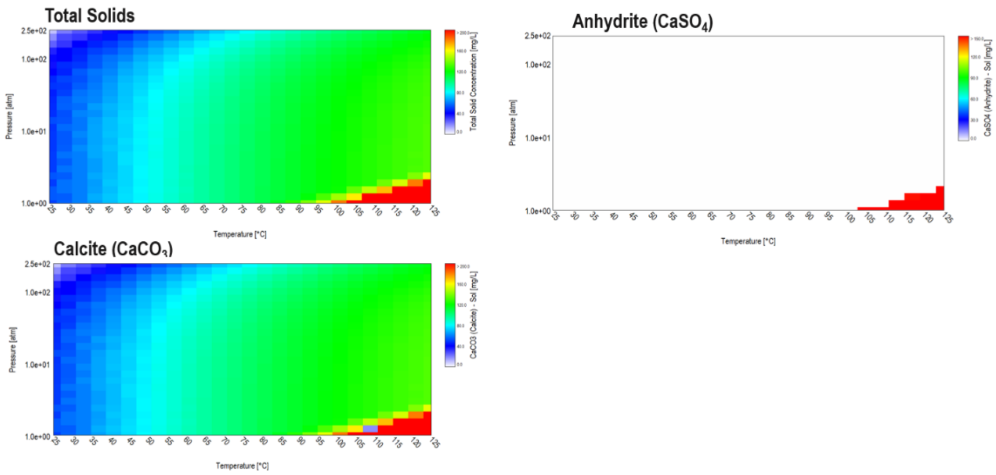

Figure 77 – 70% Injection (A-59) + 30% Reservoir (A-57)

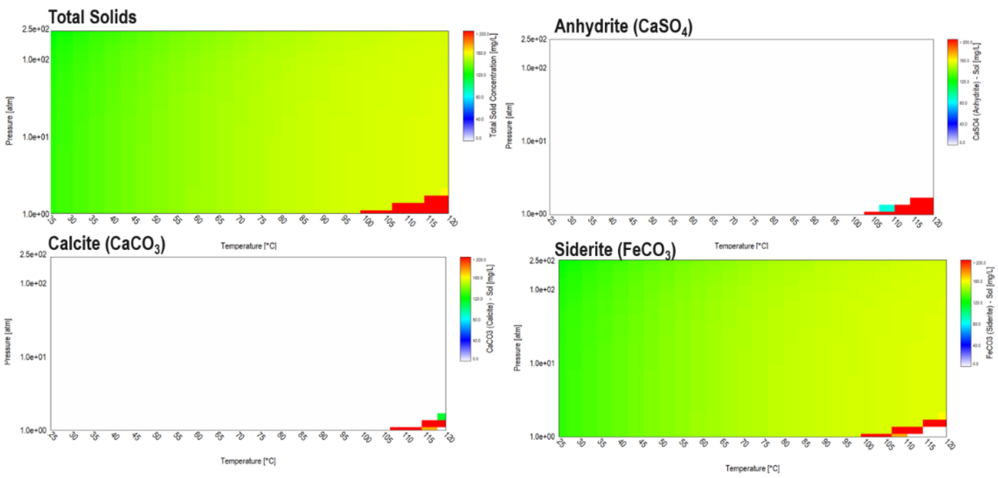

Figure 78 – 50% Fracturing Water (A-411) + 50% Reservoir (A-57)

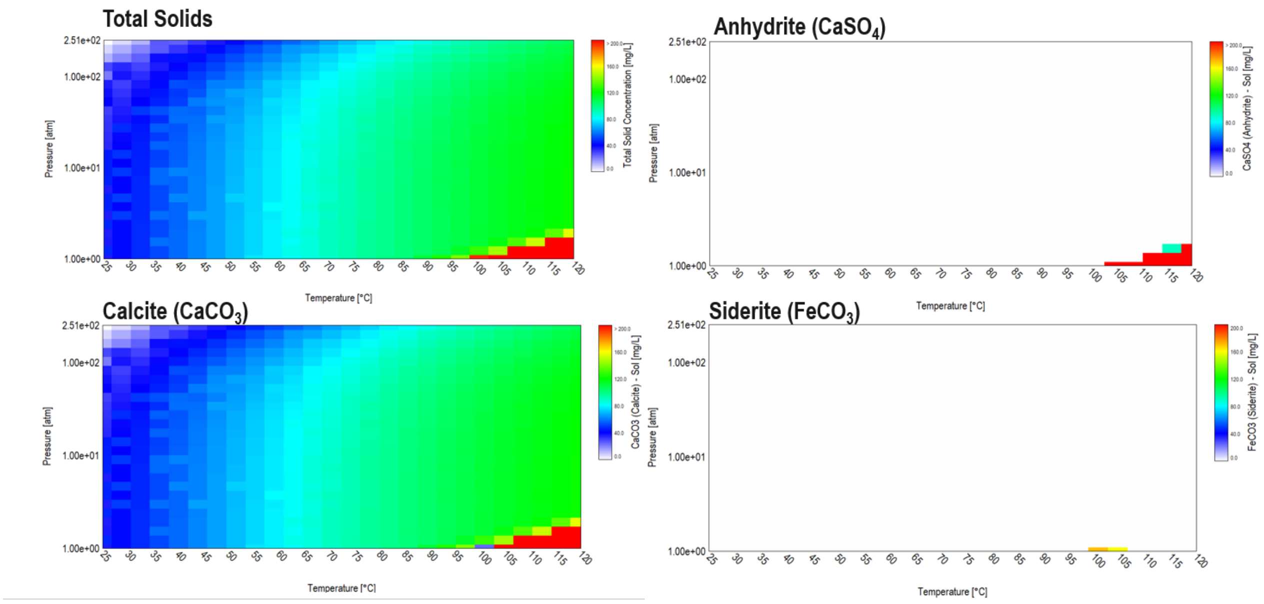

Figure 79 – 20% Fracturing Water (A-411) + 40% Reservoir (A-57) + 40% Injection (A-59)

Analysis of the water pre-heating as a scale control method

If Injection Water (well A-59) is preliminary heated to 90°C, followed by solids (133 mg/L) separation, the following scale tendency is projected for a mixture of 50-50% Injection Water (A-59) and Reservoir Water (A-57) for 120°C, 250 atm (figure 80).

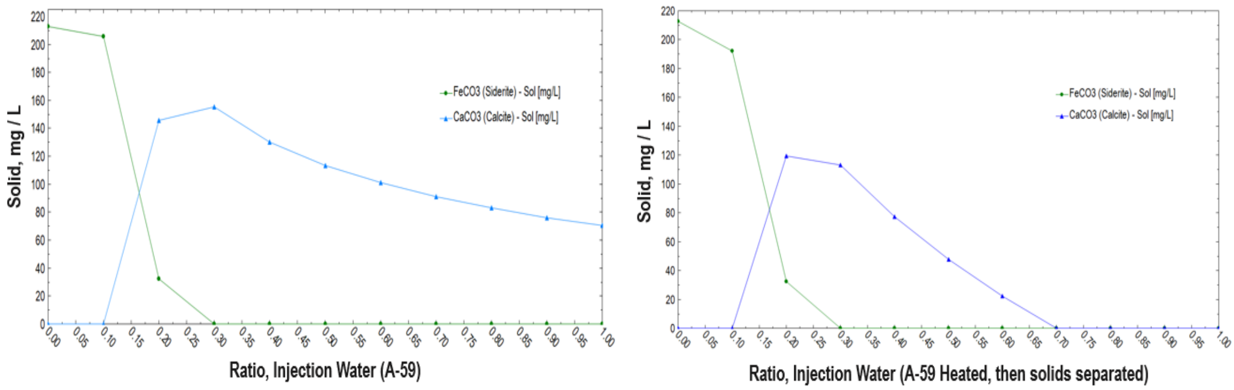

Figure 80 – Injection Water (A-59) and Reservoir Water (A-57) for 120°C

The following change in thermobaric charts is expected after pre-heating of a mixture of 50-50% Injection Water (A-59) and Reservoir Water (A-57) (figure 81).

Analysis of the water pH change as a scale control method

If Injection Water (well A-59) is preliminary subjected to pH increase, followed by solids separation, the following scale tendency is projected for a mixture of 50%-50% Injection Water (A-59) and Reservoir Water (A-57) for 120°C, 250 atm.

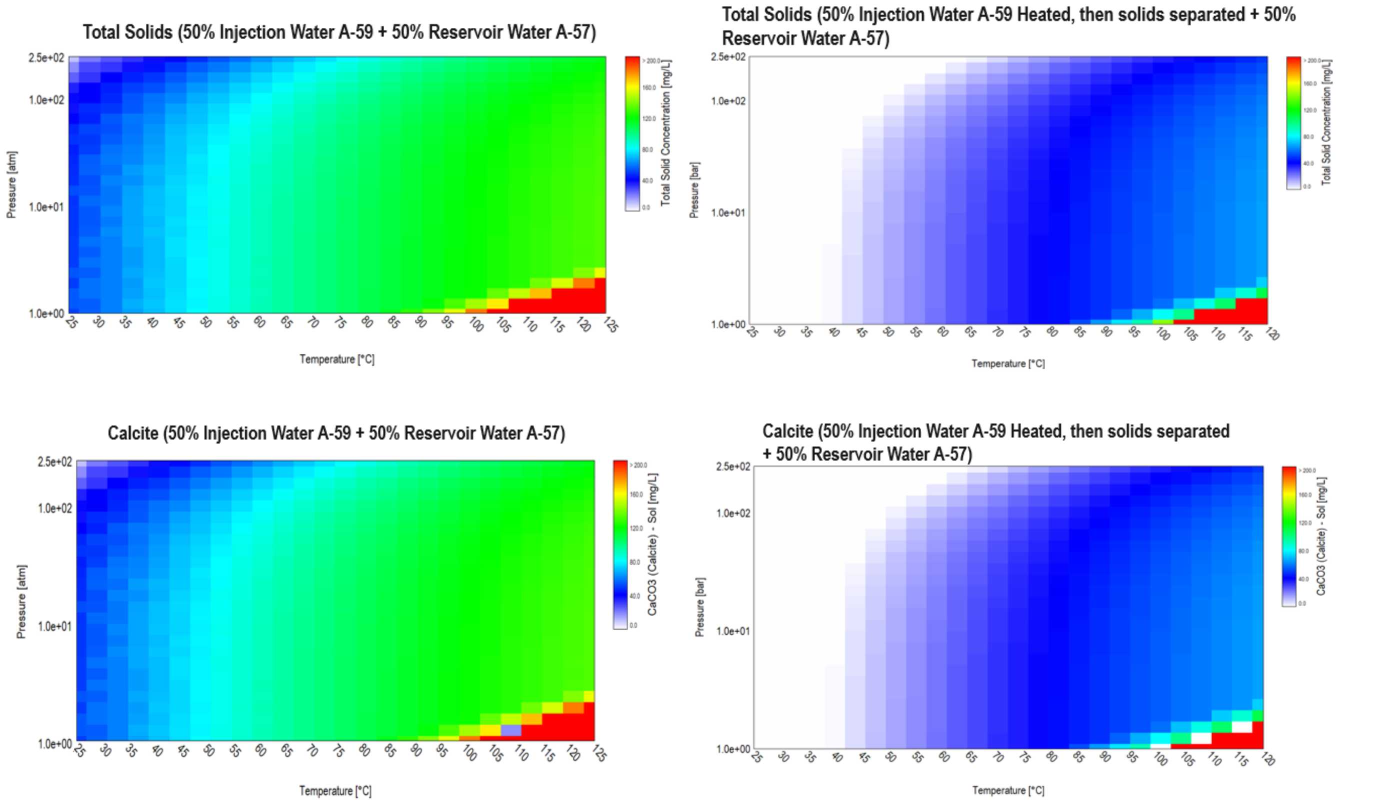

Figure 81 – 50-50% Injection Water (A-59) and Reservoir Water (A-57)

Analysis of the injection water source change as scale control method.

If Injection Water (well A-59) is changed to a water with less concentration of ions, the comparison between these two scenarios will be as following (note the ions concentration table) (figure 82).

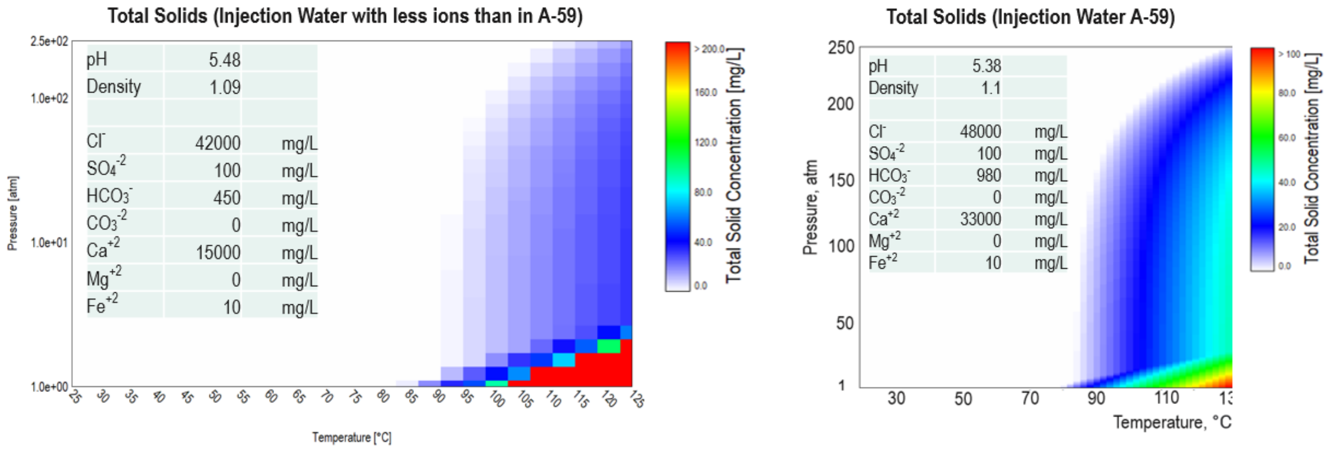

Figure 82 – Water source change

If Injection Water with less ions is mixed 50-50% with Reservoir Water (A-57), then for 120°C, 250 atm the following plot is expected (figure 83).

The following change in thermobaric charts is expected if water from well A-59 is changed to Injection water with less ions in a *50%-50% mixture with* Reservoir Water (A-57).

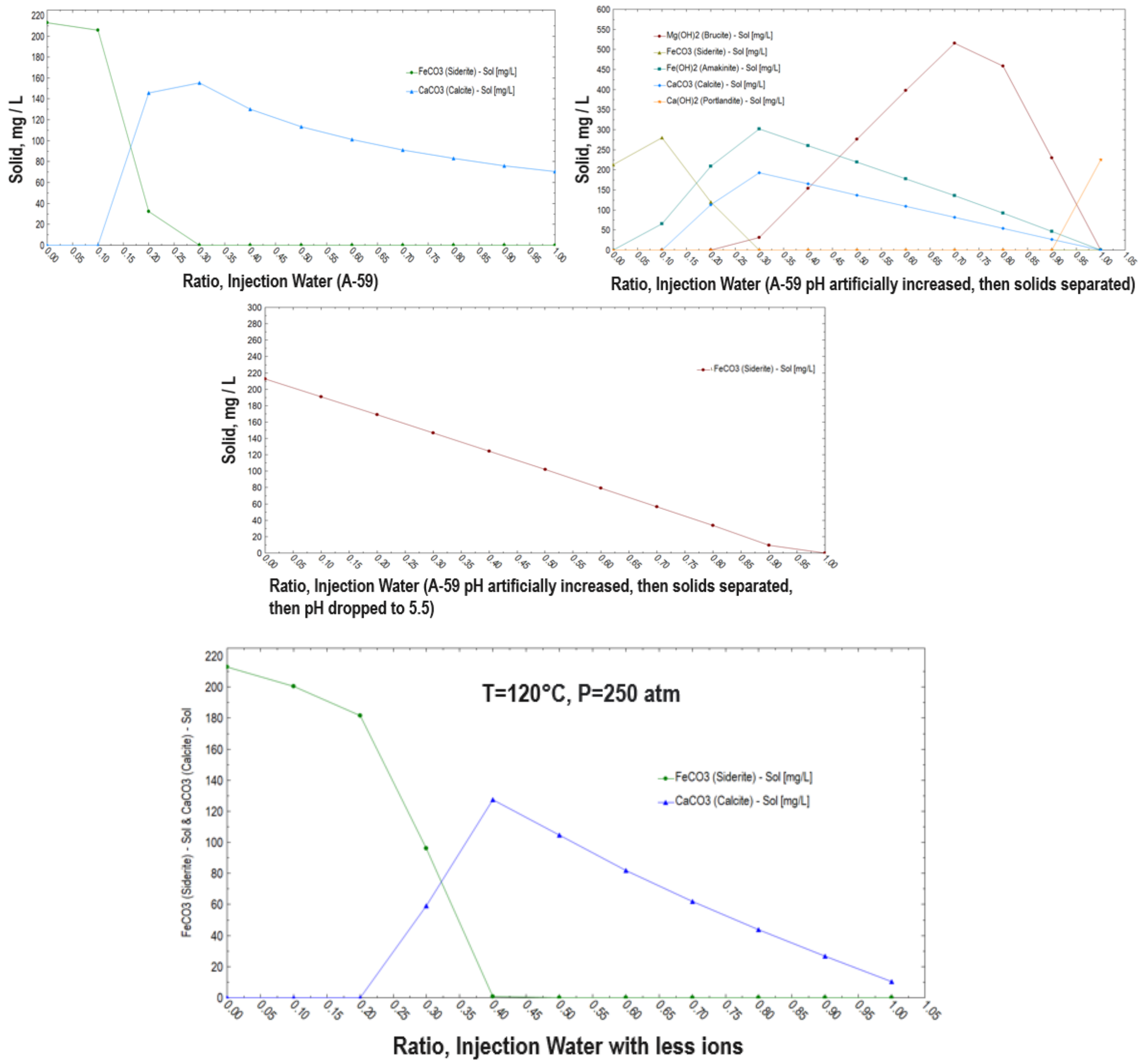

Figure 83 – Ratio injection water

Application of the results to the Field conditions.

In order to translate scale study results into the real injector well conditions, the Kinetix Matrix simulator was used.

Kinetix Matrix, a plug-in of Techlog, is the latest generation of the wellbore matrix treatment simulators. It models more than 100 acids, chelating agents, brines, solvents and other fluids reaction with rocks of different lithology. For carbonate rocks it is capable of calculating the wormholing regime based on the advanced theories (Tardy et al. An Experimentally Validated Wormhole Model for Self-Diverting and Conventional Acids in Carbonate Rocks Under Radial Flow Conditions, Panga et al. A New Model for Predicting Wormhole Structure and Formation in Acid Stimulation of Carbonates). For sandstone rocks, it is capable of calculating the whole complexity of the clay, silicates and other minerals interaction with acids, accounting for primary, secondary and tertiary reactions (figure 84). The Kinetix Matrix is used for analysis of the acidizing, placement of scale squeezes, water control treatments, chemical sand control etc [43].

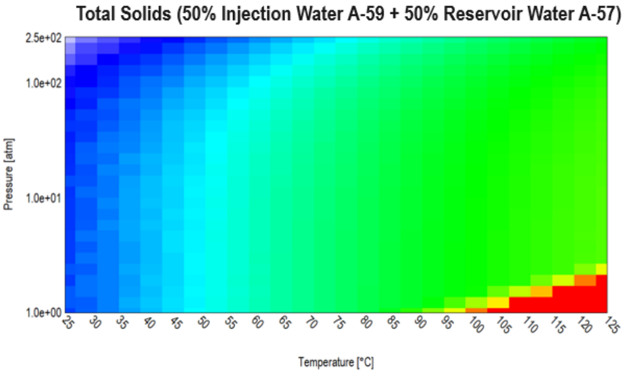

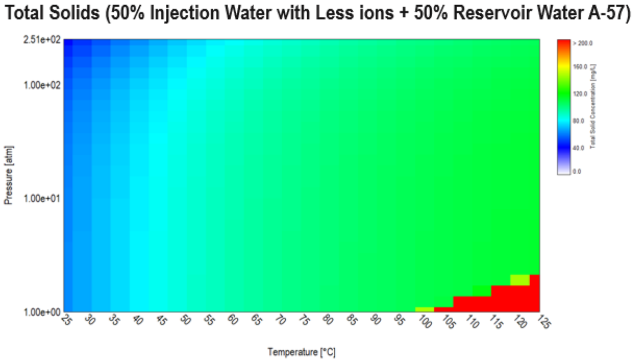

Figure 84 – Total solid

To analyze the potential damage of the permeability from scale tendencies defined in previous part of this report, the typical period of the water injection is selected. The period is limited by the given simulator's maximum stage volume. The advanced simulator Kinetix Matrix used for this study allows calculation of 1800 m^3 of fluid injection.

Fluid front movement

1800 m^3 of fluid can be distributed as 15 days of injection with the rate 120 m^3/d. Table 5, below shows typical injector well with lower permeability conditions for Arystanovskoye.

Table 5 – Typical injector well with lower permeability conditions for Arystanovskoye

Zone	Perm, mD	Porosity, %	Reservoir pressure, kPa	Top TVD, m	H, m
Shaly	0.5	5	110000	3015	9
Net pay	4	9	100000	3024	17
Shaly	0.5	5	110000	3041	9

By running a schedule of 15 days injection at 120 m^3/d into the reservoir model shown in table above, the following penetration plot can be expected (figure 85).

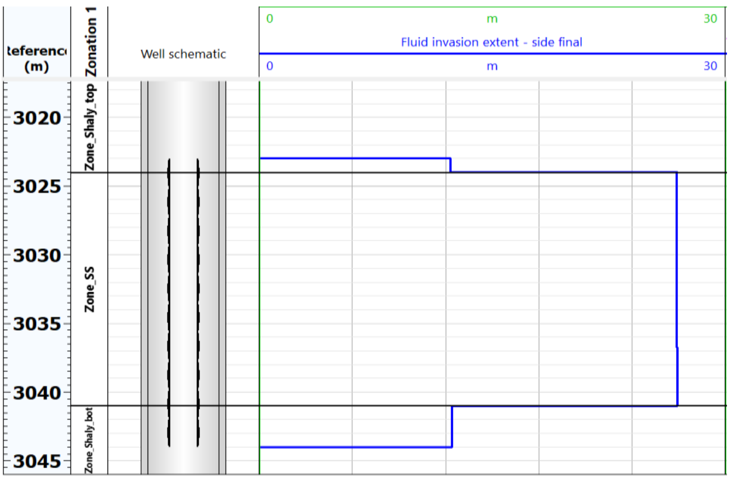

Figure 85 – Penetration plot

The same 1800 m^3 of fluid can be distributed as 9 days of injection with the rate 200 m^3/d into the higher permeability reservoir. Table 6, below shows typical injector well with higher permeability conditions for Arystanovskoye.

Table 6 – Typical injector well with higher permeability conditions for Arystanovskoye

Zone	Perm, mD	Porosity, %	Reservoir pressure, kPa	Top TVD, m	H, m
Shaly	0.5	5	110000	3015	10
Net pay	10	11	100000	3025	7
Shaly	0.5	5	110000	3032	10

By running a schedule of 9 days injection at 200 m^3/d into the reservoir model shown in table above, the following penetration plot can be expected (figure 86).

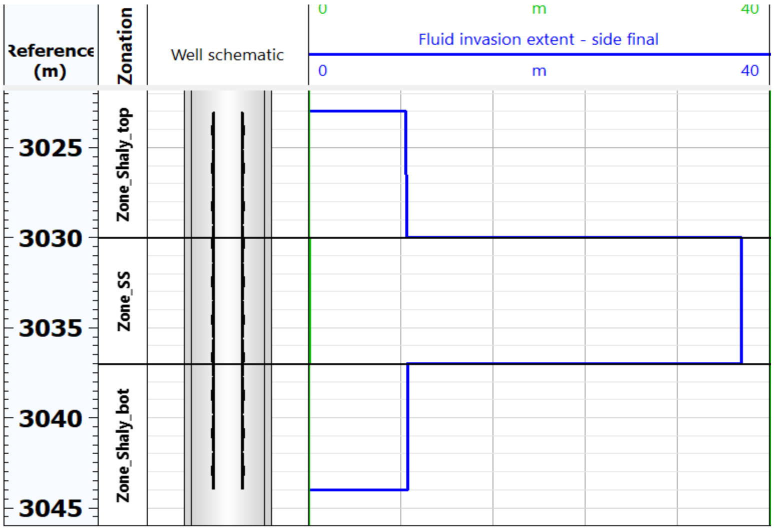

Figure 86 – Penetration plot

The fluid fronts above can be used to predict the scales tendency as per plot shown in 4.8.1 at any given point of time. For example, in a lower permeability injector, after 15 days of injection with rate 120 m^3/d, the formation of the ferrous carbonate is possible at the radius 28-30 m away from the wellbore (where the injection water to reservoir ratio is smaller), and the most pronounced calcium carbonate scaling is expected at 20-25 meter away from the wellbore. This analysis contains uncertainty because exact mixture of fluid is not known, however it gives some sense of where the main scaling activity is happening at a given point of time.

Quantitative analysis of the scales effect during injection

From the total solids plot shown in 4.8.4, which describes the closer-to-the-wellbore region, the maximum amount of scales expected to be within 70 to 120 mg/l (dotted circle on the plot below). The same amount of scales may be formed once reservoir pressure drops by 100-120 atm (figure 87) [44, 45].

The above-mentioned scales concentration, multiplied by monthly volume 3600 m^3 of water injected, yields in 250 to 430 kg of potential scales distributed in the whole pore volume invaded during injection of the given 3600 m^3.

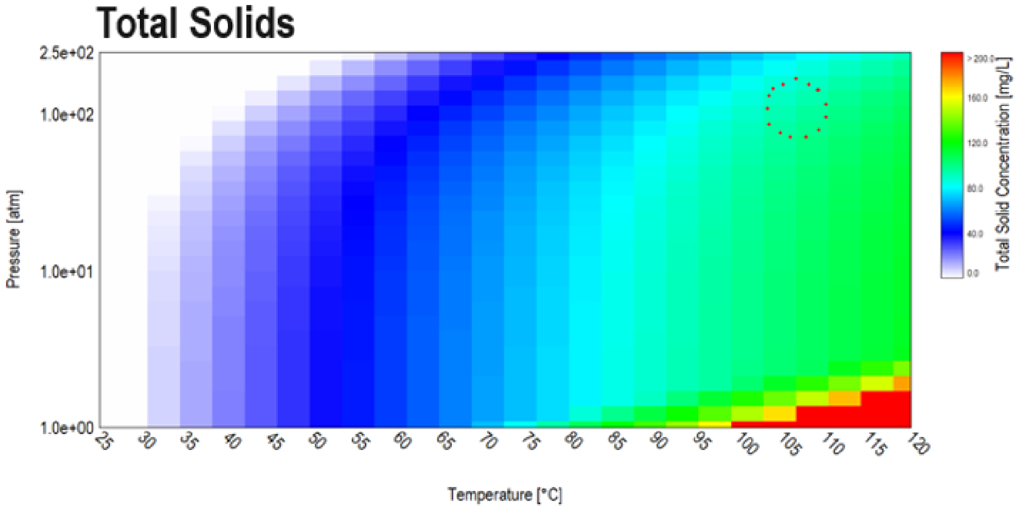

Figure 87 – Total solid

To simulate this volume of potential scale, the digital model of the injection water was created, with CaCl2, NaCl, KCl salts introduced into the solution. The salts concentration was adjusted to yield about 1000 kg of salts in total for 10 m^3 of solution. The pumping of this solution was then simulated on the model of the typical injector well with lower permeability conditions for Arystanovskoye (table shown above).

The pumping schedule assumed injection of long fresh water preflush stage for 600 min, then pumping 10 m^3 of salts solution, followed by the flush stage with regular water, all stages pumped at 120 m^3/d rate.

The software output was the skin evolution, and the calculated output is the apparent permeability decrease at the fluid front. Important assumption is that all scale is forming within the timeframe of salty brine solution downhole stage (10 m^3 pumped in 120 min).

The following are the observations from the simulations.

Well skin increase from 1 to 4 when pumping fluid with scale potential of up to 420 kg. Using the radial flow equation, and formation properties shown above in the table of lower permeability injector well, this skin increase is equivalent to permeability drop from 4 md to 2.8 md.

Refer to the figure 88 below.

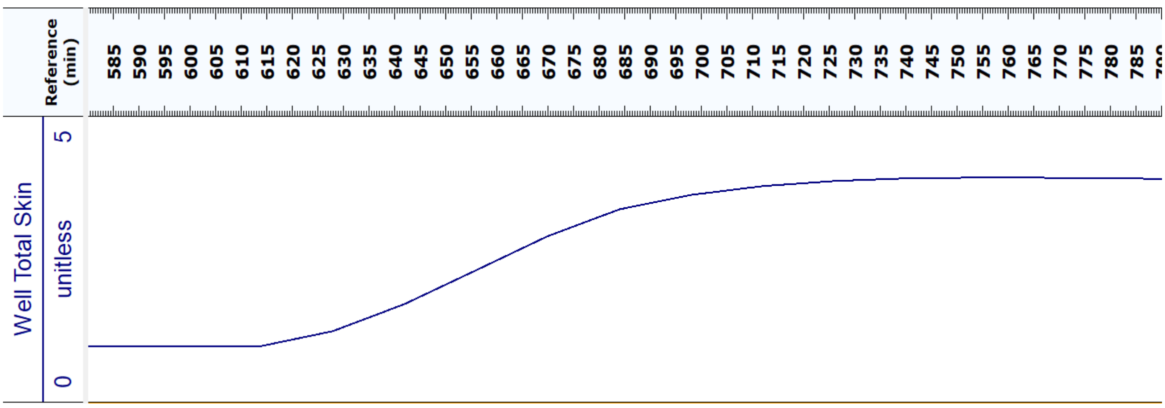

Figure 88 – Formation properties

When the scale inhibition is introduced into the simulation, via decrease of scale-prone ions content, the skin increase from 1 to 1.05 only: this is equivalent to permeability decrease from 4 md to 3.96 md only (figure 89).

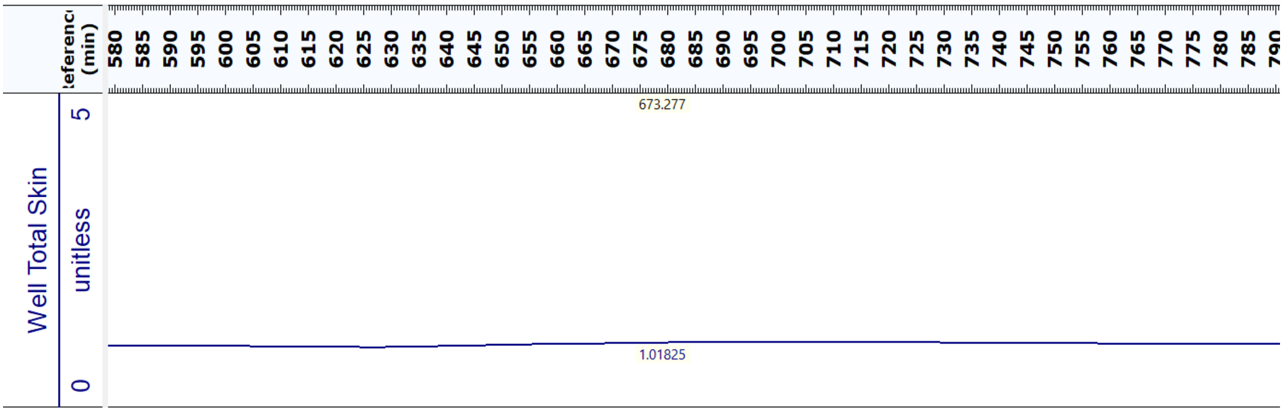

Figure 89 – Quantitative analysis of the scales effect during production

If we consider the condition of ESP work, when pressure can be as low as 20 to 30 atm, the temperature increase to 130 degC, the scaling severity can be as high as 20 mg/L of produced reservoir water (figure 90). Assuming 15 m^3 of produced water per day, the expected scaling potential can be as high as 300 gr of scales per day, distributed along the whole fluid path where fluid experience the pressure drop: in the near-wellbore reservoir zone, wellbore itself, inside the pump, and inside the upward moving fluid stream.

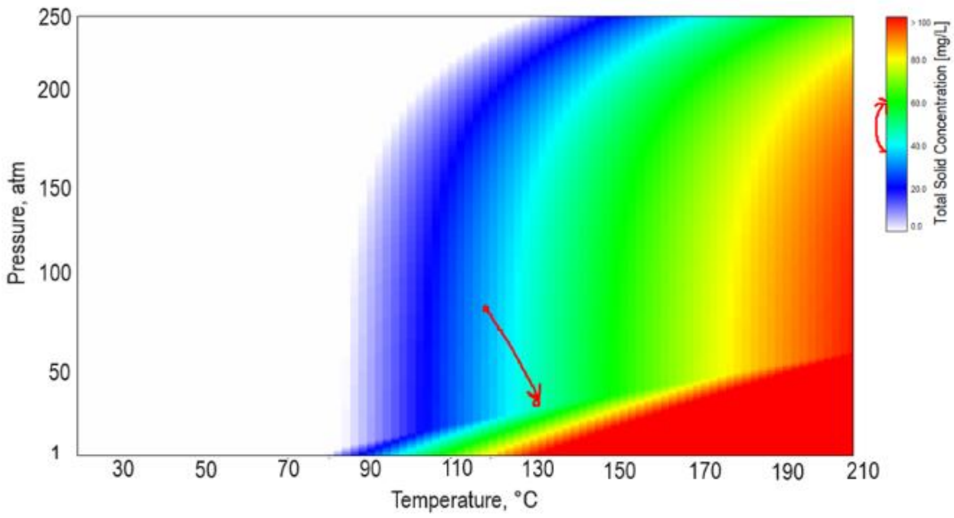

Figure 90 – Scale inhibition strategy

Considering significant amount of scale which may be formed during injection, and production, the use of scale squeezes is recommended. There is a wide variety of the scale inhibitors are available. Plot below shows comparison of two potential solutions: standard DTPMP (diethylenetriamine penta [methylene phosphonic acid]) inhibitor and more robust L076 inhibitor, intended to expend life of ESP pumps, and extend time between interventions.

The dotted lines on the figure 91 below is the minimum effective inhibitor concentration which is required for inhibitor to work. It can be seen that the time to reach minimum effective concentration can be extended by 2-2.5 times by selecting a proper inhibitor.

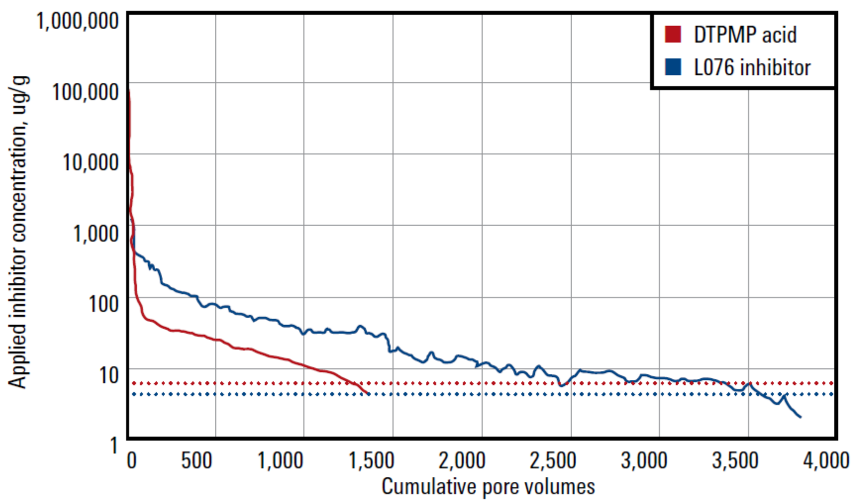

Figure 91 – Inhibitor concentration

The temperature range of the inhibitor shown on the plot is 24 to 190 degC. Note that it doesn't mean that inhibitor will lose the efficiency for the conditions when downhole pumps are heated above 190 degC: inhibitor will be effective because it works as a adsorbed substance inside the source of the scales - reservoir itself - where the temperature will not exceed the above mentioned range.

Inhibitor introduction into reservoir can be performed in the following ways:

– separate inhibitor Squeeze, when the well is stopped, and inhibitor solution is injected via bullheading, at matrix rates. Scale squeeze volume may vary and depends on the desired radius of penetration and concentration of the inhibitor;

– inhibitor added into the fracturing water. In the presence of temperature (> 175degF) or Ca2+ (< 1500 ppm), the fracturing fluid-compatible inhibitor precipitates as a glaze, and "plates" onto the reservoir and/or proppant pack. This glaze is insoluble in oil and gas and is sparingly soluble in produced water. As water flows into and through the fracture, the "plated" polymer is slowly solubilized into the water. It inhibits the scale crystallization process by poisoning the crystal deposition sites. This is a suitable and cost-effective solution because inhibitor may chelate the Ca and Mg ions contained in fracturing water. At the same time, inhibitor will penetrate the hydraulic fracture wall with the leakoff. The inhibitor may be added into the injection test fluid, or the main crosslinked gel, providing the gel is crosslinked with borate [46].

Conclusions on the 4st section

Fracturing related scaling conclusions:

– currently used fracturing water is close to neutral at the standard conditions. At temperatures and pressures expected during the fracturing treatment (from pumping to cleanup), the maximum concentration of potential scales should not exceed 20 mg/l;

– Introduction of fracturing water into the reservoir water layers or into the injection+reservoir water layers doesn't result in increase of the scaling tendency.

Long-term injection related scaling conclusions:

1. For the reservoir temperature of 115 degC, the given injection water per se may be source of scale once the reservoir pressure drops below 220 atm. Three regions of scaling exist: rapid scaling up from 0 mg/l to 20 mg/l within 220-190 atm window, then slow scaling from 20 to 40 mg/l within 190-30 atm window, then very fast scaling below 30 atm.

2. For temperatures below 80 degC, no scales are expected to form for injection water at any pressure

3. During injection, when Injected water is mixed with Reservoir water, the highest calcium carbonate scaling tendency is at the mid-distance from the wellbore (where Injected water to Reservoir water ration is within 20 to 40% window). At the far-distance, where injected water percent is very low, Calcium carbonate scale is unlikely to form. At the near-wellbore distance, calcium carbonate accumulation tendency is 2 times lower than at the mid-distance.

4. During injection, when Injected water is mixed with Reservoir water, the highest ferrous carbonate scaling tendency is at far-distance from the wellbore (where Injected water to Reservoir water ration is less than 20%). At the mid and near wellbore distance, no ferrous carbonate is formed.

Recommendations on scale control methods

Pre-heating of injected water with subsequent removal of the precipitated scale may decrease the tendency to the scaling. In the near-wellbore zone (ratio of injected to reservoir water = 0.7-1) the scaling risk may even be eliminated, but at the mid-distance (ratio of injected to reservoir water = 0.15-0.35) the scaling activity may drop only by 20-30%.

Increase of pH with subsequent removal of the precipitated scale has somewhat similar effect to temperature methods for Calcium carbonate. In the near-wellbore zone (ratio of injected to reservoir water = 0.95-1) the scaling risk may even be eliminated for Calcium carbonate, but at the mid-distance (ratio of injected to reservoir water = 0.15-0.35) the scaling activity for Calcium carbonate doesn't change. However, the highest risk in this approach is related to significant accumulation of $Mg(OH)_2$ in near-wellbore zone, and increasing tendency for ferrous carbonate scale in far zone. Further decrease of pH to 5-5.5 may positively affect the scaling tendencies, however without full elimination of the problem.

Change of water source to the one with two times less Calcite content, and 20% less Chlorine content, doesn't eliminate the scaling problem either, just mitigating not more than 20-30% of scale volume for certain P-T range.

Taking into account the three recommendations above, the most effective strategy for scale control would be either use of water with significantly less ion concentration (close to the Fracturing water one), or use of periodic scale inhibitor treatments [47, 48].

In case scale inhibition treatment is selected, the Scale Inhibitor type, concentration and treatment frequency should be modeled. Scale inhibitor treatment can be performed as a standalone bullhead job, or as part of fracturing job. Scale

Inhibitor retention in the formation and slow desorption and dissolution allows partial protection against scaling. The injected water slowly dissolves the inhibitor precipitate, and the trace presence of inhibitor in the water slows the formation of scales. Scale inhibitors should be tolerant for Fe^{3+} up to 2,000-ppm in a Ca rich environment.

5 ADVANCED METHODS OF FRACTURE GEOMETRY ANALYSIS, AND FRACTURE PARAMETERS SENSITIVITY STUDY

Objective

Introduction of Advanced Methods of Fracture Geometry Analysis, and Fracture Parameters Sensitivity Study" is a second part of the Integrated laboratory, software and research study under the dissertation scope.

The Research and Scientific nature of this work is supported by the fact that Lagrangian approach-based Multiphysics hydraulic fracturing modelling software in combination with fracture height measurement techniques is a new approach to the production stimulation industry in Kazakhstan [49].

Multiphysics hydraulic fracturing modeling is a complex problem that requires the coupling of different physical processes, such as fluid flow, solid mechanics, and heat transfer. One approach to solve this problem is through the use of Lagrangian methods [50-52].

In Lagrangian methods, the domain is discretized into particles that move with the fluid flow. These particles carry information about the properties of the fluid and its interaction with the solid matrix. The Lagrangian approach is particularly well-suited to modeling hydraulic fracturing because it allows for the simulation of fracture propagation and the interaction of the fluid with the surrounding rock.

To model hydraulic fracturing using a Lagrangian approach, one typically starts by creating a three-dimensional mesh of the domain. This mesh is then populated with particles that represent the fluid and solid materials. The particles are assigned properties such as density, viscosity, and elasticity. The governing equations for fluid flow, solid mechanics, and heat transfer are then solved for each particle in the mesh.

The simulation typically starts with the injection of a fluid into the fracture. As the fluid flows through the fracture, it interacts with the surrounding rock, creating new fractures and propagating existing ones. The simulation continues until the fracture network has reached the desired extent or until the injection of the fluid is stopped.

One advantage of the Lagrangian approach is its ability to model the interaction of the fluid with the rock matrix. This interaction can be modeled using different approaches, such as the use of cohesive zone models or the implementation of damage models. Additionally, the Lagrangian approach can be used to simulate complex fracture networks, including non-planar fractures and branching fractures.

In summary, the Lagrangian approach is a powerful tool for modeling multiphysics hydraulic fracturing. It allows for the simulation of fluid flow, solid mechanics, and heat transfer, and is particularly well-suited to modeling fracture propagation and interaction of the fluid with the surrounding rock.

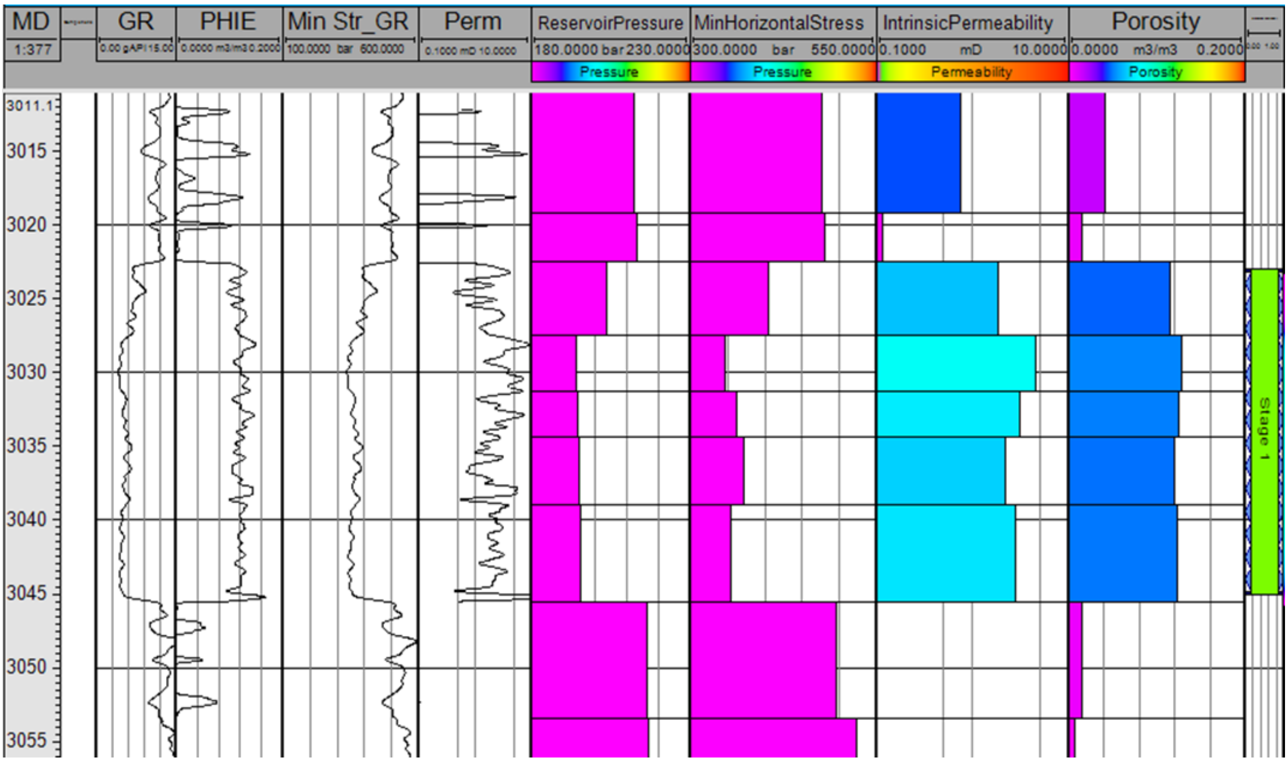

Figure 92 – Well A-210 Fracturing Job using Advanced Methods of Fracture Geometry Analysis

Based on the prepared well model (figure 92), the main hypothesis to check was: Do we correctly predict the Fracture geometry, and if no – how to optimize it?

5.1 Diagnostic tests analysis using Bottomhole Pressure Gauge data

Diagnostic tests determine the in-situ parameters critical to optimum fracture treatment design. Assumed or inaccurate parameter values can result in the following:

1. Reduced fracture penetration caused by pad fluid depletion.
2. Increased treatment cost because of excessive pad volume.

Diagnostic tests typically consist of two tests:

1. The closure test: it determines closure pressure, which is the minimum in-situ rock stress. Accurate determination of closure pressure is important because all fracture analysis is referenced from it.
2. The calibration test: it is an injection/shut-in/decline procedure. A viscosified fluid is pumped at proposed fracturing treatment rate. The well is then shut in and a pressure decline analysis is performed.

The following data can be obtained during on different stages of diagnostic tests analysis:

1. Pressure falloff after shut-in.

– fracture extension pressure, rate, and net pressure;
– fracture closure pressure;
– fluid efficiency and leakoff coefficient;
– dominant leakoff mechanism;
– matrix or natural fractures;

– variable storage.

2. After-closure analysis

– identification of reservoir transient flow regimes;

– reservoir pressure;

– reservoir flow capacity (kh/m) or permeability.

For this particular study on well A-210, the Diagnostic testing was improved by.

3. Introduction of the dynamic analysis (breakdown part of the injection tests and step-up/step-down part of the additional injection tests). The dynamic analysis helped to determine the following:

– breakdown pressure;

– fracture propagation pressure;

– friction analysis.

4. Use of downhole gauges to distinguish near-wellbore frictions and effects from the tubing effects and calibrate the tubing frictions data.

5. Use of temperature logging data after the calibration test to estimate the fracture dominating injection point and fracture height

Below is the technical interpretation of the tests.

Breakdown/Injection tests analysis

Injection Test 1: Surface data Breakdown pressure: 3290 psi at surface at 3.7 bpm. Fracture propagation pressure: 2106 psi at surface at 3.7 bpm (figure 93).

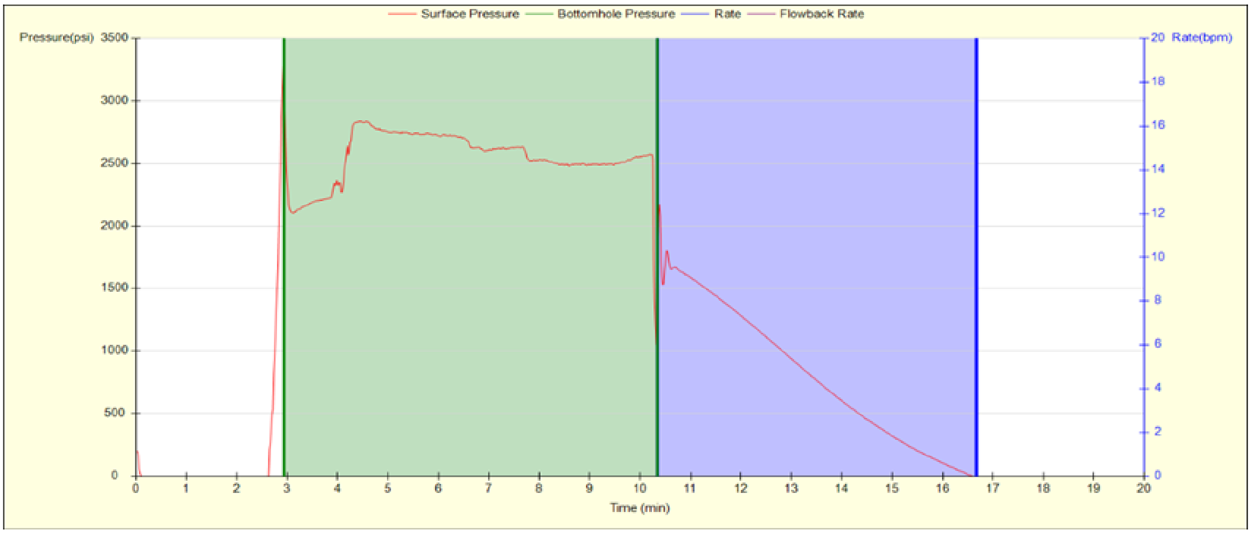

Figure 93 – Injection Test 1

Closure pressure – 5027 psi (gradient 0.506 psi/ft).

Res. Pressure – 2870 psi Kh/mu – 400 md*ft/cp (120 md*m/cp).

No signature of height growth (figure 94).

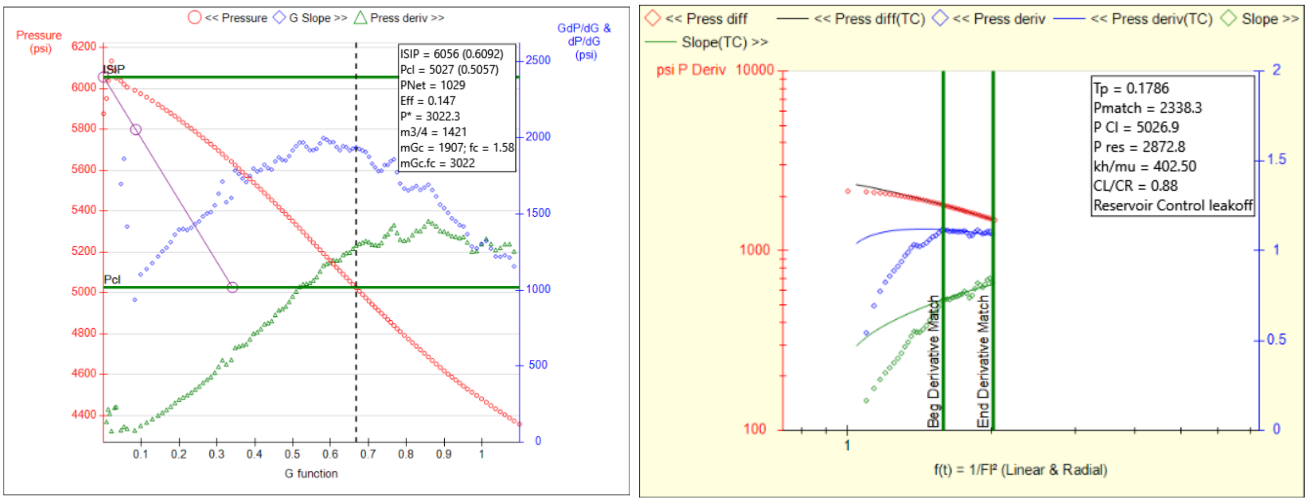

Figure 94 – Slope1 – 15713 psi/min, Slope 2 – 216 psi/min

Injection Test 1: BHPG data

Breakdown pressure: 7250 psi: Fracture propagation pressure: 5940 psi (figure 95).

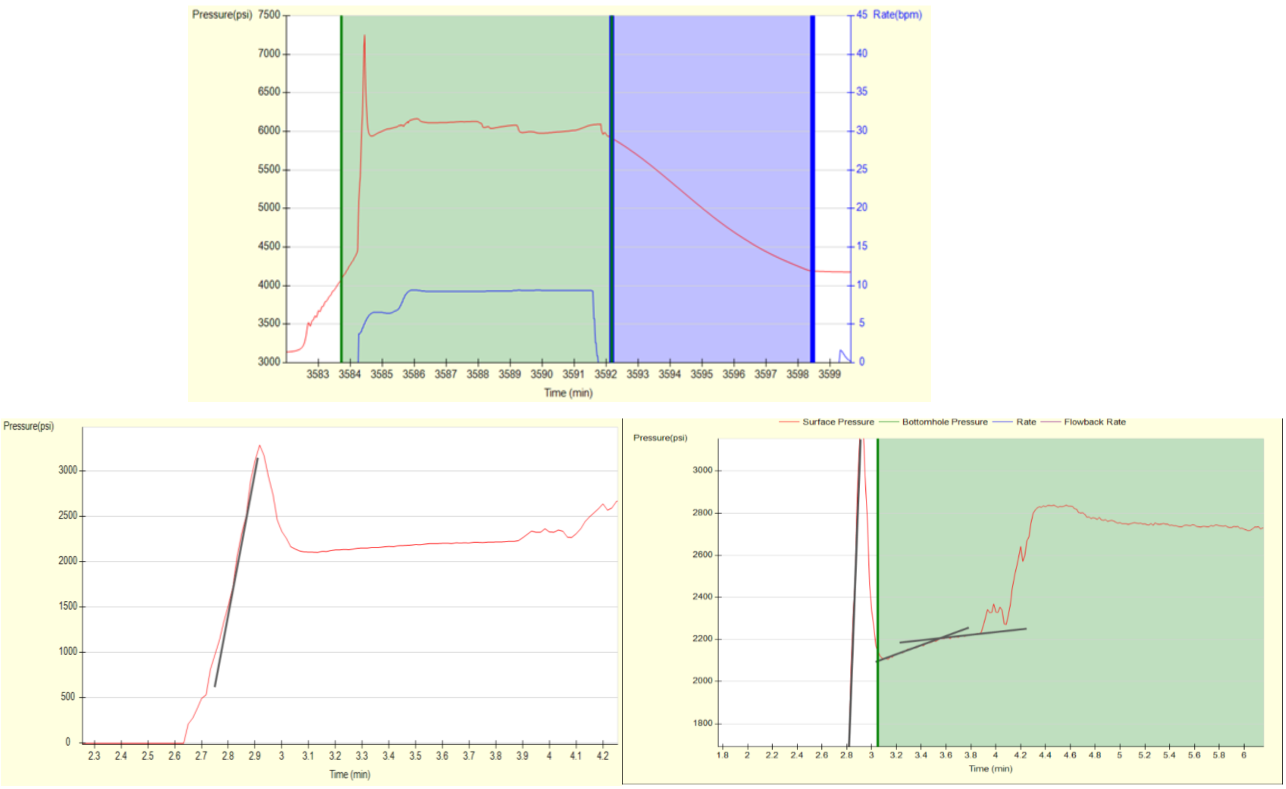

Figure 95 – Slope 3 – 64 psi/min

Closure pressure – 5013 psi (gradient 0.506 psi/ft)

Res. Pressure – 2824 psi: Kh/mu – 400 md*ft/cp (120 md*m/cp), (figure 96).

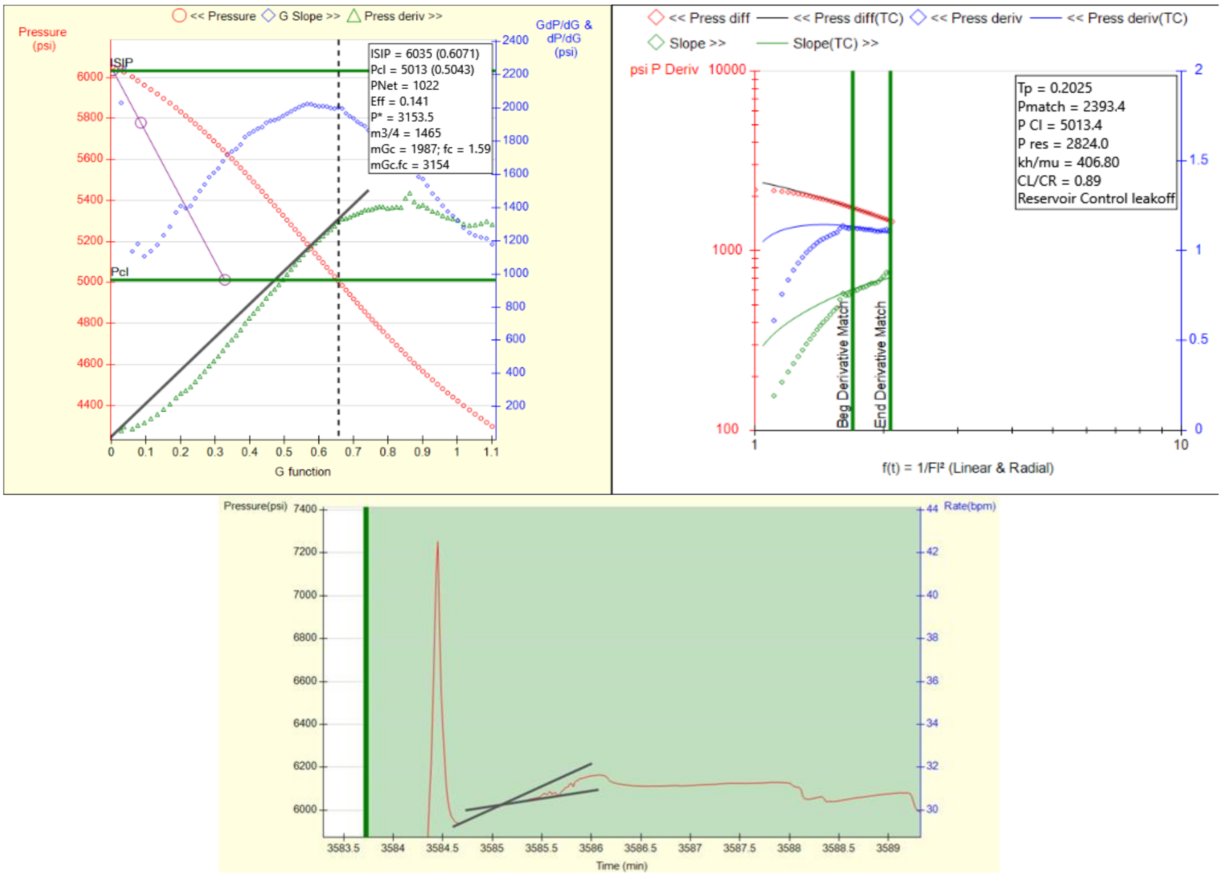

Figure 96 – Slope 2 – 210 psi/min, Slope 3 – 71 psi/min

Conclusion from Injection Test 1.

1. Fracture was initiated at the weakest point, and propagated in length in very confined and quite permeable thin layer (not more than 7-10 meters in height with average permeability about 5 to10 mD).

2. Formation has significant toughness, probably the Young's Modulus (YM) in the models is underestimated.

Injection Test 2: Surface data.

Breakdown pressure: 3287 psi :Fracture propagation pressure: 2800-2600 psi.

Closure pressure – 5536 psi (gradient 0.557 psi/ft), (figure 97).

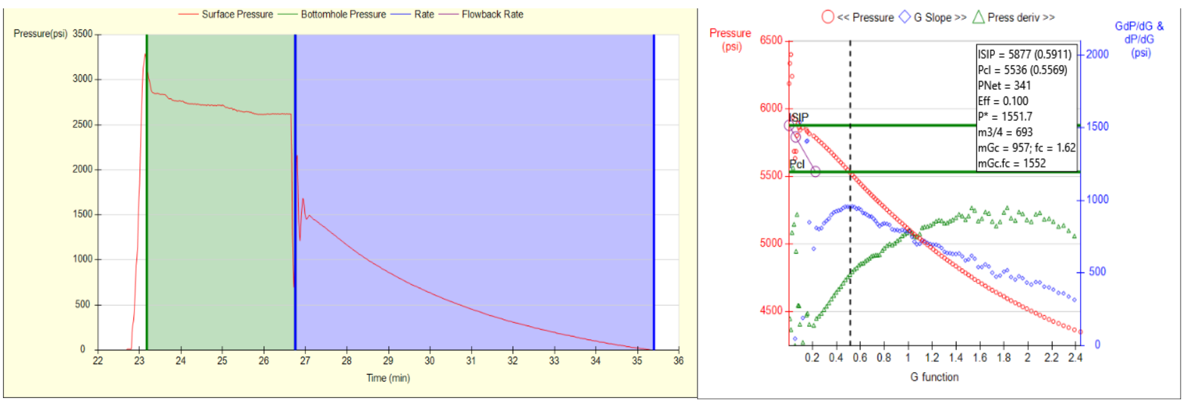

Figure 97 – Injection Test 2

Injection Test 2: Bottomhole data

Breakdown pressure: 6510 psi : Fracture propagation pressure: 6070 psi (figure 98).

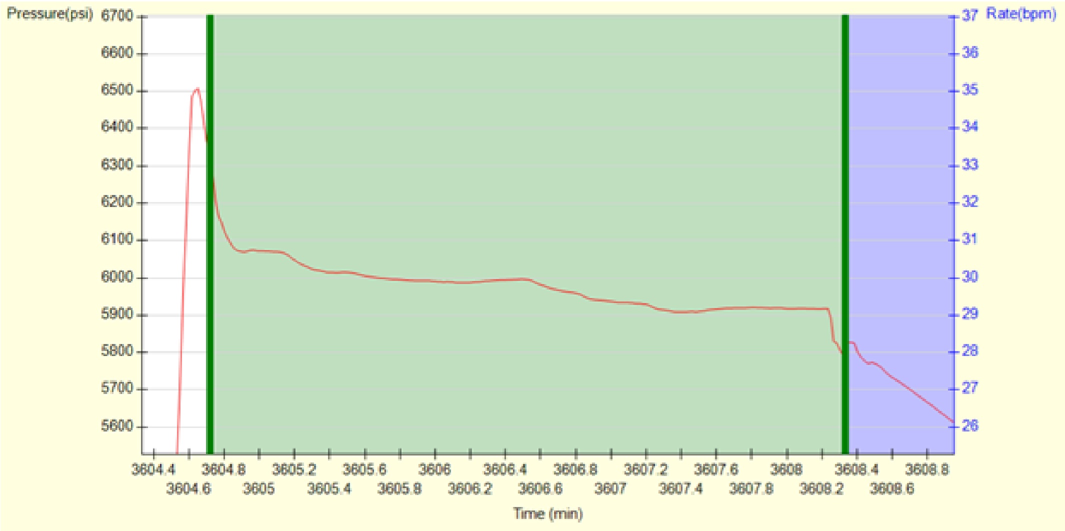

Figure 98 – Fracture propagation pressure

Closure pressure – 5270 psi (gradient 0.53 psi/ft).

Res. Pressure – 3533 psi : Kh/mu – 527 md*ft/cp (160 md*m/cp), (figure 99).

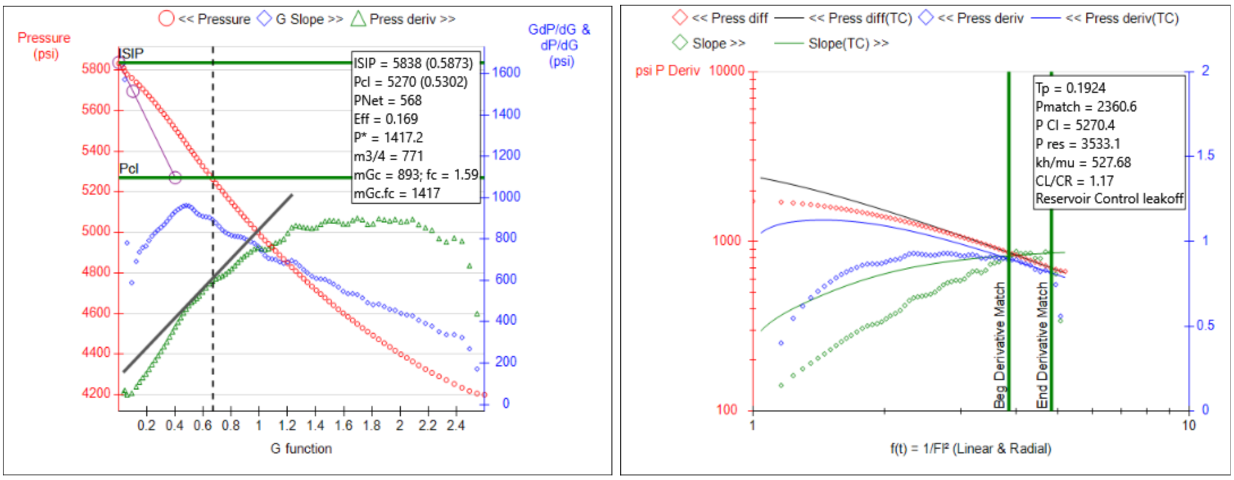

Figure 99 – Closure pressure

Conclusion from Injection Test 2

Fracture propagated in length-dominating mode, but broken through at least two higher-stress zone, which provided some height recession during closure. Height is higher than during injection test 1, but still less than 15-20 m. with average permeability 4 to 8 mD.

Formation has significant strength, because the repeated breakdown was observed Step-rate tests analysis : Surface data.

Closure pressure – 5450 psi (gradient 0.548 psi/ft), (figure 100).

Step-Rate Test: Bottomhole data (figure 101).

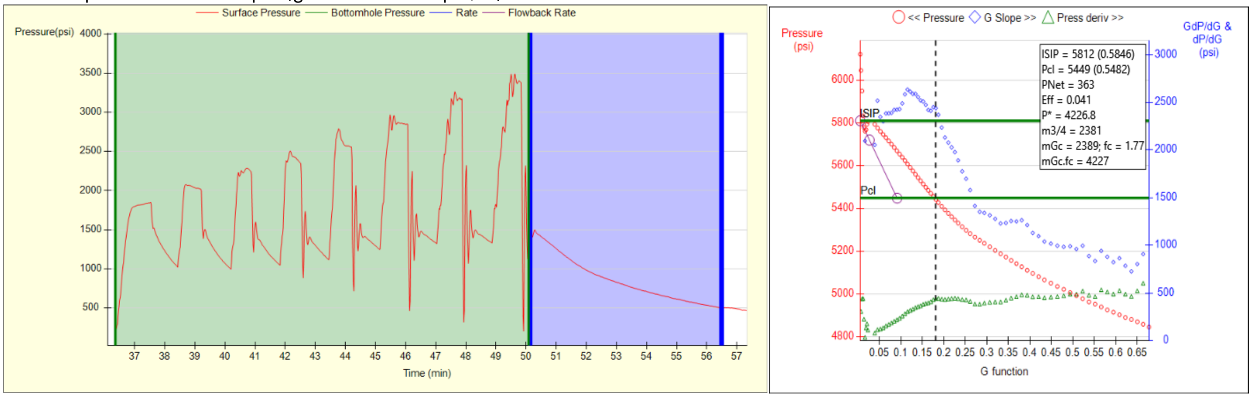

Figure 100 – Closure pressure

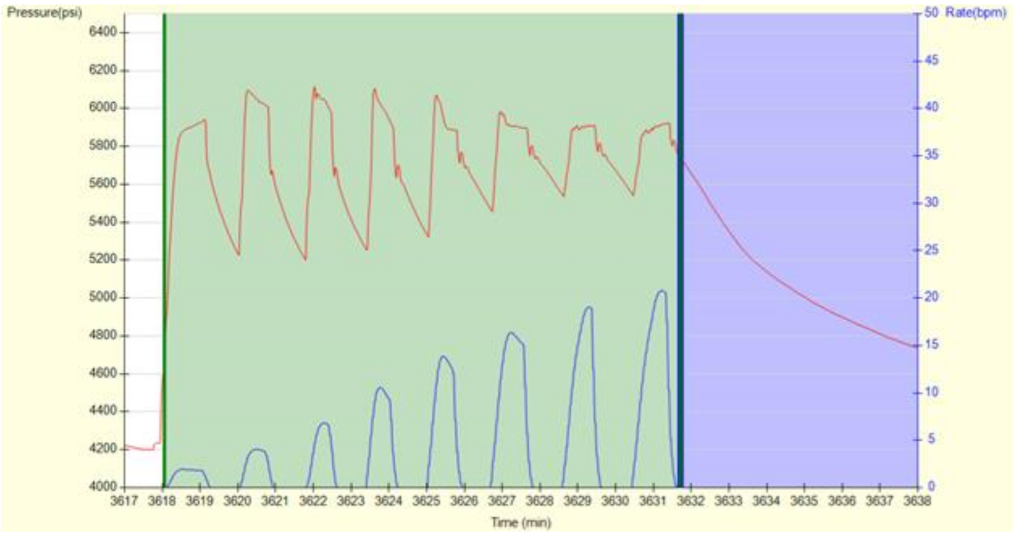

Figure 101 – Step-Rate Test

Closure pressure – 5800 psi.
Conclusion from Step-Rate test (figure 102).

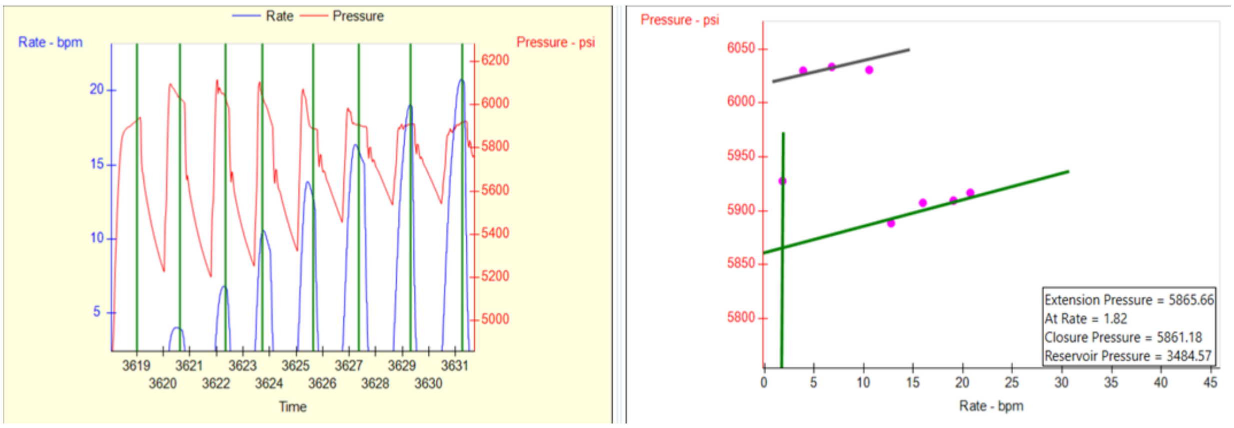

Figure 102 – Closure pressure

Tortuosity dominated regime at low rates (high near-wellbore frictions when fracture is confined at rates below 10 bpm), then NWB frictions rapidly drop at rates

>10 bpm) confirms the small height and fracture width (thus high YM) at low rates

Step-rate test data for the given formation provide overestimated closure pressure. The G-function analysis is the main tool to determine fracture closure pressure for this particular well-reservoir system (figure 103).

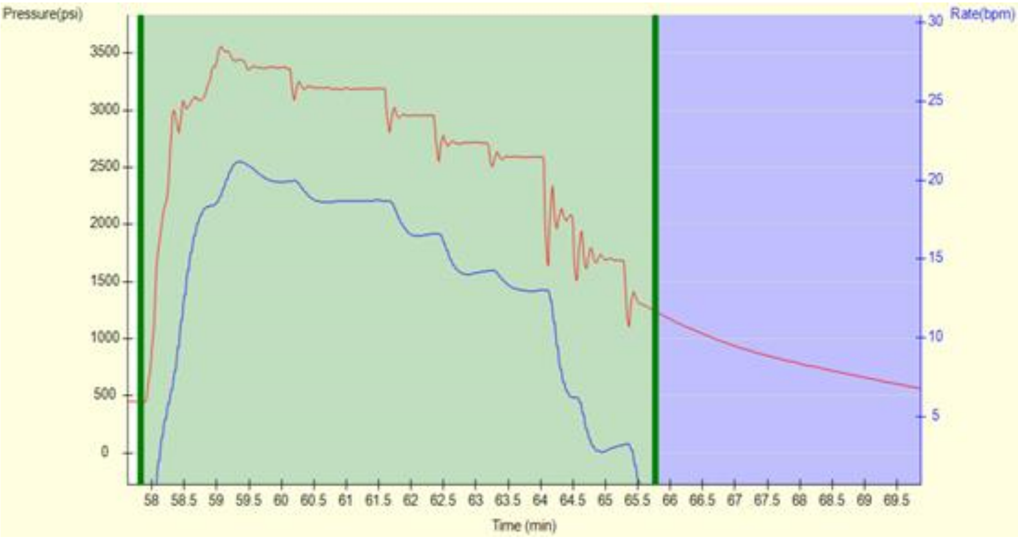

Figure 103 Step-Down Test

Step-Down Test (SDT): Surface data.

Step-Down Test: Bottomhole data (figure 104).

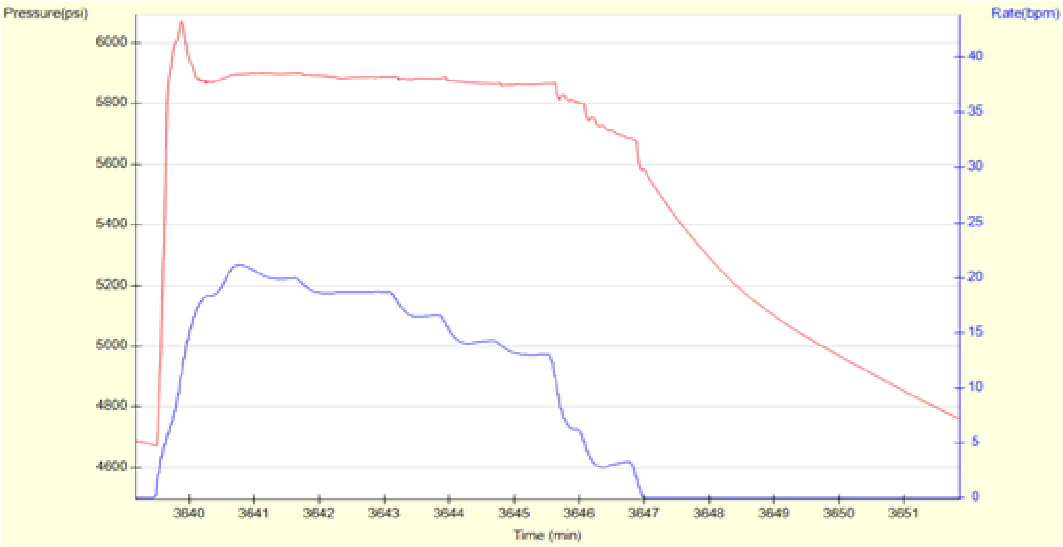

Figure 104 – Step-Down Test

Regime: Tortuosity dominated Open perfs: >130, <320 (figure 105).

Conclusion from Step-Down test.

With properly calibrated tubing frictions, the step-down test can be used in future to determine approximately the friction source.

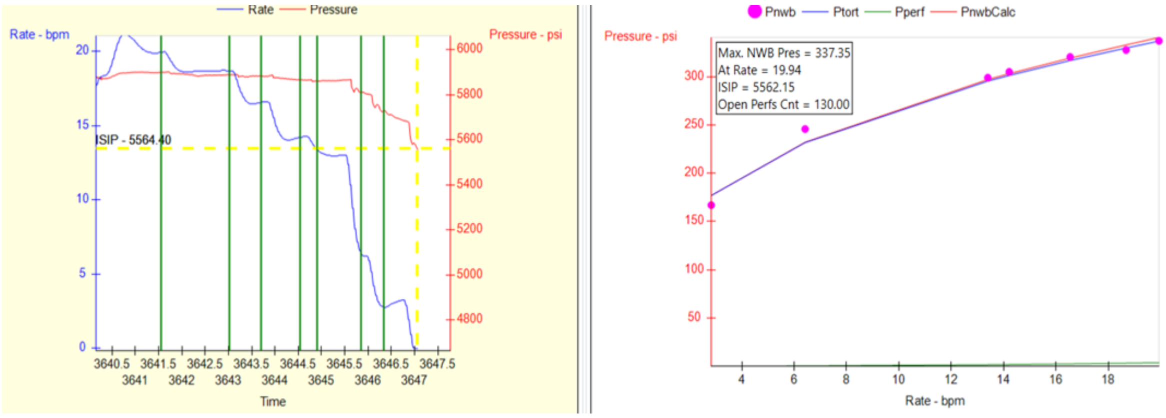

Figure 105 – Regime

However, the exact number of perforation holes opened cannot be properly estimated with SDT from surface readings: the bottomhole data showed that the discrepancy in open perfs estimation can be as much as 40%.

Calibration tests analysis: Surface data (figure 106).

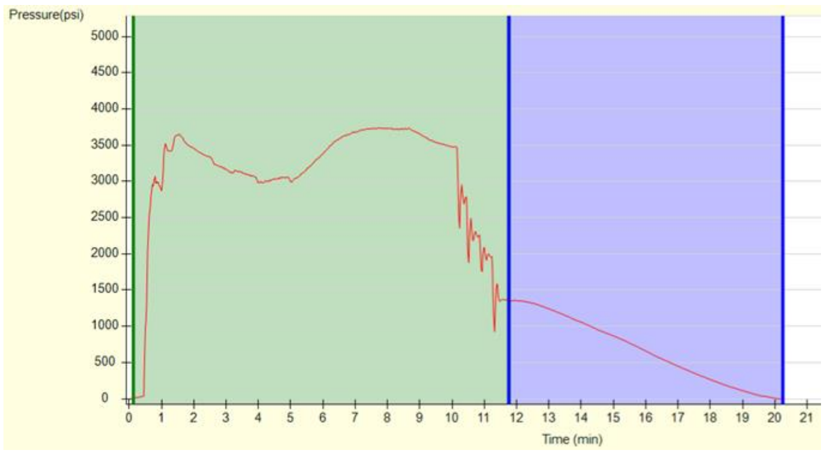

Figure 106 – Calibration tests

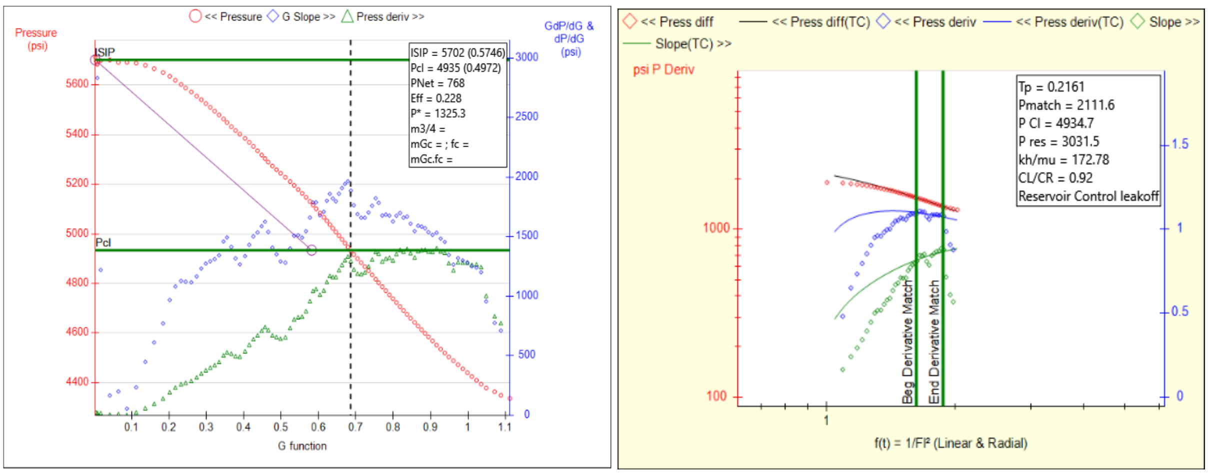

Figure 107 – Closure pressure

Closure pressure – 4935 psi (gradient 0.497 psi/ft) : Res. Pressure – 3030 psi.

Kh/mu – 172 md*ft/cp (52 md*m/cp): Efficiency – 23% (figure 107).
Calibration Test: Bottomhole data (figure 108).

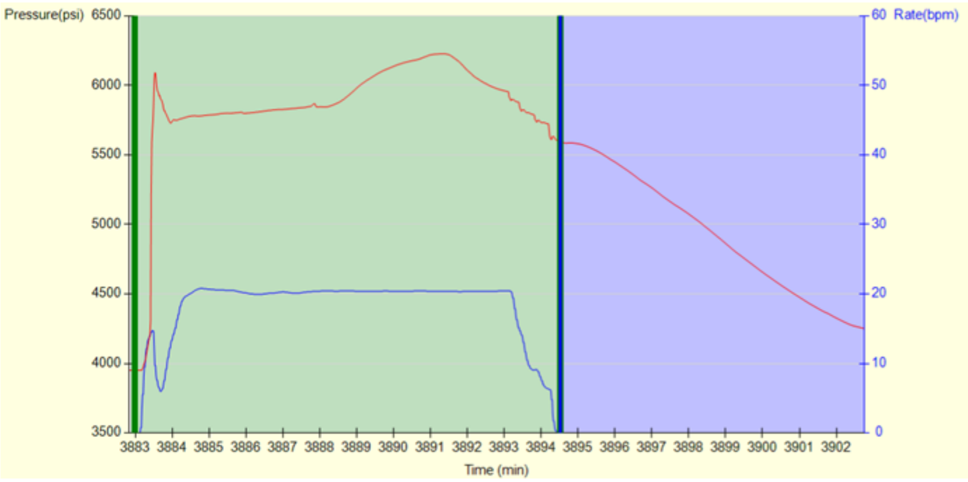

Figure 108 – Calibration Test

Closure pressure – 4842 psi (gradient 0.487 psi/ft) : Res. Pressure – 2717 psi.
Kh/mu – 839 md*ft/cp (255 md*m/cp): Efficiency (corrected) – 20% (figure 109).

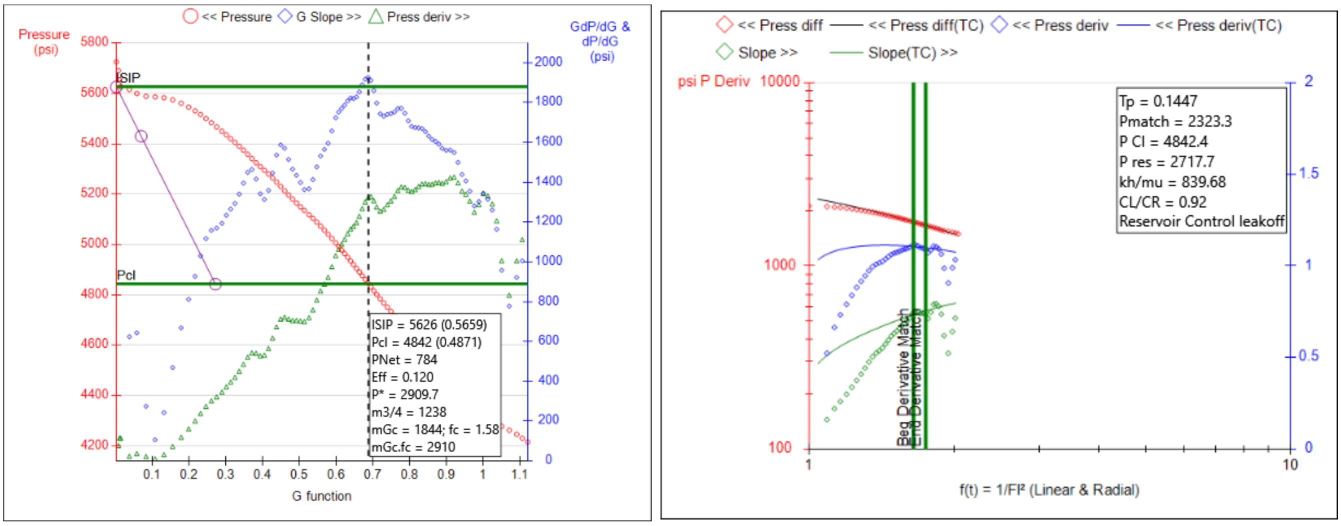

Figure 109 – Closure pressure

Conclusion from Calibration test.

Calibration test opened the whole kh of the target sand layer, with average k lying in a range from 3 to 6 mD. The downhole gauge data are extremely important to determine after-closure transmissibility at the crosslinked stage, because the surface readings showed underestimated kh.

5.2 Temperature Log Analysis

Temperature log analysis is a useful technique for evaluating hydraulic fracture performance. By analyzing temperature changes in the wellbore during and after a hydraulic fracture treatment, engineers can gain valuable insight into the efficiency and effectiveness of the treatment [53-55].

Once the temperature logs are acquired, analyze the data to determine the temperature changes that occurred during and after the hydraulic fracture treatment. Look for any temperature anomalies, such as sudden temperature drops or rises, which may indicate fracture growth or other changes in the formation (figure 110).

Fracture top: ~3015 (High probability).

Fracture bottom: between 3045 and 3055 (Significant Uncertainty).

Fracture Initiation zone: ~3032 (High probability).

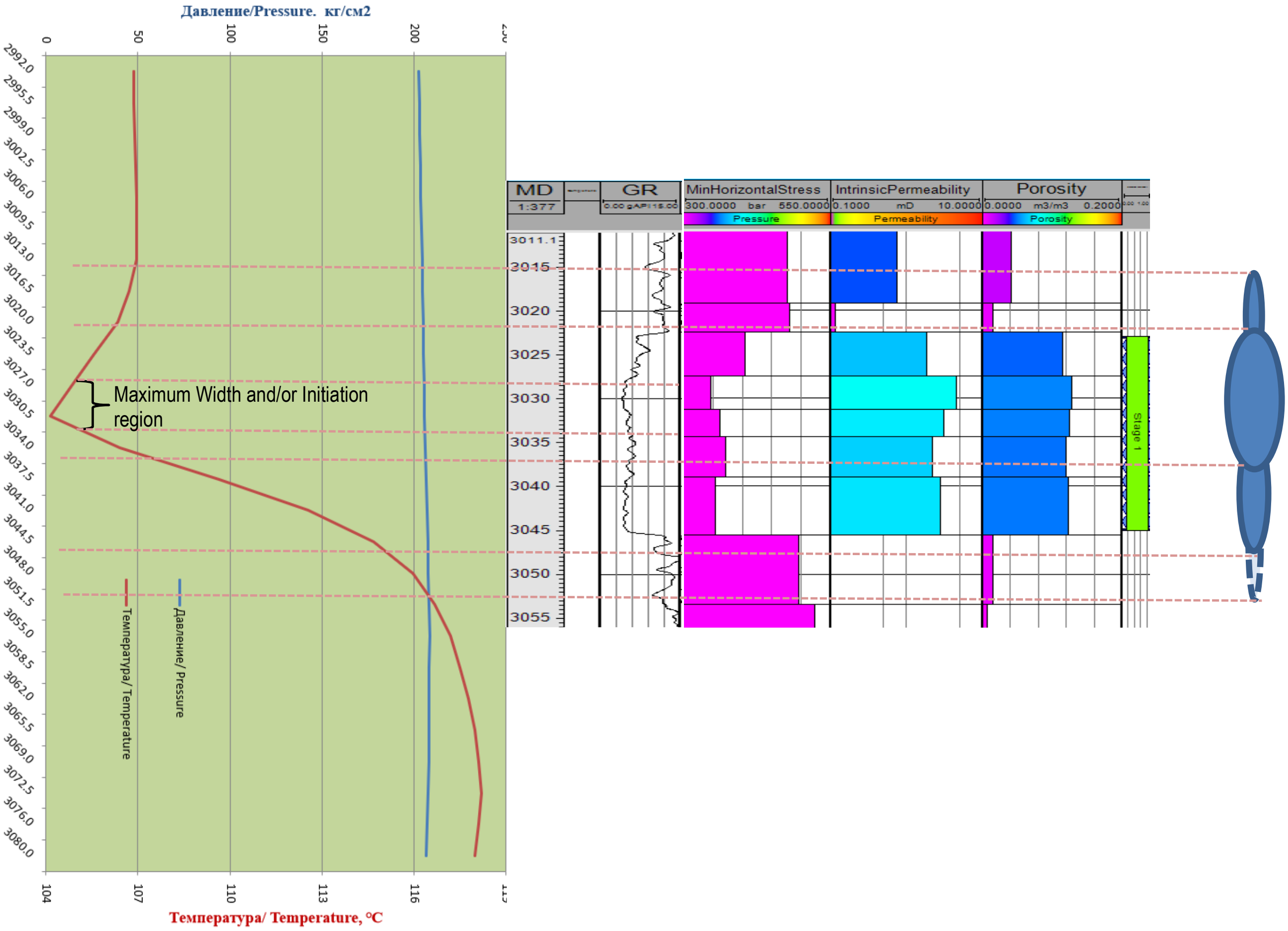

Figure 110 – Temperature log

Conclusion from Temperature log.

Fracture initiated, and most probably has the maximum width somewhere at 3030-3031 m. The reservoir model in fracture simulator was adjusted accordingly.

Using fracture initiation point from temperature log, and step-like breakthrough signatures during injection test 2, the maximum reasonable number of zones with varying minimum-in-situ stress in target net pay can be 4 or 5. There is no practical need to finer layering of reservoir model in fracture simulators [56, 57].

The fracture top height is determined with satisfactory error +/- 2 meters; however, the fracture bottom determination is questionable (sonic tool helped to solve this – see below) [58, 59].

5.3 Dipole Acoustic Log Data Analysis

Shear slowness was extracted from Dipole data using 5 receiver's multi shot technique and the final results are good in the expected range of values (figure 111).

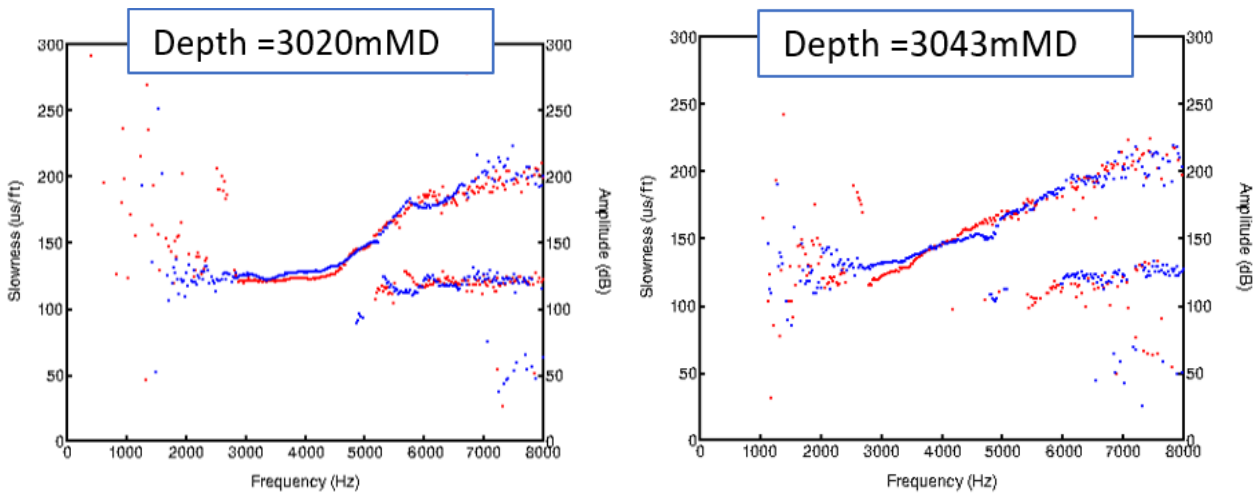

Figure 111 – Dipole Acoustic Log Data Analysis

Analyze the post-treatment dipole acoustic log: Analyze the post-treatment dipole acoustic log data to gain insight into the hydraulic fracture performance. Look for changes in the formation, such as changes in acoustic impedance, that may indicate the presence and extent of the created hydraulic fracture [60, 61].

Interpret the dipole acoustic log data: Interpret the dipole acoustic log data to gain insight into the efficiency and effectiveness of the hydraulic fracture treatment. Look for areas where the treatment may have been less effective than expected or where the fracture may have grown more than anticipated.

Definite presence of fracture in 3016-3044 m:

– 3046-3060 – presence of wellbore diameter change. The fracture bottom may be masked by this fact (formation signal coherency becomes week and casing arrival appears to be visible), but presence of isotropic points at 3046 and 3055 may indicate that the fracture stopped at 3045, and the induced anisotropy signals below are caused by pumped fluid entry and work in washed out zone [62].

Another important piece of information obtained from acoustic data is direction of the fracture plane. The deviation of the well is very low, so the precision of the fracture azimuth determination can be low. In general, the fracture azimuth is expected to be in WNW direction, in a range of 105 to 135 deg (refer to the log below, Fast Shear Azimuth red line). This fracture azimuth reflects the local maximum horizontal stress direction. The local maximum horizontal stress direction can be different in the vicinity of the geological faults. The minimum horizontal stress gradients observed during fracturing are indicating normal regime in this field, where normal faulting is expected. In this case, the maximum horizontal stress direction is aligned with the fault line. If the faulting lines are not aligned with the maximum horizontal stress direction given above, then either this maximum horizontal stress direction is a local feature, or the faulting history contains some strike-slip movement in the past (figure 112) [63].

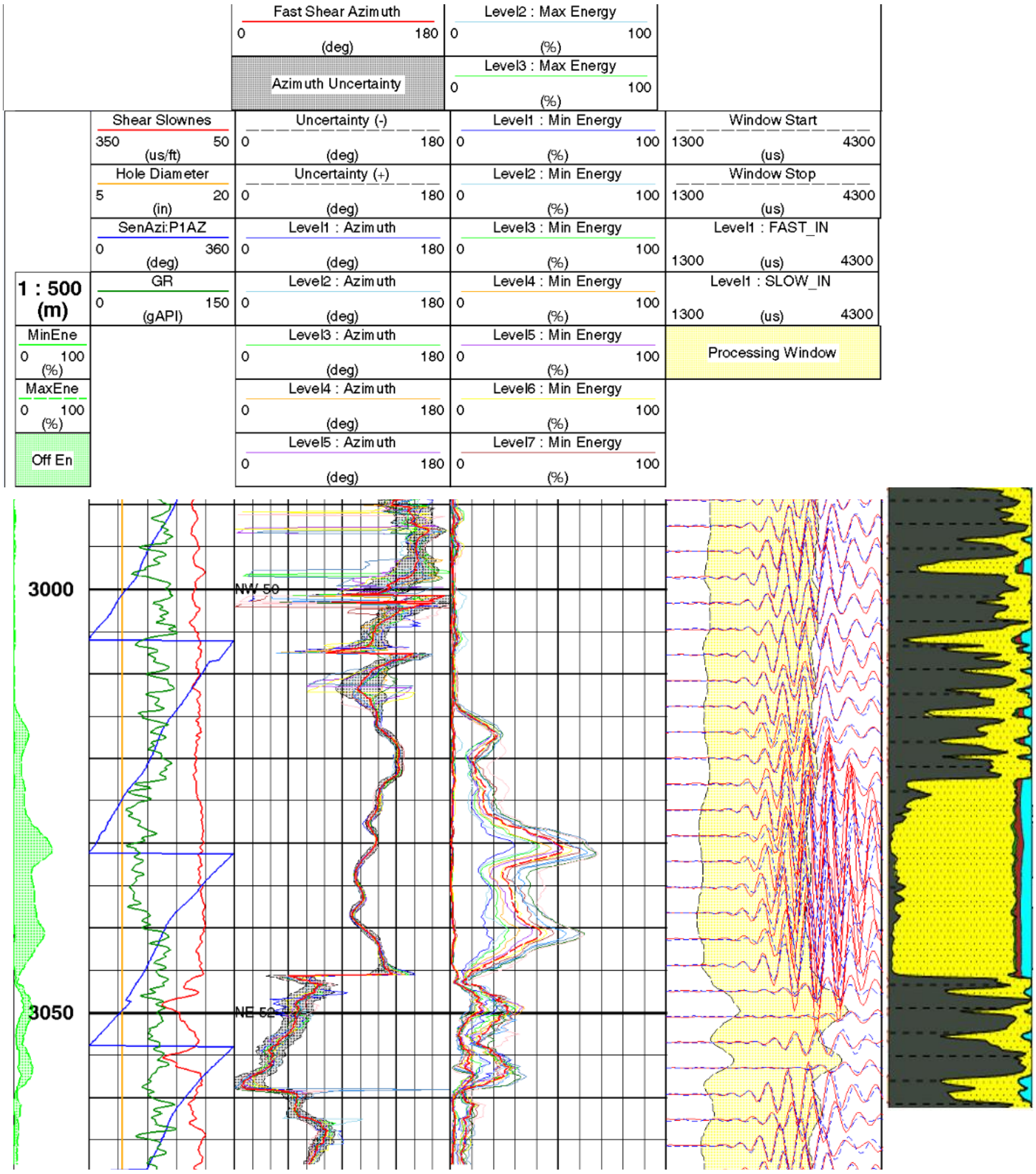

Figure 112 – Dipole Acoustic Log

5.4 Fracture Model Calibration

Using the data obtained from Mini-frac, temperature logs and Sonic tools, the Advanced Multiphysics software Kinetix was used to recalibrate the fracture design.

In the used Multiphysics method, transport equations describing the advection of proppants, fluids, and fibers via a conservative [64].

Lagrangian algorithm (particle-in-cell method) (Harlow 1964; Grigoryev et al. 2002). It has zero numerical diffusion and allows us to simulate slurry flow with no excessive smoothing. The velocity field for each component is calculated using a finite volume scheme on 2D grid in the x, y plane and closure relations for settling velocity and bridging.

The particle-in-cell method gives an exact determination of fluid/proppant location and enables the capture of many important effects, thus combining advantages of both mesh and meshfree methods. These include materials degradation via tracking temperature and shear exposure; displacement of proppant in the near-wellbore area in case of overflush; correct simulation of tail-in/resin-coated proppant stages; and complex boundaries between fluids, proppants, and fibers. Algorithm allows for tracking exposure history for all fracturing materials and account for fluid and fiber degradation. Fluid degradation affects rheology according to a given experimental table [65-67].

Below, on the figure 113 is the fracture created during Calibration test, built on calibrated reservoir, before main job [68-70].

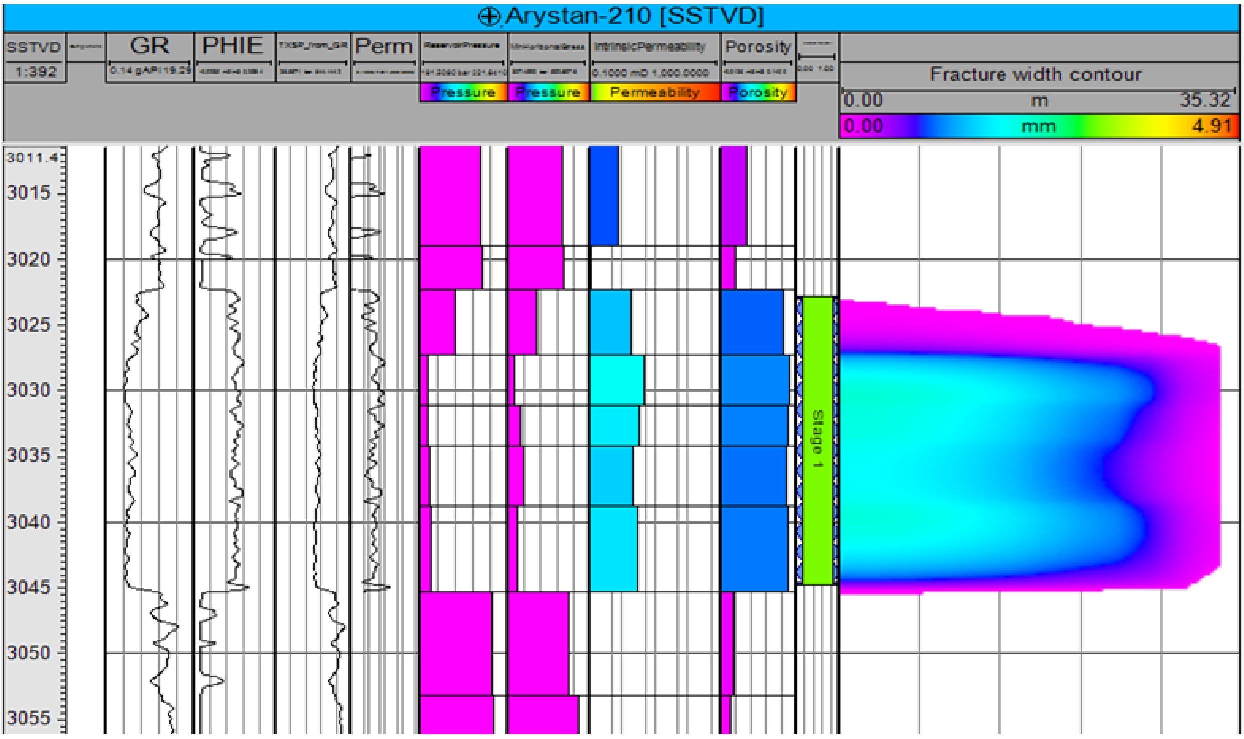

Figure 113 – Calibration test

5.5 Fracture Fluid Rheology Testing

For modelling of the actual job, the fluid rheology digital model was reconstructed. It is especially important, because the advanced fracturing software used in this study is equipped with Multiphysics fluid/proppant transportation algorithms, which are very representative, so the precision of fluid model becomes increasingly important in this case. The fluid rheology tests were performed on actual chemical and water samples from the field (table 7).

Table 7 – Temperature Stability tests : Linear gel properties

30# gel	
pH	8.23 @ 24.8 degC
Viscosity @ 170 sec-1	54 cP
Viscosity @ 511 sec-1	27 cP
33# gel	
pH	8.3 @ 24.4 degC
Viscosity @ 170 sec-1	60 cP
Viscosity @ 511 sec-1	34 cP

Then, the crosslinked fluid was prepared placed on the Chan 5550 High Temperature Viscometer and the viscosity of the fluid was monitored over a period of time at 114°C. Measurements performed on Chan 5550 High Temperature Viscometer, showed that 33# gel had a viscosity of 500-600cP at 100 sec-1 for duration of the test, approximately 45 minutes at 114 degC (figure 114).

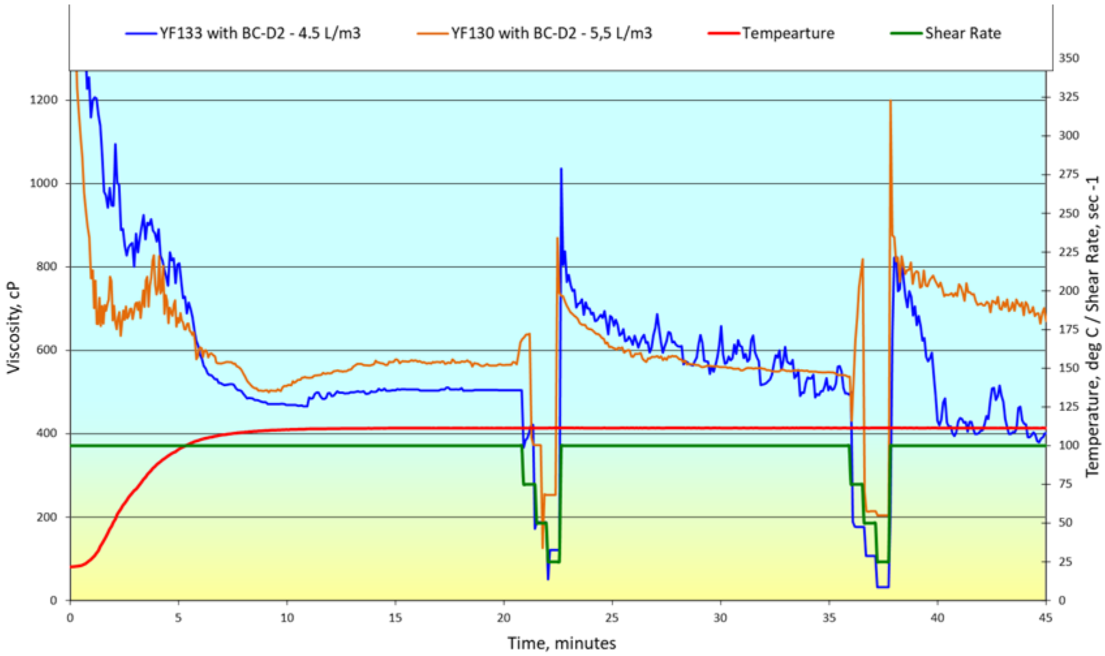

Figure 114 – Viscometer and the viscosity

Breaker tests

The break test was performed at 110 degC with various loadings of AP-2 Breaker were performed, in order to give an indication of the breaker schedule required and which would give the desired working time of 45 minutes. The working time is the length of time elapsed before the viscosity of the fluid falls below 400 cP at a shear rate of 100 sec-1 Tests were performed on the Chan 5550 High Temperature Viscometer. The results show that increasing the amount of breaker results in a reduction in the viscosity of the fluid (figures 115, 116, 117, 118).

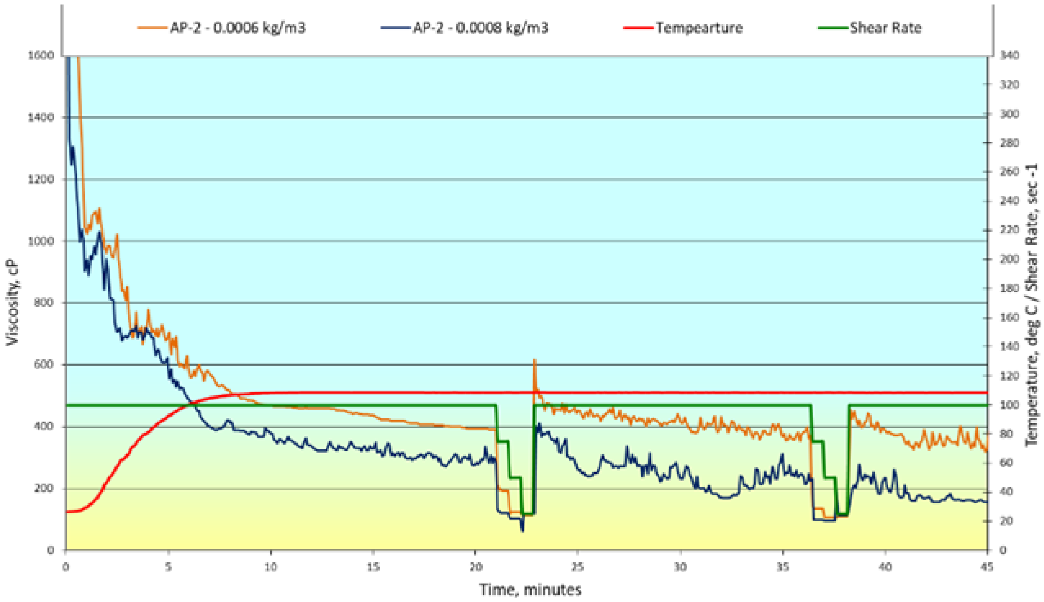

Figure 115 – 30# gel Break Testing at 110 degC

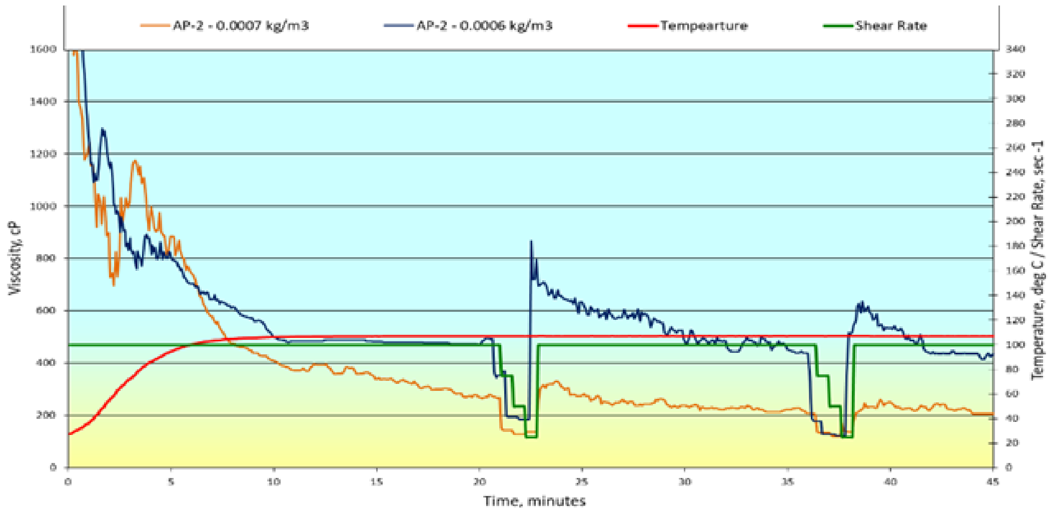

Figure 116 – 33# gel Break Testing at 110 degC

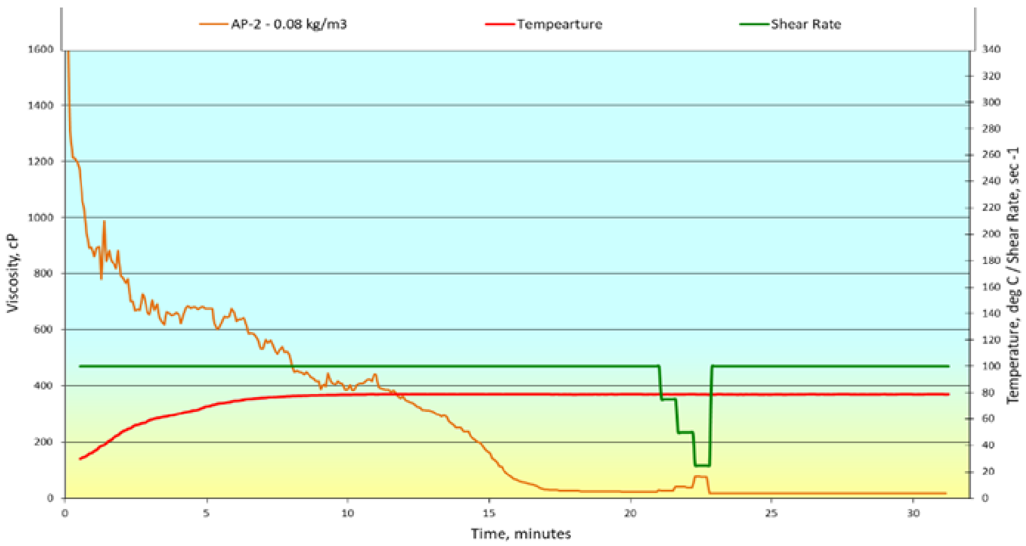

Figure 117 – 30# gel Break Testing at 80 degC

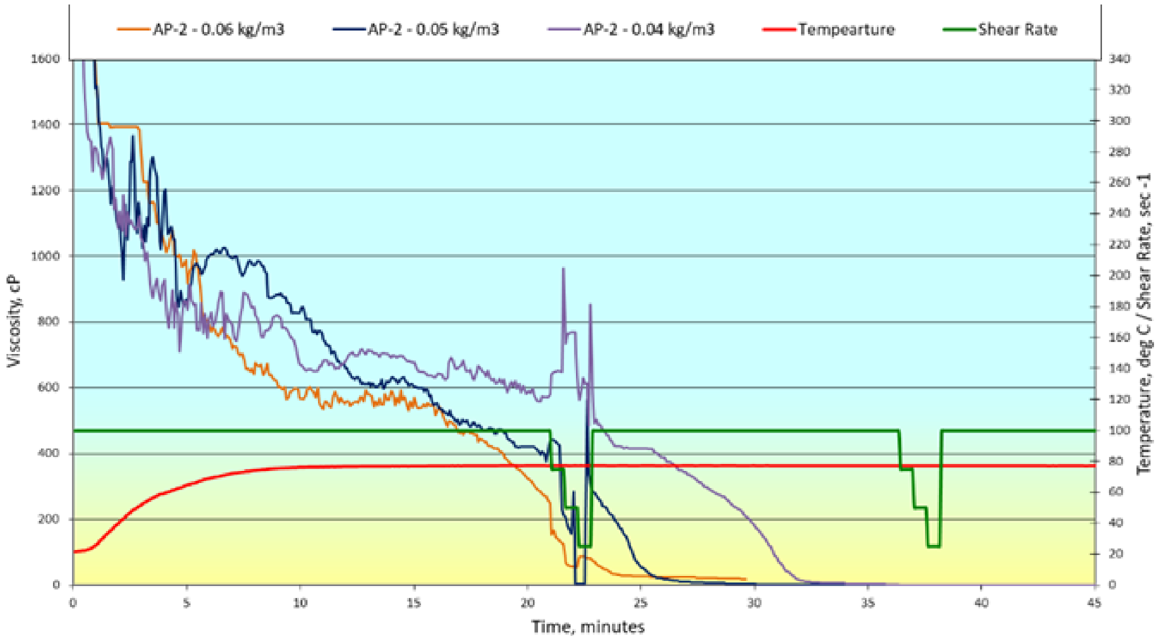

Figure 118 – 33# Break Testing at 80 degC

5.6 Sensitivity study on the Actual Fracture length

Actual pumped job was simulated on the calibrated model. Two cases were checked in order to get a range of actual fracture length [71].

P50: Less propped height due to any reason (slightly higher actual rate, less fracture width on top, more fracture toughness in vertical direction, and less in horizontal, etc.).

P90: Height seen at acoustic data.

The difference between two cases in propped length is not more than 5 meters (around 80 m for P90 vs 85 m for P50). Refer to figures 119 and 120 below.

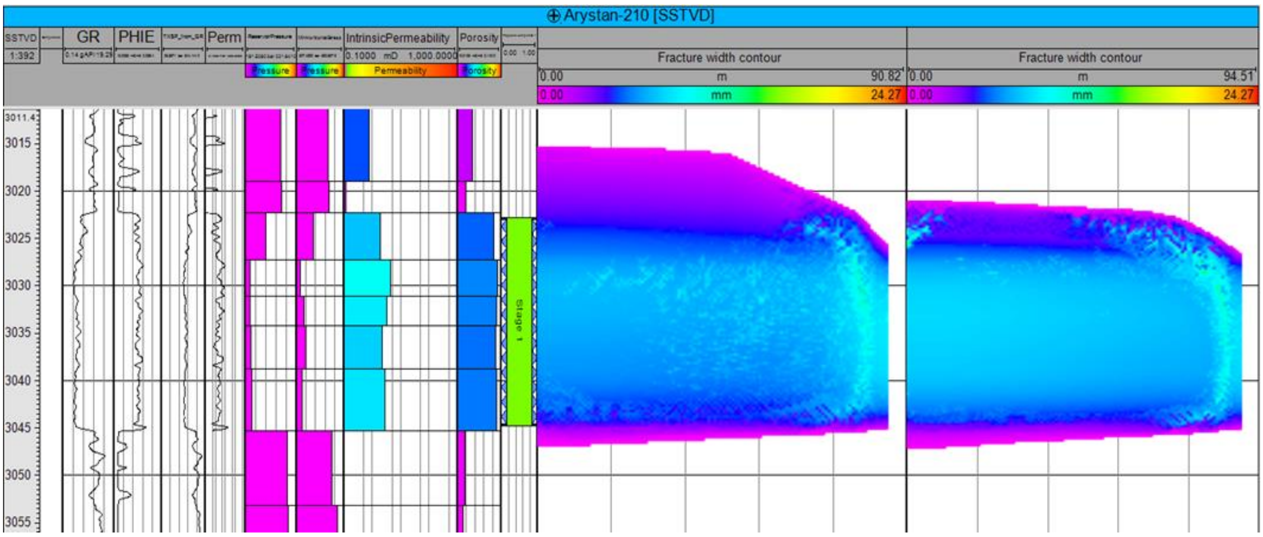

Figure 119 – Calibrated fractures after Actual job: P90 (left) and P50 (right)

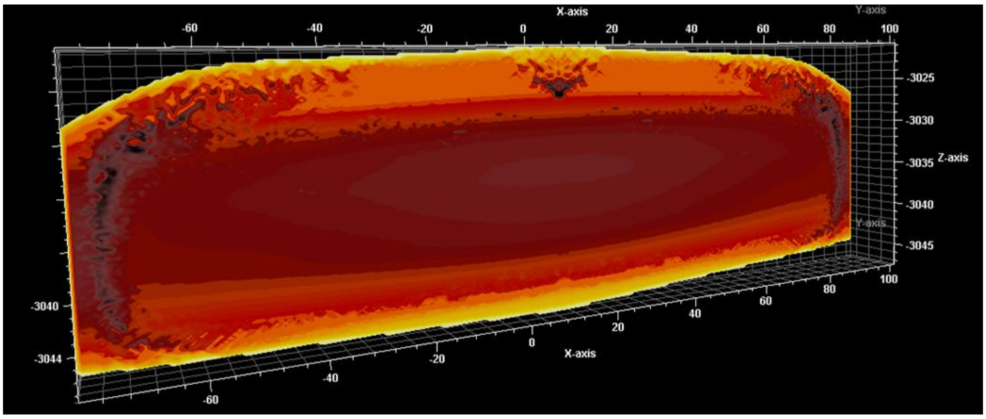

a

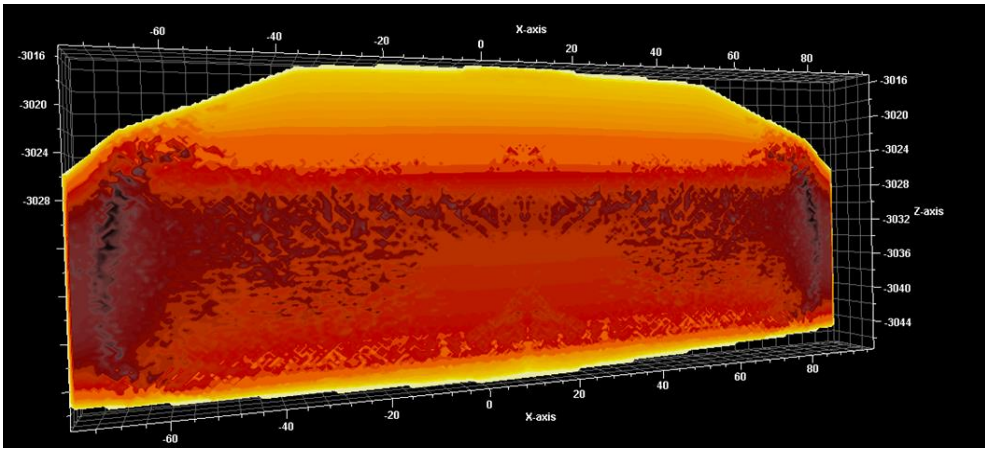

b

a – Internal structure of the fractures created during actual job: P90; b – Internal structure of the fractures created during actual job: P50

Figure 120 – Internal structure of the fractures created during actual job

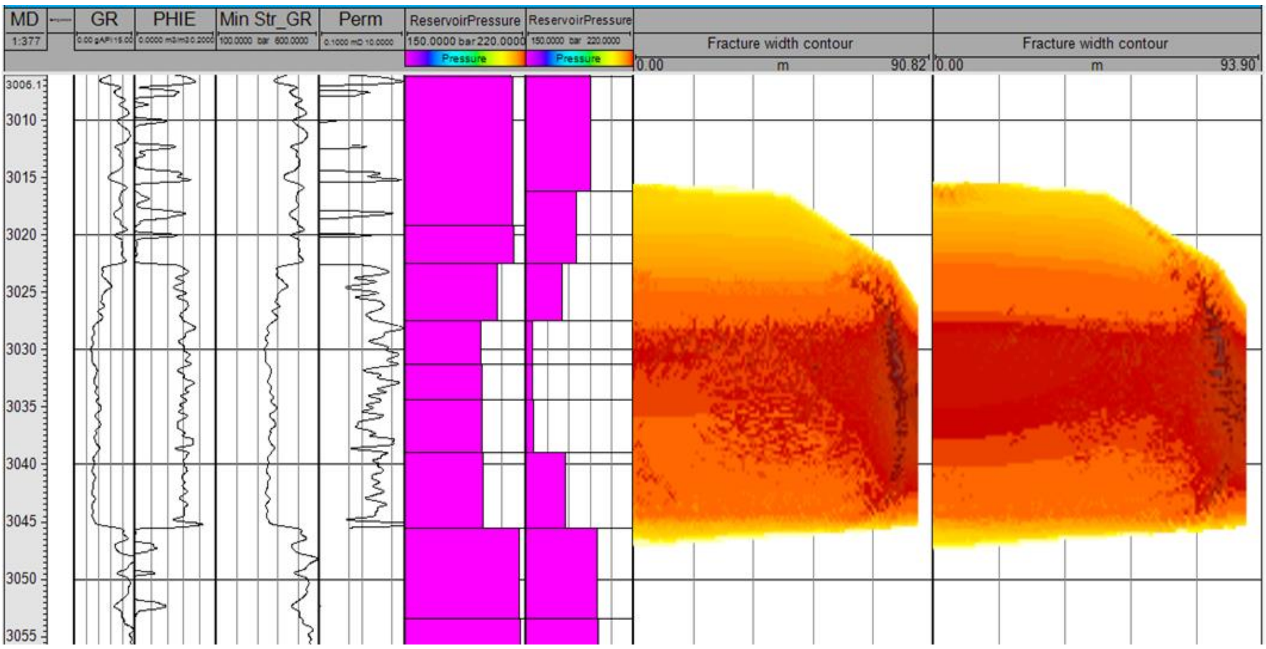

Figure 121 – Hypothetical Fracture length

5.7 Sensitivity to gel loading

Comparison of current gel loading with loading decreased to 30# shows that Initial skin can be improved from -5.45 to -5.52, taking into account assumptions that effective fracture half-length is increasing from 55 to 58 m, and Fcd from 8 to 9.

Plot on the left on the figure 122 – Pratt's correlation for actual current fracture (60-65% ratio of X_{eff} to $X_{propped}$). Plot on the right – Pratt's correlation for hypothetical fracture if gel is replaced to the gel with 5% higher retained conductivity.

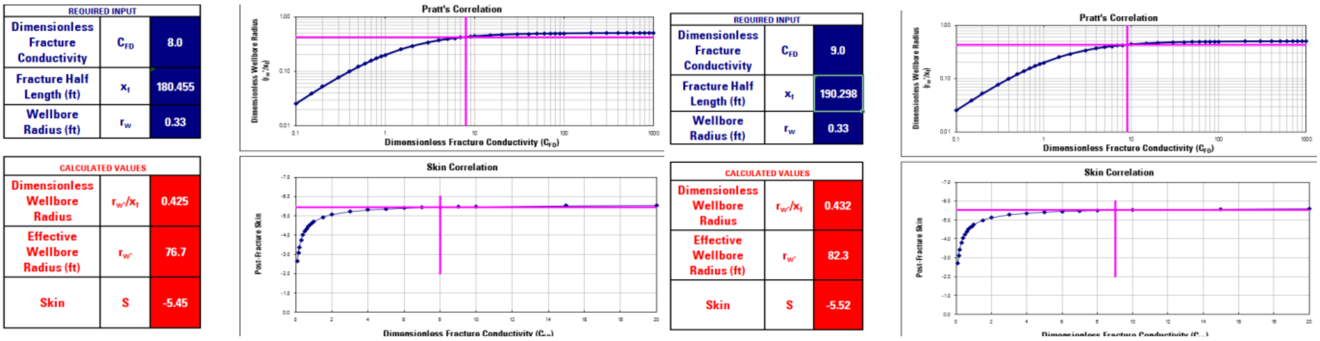

Figure 122 – Pratt's correlation

5.8 Sensitivity to proppant placement methods

Considering that volume increase and gel loading increase doesn't provide step-change in effective half-length, the proppant placement methods were analysed [72-74].

Below, on the figure 123 and 124, is the comparison of 43 t job pumped in pulsation mode (channel fracturing method) versus 60 t job pumped in standard mode, for depleted case. It can be concluded that despite total length is increased by 10%, the effective half-length is expected to increase from 58 m to 80 m, i.e. by about 40%.

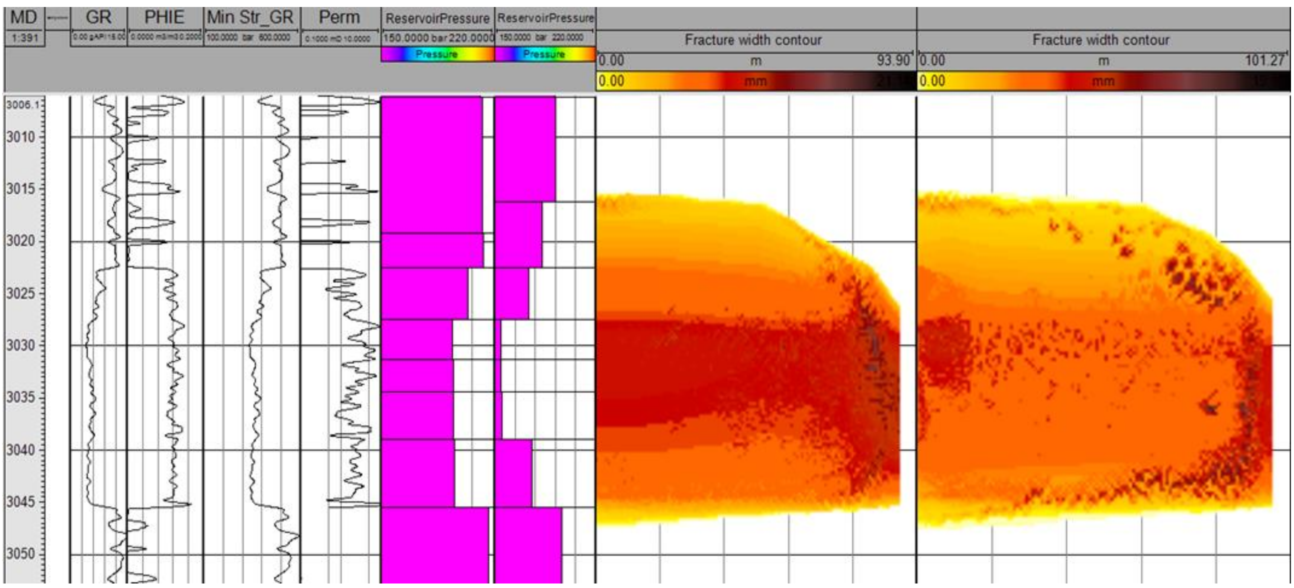

Figure 123 – Placement methods

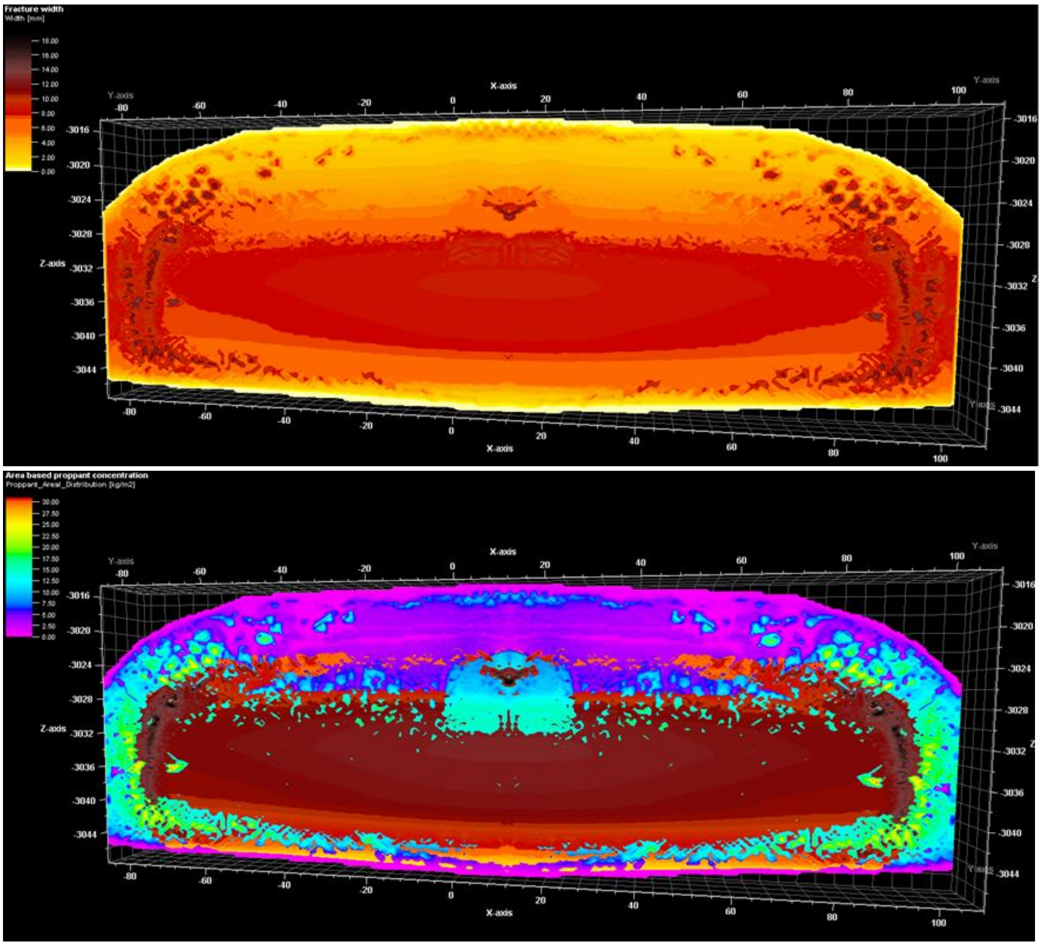

Figure 124 – placement methods

Refrac sensitivities

Modelling of the re-fracturing is a complex process, which can't be performed precisely because of the multiple factors: two different conditions of the reservoir itself, changed state of geomechanics components from the previous fractures, micro- and macro scale geometrical/completion/geology uncertainties. For this study, the following question was raised: when we perform frac, do we expect significant change of fracture plane direction, considering that crack during refracturing may be initiated in different depth than during initial fracturing [75-77].

Refrac modelling was performed in the following way:

1. The initial fracture was modeled on a less depleted zone.

2. The refracturing was modeled by giving 40% depletion, shifting the fracture initiation point 1-2 meters along the wellbore, increasing leakoff.

3. Planar3D modelling engine was used, to account for more complex processes.

4. Multiphysics simulator allowed stress shadowing effect (between two fractures) to be accounted for.

5. Job volumes were reduced, because the key parameters that we are interested in here is the initiation zone and several meters of the fracture propagation in a preferrable fracture plane [78-80].

Results of simulations are shown below (figure 125).

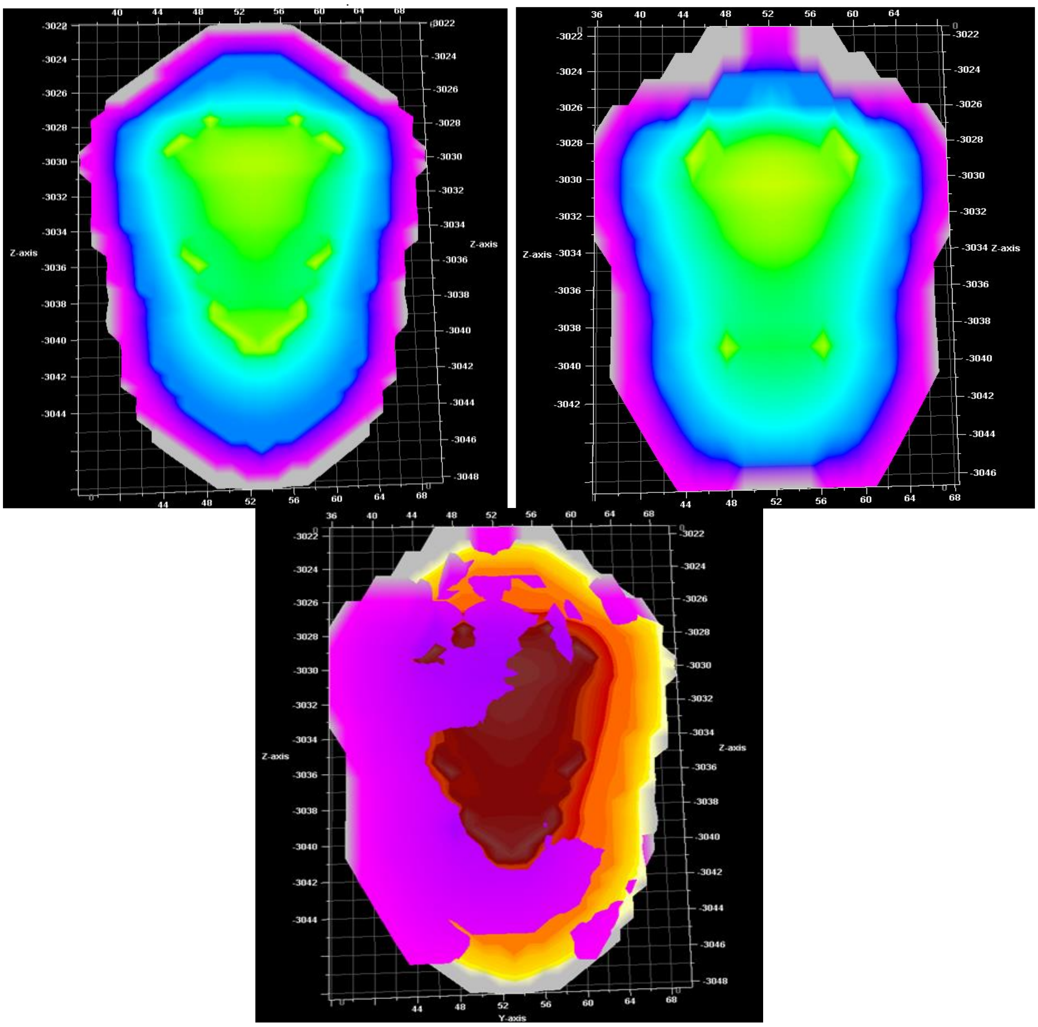

Figure 125 – Fracture simulation

On the left – initial fracture, on the right – re-fracture. At the bottom – overlapped picture of both fractures, where yellow-orange-brown colours are reflecting refracture, and purple colours are initial fracture. Note, the cross-section is shown, the distance between two fractures from the top view is less than radius of the wellbore.

Conclusions for refracturing modelling are:

1. For the given conditions of the viscous frac fluid, conventional rate fracturing, the branched wings/multiple wings are not formed in this reservoir

2. Main body and the tips of both fractures are following the same preferrable fracture plane (PFP), so the stress shadow effect for this reservoir setup and pumping schedules, is not affecting the fracture geometry. However, the local depletion in the net pay may cause local stress rotations, this effect may cause conditions when refrac creates a fracture with different PFP from the initial fracture, though this case is not expected to be frequent.

3. Refractured fracture has decreased in size (though not drastically) for the same volume pumped, due to more aggressive leakoff, so in order to create the same fracture during refract, bigger job should be pumped.

4. The main risk of refracturing is proved to be close position of the fractures, even coinciding of them, with subsequent problems like increased leakoff, and sudden screenouts.

Note on stress rotation:

It is noted in some publications in industry, e.g. SPE-106140 (picture below), that fracture reorientation may happen. In locally depleted zone. Thus, for refracturing candidates, it is recommended to observed the fracture efficiency. If fracture efficiency is close to that of during initial fracture, then probably fracture is created in new plane. However, if fracture efficiency is significantly lower, then, probably, the fracture is created along the initial fracture (figure 126).

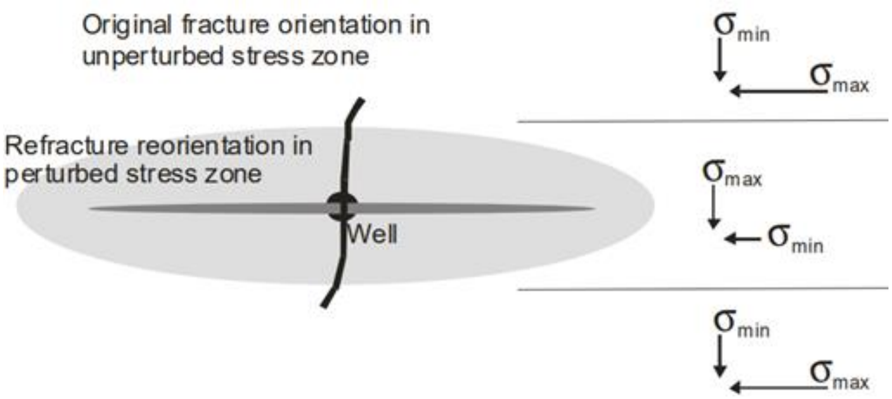

Figure 126 – Stress rotation

5.9 Well A-233 Fracturing Job Analysis

Design and Hypothesis: For well A-233, similarly to well A-210, the well model was prepared. Based on this model, the main hypothesis to check was: Do we correctly predict the Fracture geometry, and if no – how to optimize it?.

Diagnostic tests analysis: To work on hypothesis confirmation, injection, calibration, and main propped fracturing job data were used. First step was to analyse the diagnostic tests, based on explanations given in 2.2.

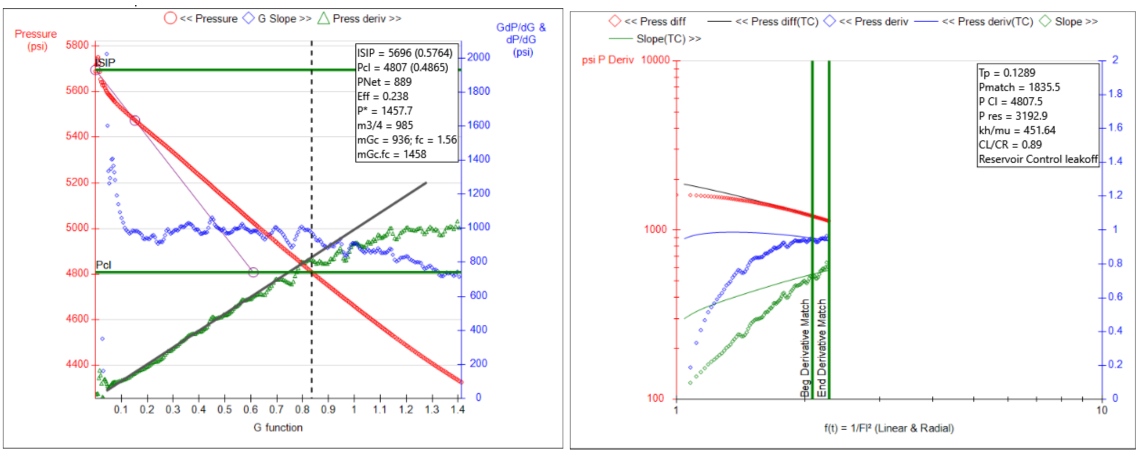

Res. Pressure – 3192 psi; Kh/mu – 450 md*ft/cp (137 md*m/cp) – low confidence, most probably exaggerated

Figure 127 – Closure pressure – 4810 psi (gradient 0.49 psi/ft)

Wellbore fill up – breakdown test (figure 127).
Step-rate test (decline after pre-final step) (figure 128).

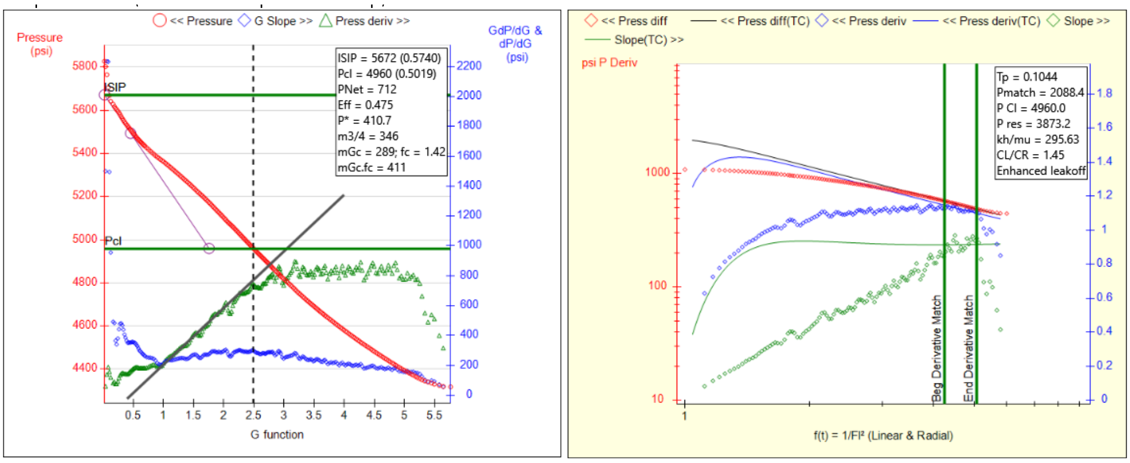

Res. Pressure – 3870 psi; Kh/mu – 295 md*ft/cp (90 md*m/cp) – medium confidence

Figure 128 – Closure pressure – 4960 psi (gradient 0.50 psi/ft)

Step-rate test (decline after final step completed in Step-down mode) (figure 129).

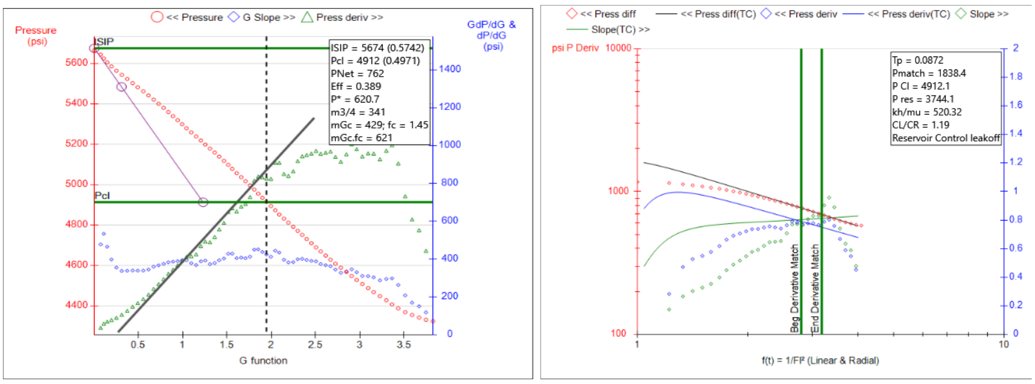

Res. Pressure – 3745 psi; Kh/mu – inconclusive

Figure 129 – Closure pressure – 4910 psi (gradient 0.50 psi/ft)

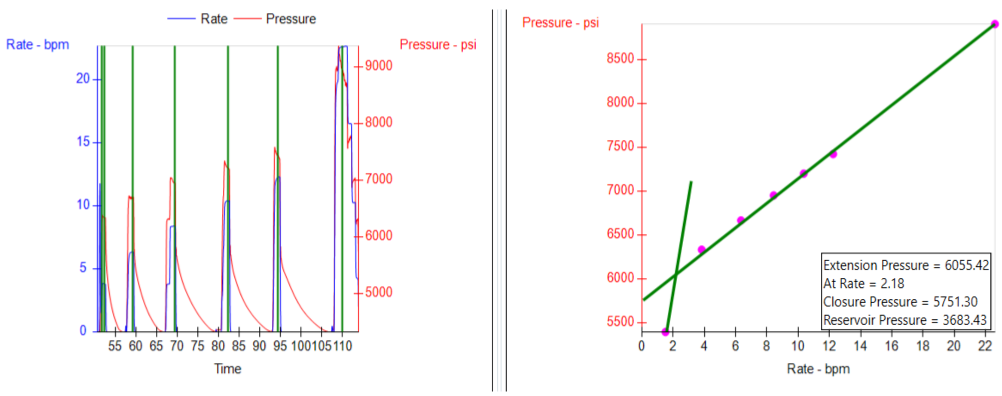

Res. Pressure – 3600-3800 psi (approximate value due to absence of matrix mode points)

Figure 130 – Upper bound for the closure pressure – 5750 psi

Step-rate test dynamic analysis (figure 130).

Closure pressure – 4915 psi (gradient 0.50 psi/ft) : Res. Pressure – not reached Fluid efficiency – 50% (figure 131).

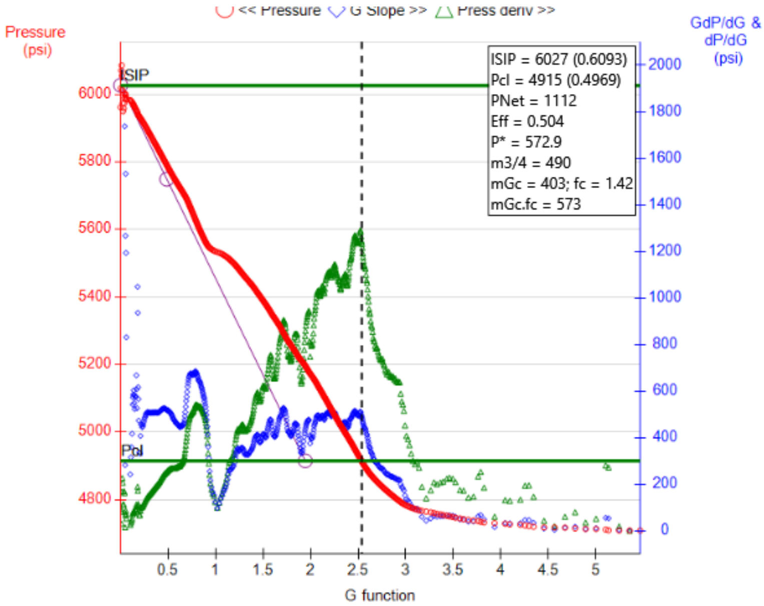

Figure 131 – Decline after the calibration

Conclusions from the diagnostic tests analysis

1. Minimum horizontal stress gradient is ~0.49 psi/ft

2. There is no height recession signature in injection tests, which means the simple 2 fracture walls opening in the net pay without significant growth into barriers for all tests. High Net pressure during calibration is also explained by this fact.

3. The short apparent enhanced leakoff observed during the early period of Step-rate test decline is an artefact of the slight fracture geometry variations because of the fracture opening and closure during previous step-rate tests.

4. The fact that calibration test's closure pressure is almost equal to that of the injection test means that there are no distinctive weak thin layers.

5. Calibration test opened the whole kh of the target sand layer.

5.10 Temperature log analysis

After the calibration test, the temperature log was run, to estimate the top and bottom of the fracture. Unlike in well A-210, the quality of temperature log in A-233 was much higher.

On the left figure 132 below, the 3 temperature profiles are given. They represent 3 down passes: first, then after 2 hours the second pass, then after 3 more hours the third pass. In order to distinguish the fracture signatures and increase sensitivity of the data, the warmback dynamics plot is shown on the right, it presents the difference in temperature between pass 2 and pass 1, and between pass 3 and pass 2.

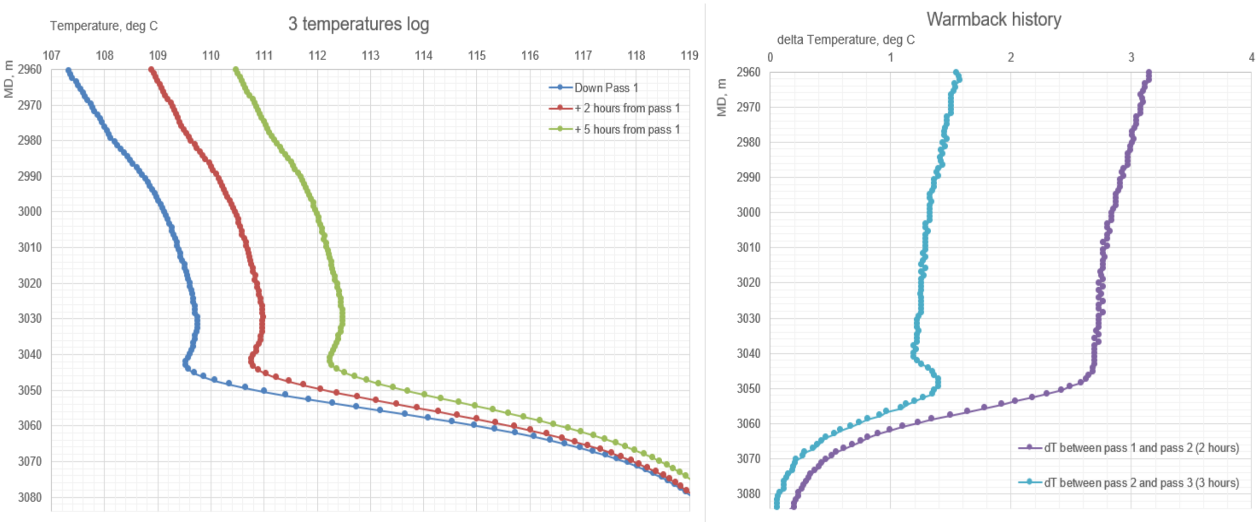

Figure 132 – Temperature logs

Conclusions from the temperature logs

1. The fracture bottom is located at 3040-3045, with the more permeable part ending at 3040 (warmback plot between pass 1 and pass 2 shows the beginning of the so-called "nose"), and less permeable (bottom tip) of the fracture at 3041-3045.

2. Several distinct intervals with uniform warmback inside the fracture can be seen on the blue line (warmback between pass 1 and pass 2). Uniform warmback may indicate that this part of the fracture is hydrodynamically uniform, and potentially has more or less uniform width and near-wellbore pack width. These intervals are: 3030-3040; 3018-3028; 3005-3010. The interval 3018-3028 is showing the vertical line on both warmback lines, which means this can be the most conductive part of the fracture which received the main mass of frac fluid. The intervals with uniform warmback are matching the lithological layers, which means that the fracture width is following the lithology profile (maximum width in cleaner sandstone, less width in more shaly zones).

3. The top of the fracture is somewhere in interval 2994-2996, because above this depth the warmback line doesn't show any layers with uniform warmback. However, the top of most conductive part of the fracture is somewhere between 3005 and 3010.

Fracture model calibration.

Based on the injection test, calibration test, and temperature log data, the model of the reservoir was calibrated.

On the plot below, the purple fracture contour (third track from the right) represents the fracture created during calibration test, this fracture results from the net pressure and fluid efficiency match.

Then, on the calibrated model, the actual propped job schedule was run. The Advanced Multiphysics software Kinetix (refer to 2.5 for details of the Advanced Multiphysics simulation) was used to recalibrate the fracture design.

The use of advanced proppant transport software helped to understand the key feature of the fracture:

1. The proppant tends to accumulate in narrow 3020-3024 m layer.

2. The most productive part is concentrated in 3011-3024 m layer.

3. The fracture have drop from 3 proppant grain width to less than 3 proppant grain width somewhere at 60-70 m half-length. Considering that part of the proppant pack will be embedded into the rock, and that the retained permeability of the given gel is below 45%, most probably the effective half-length doesn't exceed 70 meters, whereas the propped half-length is approaching 110-115 m, which means effective to propped length ratio of about 60-65% (figure 133).

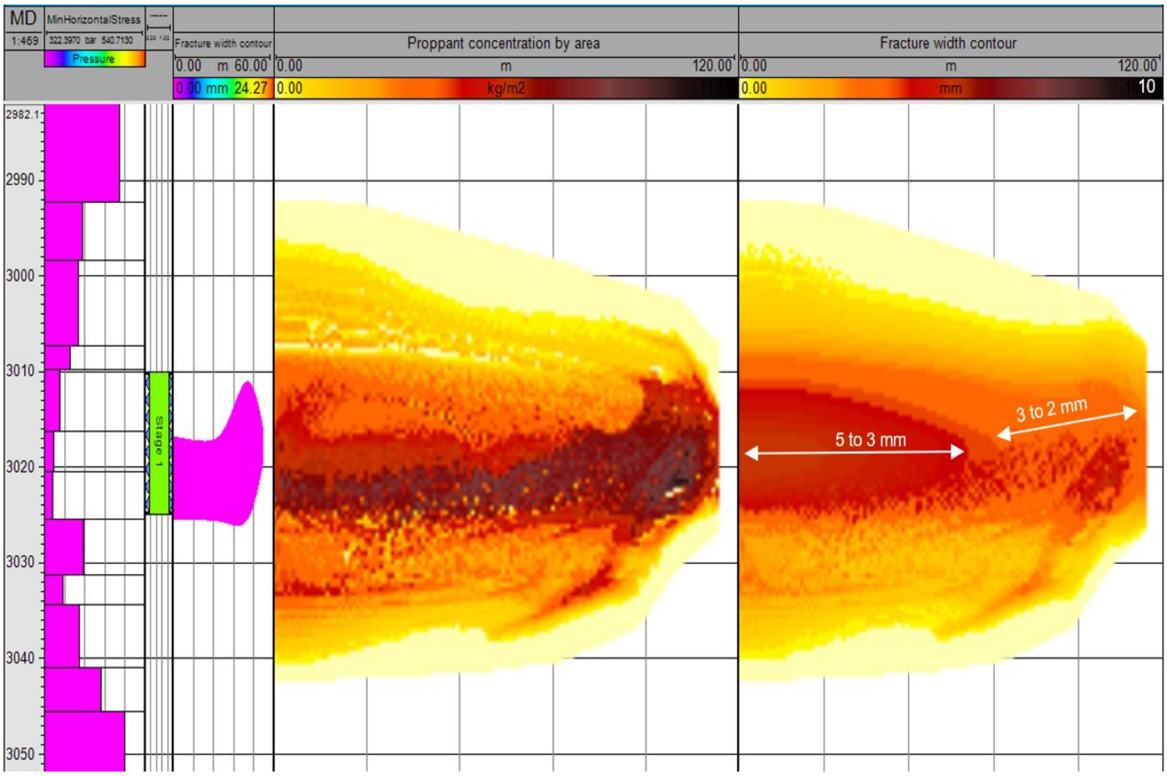

Figure 133 – Recalibrate the fracture design

From the calibrated model, the following recommendations should be considered for lower permeability, higher fluid efficiency (>45%) wells like A-233, in order to increase the effective half-length:

1. Consider gradual replacement of some PAD volume from crosslinked to linear gel in the beginning of PAD stage. Start with replacement of 20% of X-linked PAD to linear gel, on first well, then try 30% on the next well. After each job analyze the net pressure gain. Stop increasing linear gel percentage if the net pressure gain becomes too aggressive.

Consider addition of 20/40 or 30/50 proppant in the initial stages of jobs if the fracture half-length exceeds 100 meters for wells with efficiency more than 45%. It may help to prop the near-tip region (10-20 m) of the fracture.

Note on pressure drops

During production at A-233, the pressure drops was observed. It may indicate proppant flowback and fracture choke effect at interval 3010-3014 m, where the proppant concentration is lower (see the fracture plot above), causing apparent skin increase.

5.11 Production Decline Analysis

In order to estimate how the fracture conductivity and half-length deterioration with time affect the production, the following study was performed.

The well A-223 was taken for analysis (since it contains long production history data after hydraulic fracturing) (figure 134). The hydraulic fracturing report was checked, corrected a bit, and this corrected fracture geometry was taken for estimations. Assuming the effective to total length ratio defined in 3.4, the initial fracture's dimensionless conductivity and apparent Skin from Pratt's correlation were calculated. Then, using the historical reservoir pressure, bottomhole flowing pressure and apparent skin, the Calculated Rate was estimated, to define the rate which the given hydraulic fracture should provide. This is performed for 5 random points in the past, when the production was stable. Note that the adjustment of facture half-length, and apparent skin is performed for each point, based on the expected fracture deterioration experience in the similar reservoirs.

The comparison showed that for the given skin evolution scenario (refer to table below), the actual fracture behaviour shows satisfactory match with calculations. Some discrepancy in points B and C can be caused by error in reservoir/bottomhole flowing pressure data input, or by the production restriction factors like non-optimum ESP regime, scaling etc [81].

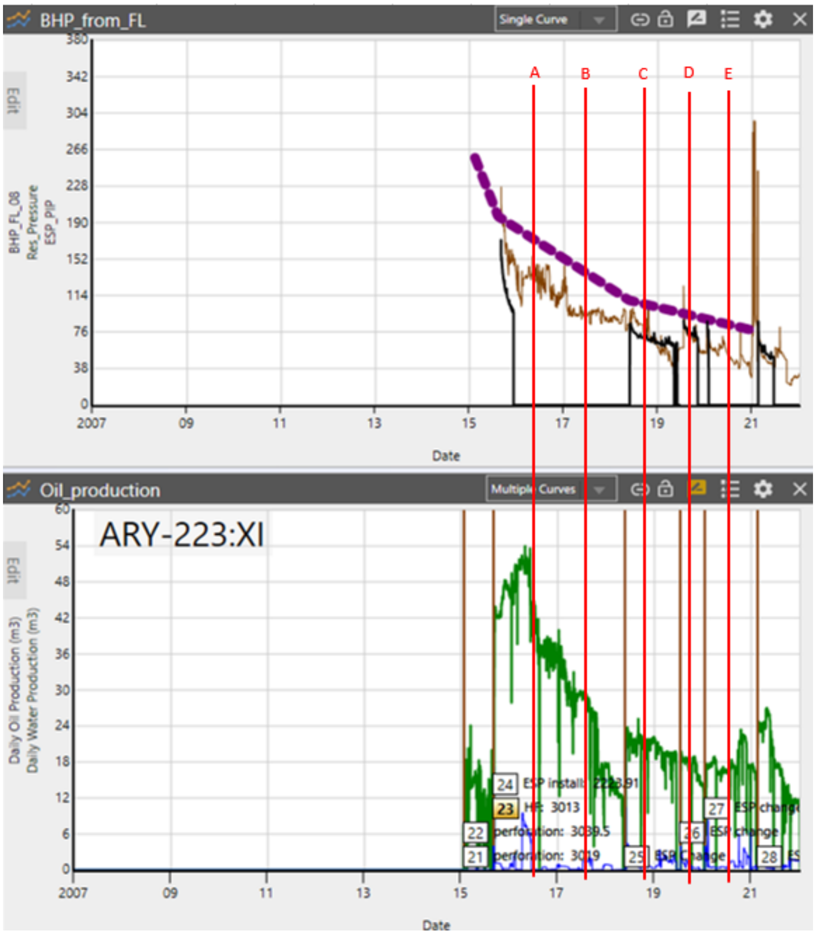

Figure 134 – Production decline

Overall, this analysis indicates that for the observed actual drawdowns and rates, the fracture keeps low skin for an extended period, and *the major driver of the production drop is the depletion of the reserves in a drainage radius* (table 8).

Table 8 – Actual fracture behavior for the given skin evolution scenario

Fracture behavior	A - Sep 2015	B - Mar 2017	C - End 2018	D - Autumn 2019	E - Mid 2020
Xf propped (report), m	120	120	120	120	120
Xf eff (assumption), m	70	55	45	40	35
Fcd (report)	5.5	4.5	4.0	3.5	2.5
Apparent Skin from Pratt's correl.	*-5.4*	*-4.9*	*-4.8*	*-4.7*	*-4.5*
P reservoir, atm	190	142	112	95	80
P wf at bh, atm	150	98	80	75	55
Kh, md*m	80-100				
Re, ft	500				
Rw, ft	0.33				
Rate calculated, m^3/d	48	35	25	17	17
Rate actual, m^3/d	47	30	21	18	17

Since the depletion is the key driver of production drop, the fluid efficiency decrease will be a common trend for the next jobs. In this case, the following recommendations should be considered.

Compensation of the fluid efficiency loss should be performed with the following methods:

1. Introduce fluid loss additives. One of such examples are degradable fibers. Addition of degradable fibers, to the PAD stage (e.g. to the first 30% of PAD), can increase fluid efficiency by 5%, depending on severity of the depletion and concentration of fibers.

2. Increase the pumping rate, according to the design.

3. Increase of viscosity by 50-200 cP (adjust ratio of crosslinkers and buffering agents, then if it doesn't help – increase gel concentration etc). This will lead to increase of the proppant pack damage; thus the breaker schedule aggressiveness should be increased as well. If the gel concentration exceeds 40 pounds per 1000 gal, then further increase of gel concentration is not recommended.

4. Increase of the proppant mass volume with increase of proppant ramp aggressiveness (start with trying 10% faster ramp up, 10% more proppant at higher concentrations). At the same time, PAD volume should not be increased significantly, because it will be difficult to extract extra fluid. As for the proppant mass sensitivity – please refer to the following plots.

Below is the table of sensitivity runs, showing the half-length gain for non-depleted and depleted formations.

Main conclusion from these plots is that starting from 100 tons (for non-depleted) and 80 tons (for depleted reservoirs) – the efficiency of each added ton of proppant is decreasing, because the more gel is used, and the more difficult to extract gel residue from the fracture tip. In other words, the Effective to total half-length ratio is decreasing starting from 80 tons (depleted case) and 90-100 tons (non-depleted case).

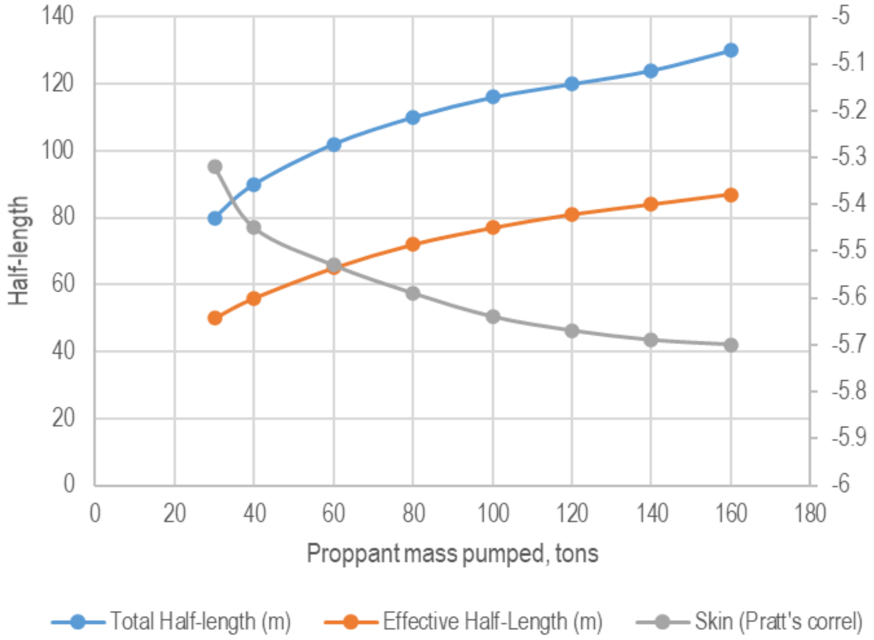

Figure 135 – Non-depleted case (fluid efficiency 25-35% for A-210, reservoir pressure ~200-220 bar)

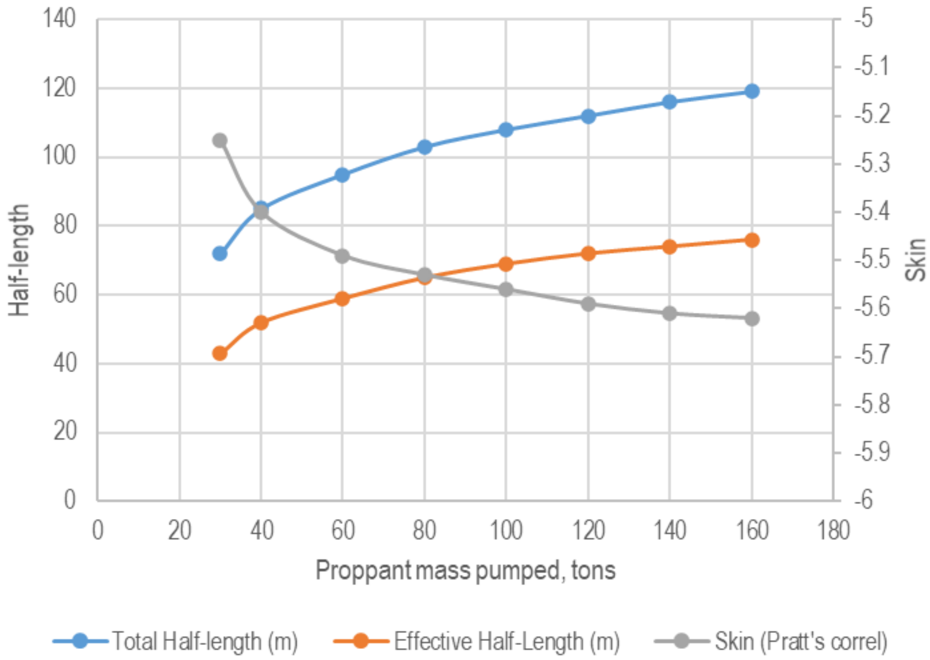

Figure 136 – Moderately depleted case (fluid efficiency 18-22% for A-210, reservoir pressure ~120-140 bar)

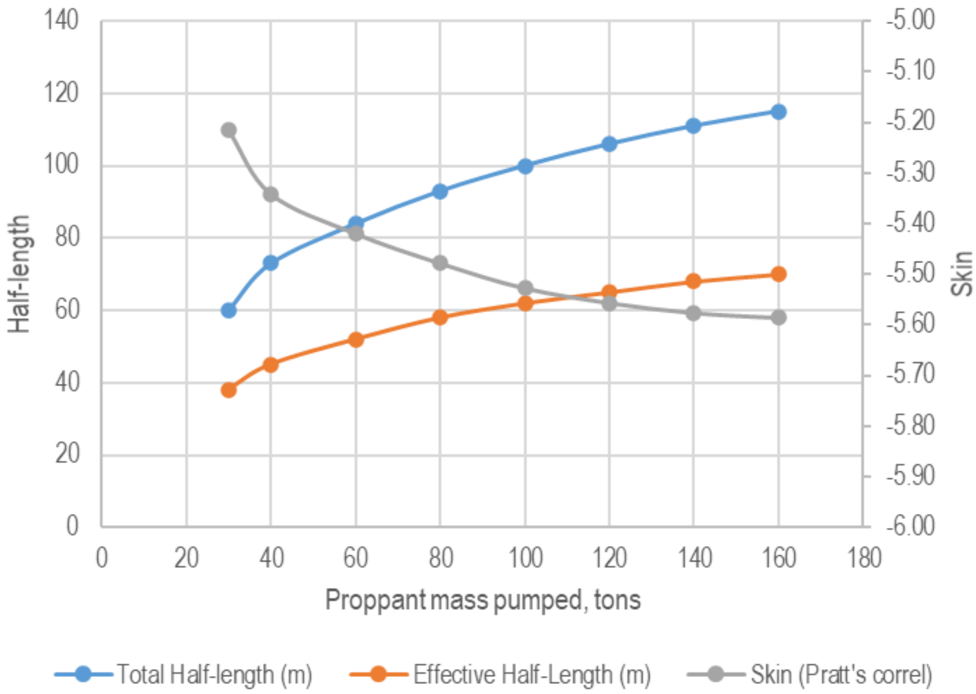

Figure 137 – Moderately depleted case (fluid efficiency 14-18% for A-210, reservoir pressure ~100-120 bar)

Based on the figures 135, 136, 137 above, the following table 9 was summarized.

Table 9 – Sensitivity run for non-depleted and depleted reservoirs

Job vol, tons	FE= 25-35% (well A-210)			FE= 18-22% (well A-210)			FE= 13-18% (well A-210)		
	Xf tot	Xf eff	Skin (P)	Xf tot	Xf eff	Skin (P)	Xf tot	Xf eff	Skin (P)
30	80	50	-5,32	72	43	-5,25	60	38	-5,21
40	90	56	-5,45	85	52	-5,4	73	45	-5,34
60	102	65	-5,53	95	59	-5,49	84	52	-5,42
80	110	72	-5,59	103	65	-5,53	93	58	-5,48
100	116	77	-5,64	108	69	-5,56	100	62	-5,53
120	120	81	-5,67	112	72	-5,59	106	65	-5,56
140	124	84	-5,69	116	74	-5,61	111	68	-5,58
160	130	87	-5,7	119	76	-5,62	115	70	-5,59

Where FE stands for Fluid efficiency, Xf tot – the total fracture half-length, Xf eff – effective fracture half-length, Skin (P) – skin calculated from Pratt’s correlation, first month after the job. For Skin deterioration trends, please refer to the table shown previously in Section 4 of this report.

Note on Fracturing feasibility:

At certain point of depletion, the fracturing may become not profitable even for permeable reservoirs. It may happen when the pumped fluid cleanup time and the pay-out time of the fracturing job significantly extends. Since it is a matter of economic indicators, this “profitability” point greatly depends on the market situation.

The table 10 below provides an example, based on well A-233, that for reservoir pressure below 60 atm, bottomhole flowing pressure below 25 atm, and assuming "clean" revenue from bbl as 25 USD, the fracturing job with 60 tons can still be profitable, if fluid efficiency is about 30-50%

Table 10 – Profitability of the project (FE = 30-50%)

P res (psi/atm)	1911	130	P res (psi/atm)	1176	80	P res	808.5	55
P wf (psi/atm)	1323	90	P wf (psi/atm)	588	40	P wf	367.5	22
S	-5.2	-	S	-4.5	-	S	-4.4	-
Rate, bopd	127	-	Rate, bopd	100	-	Rate, bopd	73	-
Rate, m3/d	20	-	Rate, m3/d	16	-	Rate, m3/d	12	-
Incremental prod in 1 year	22826	-	-	17997	-	-	13102	-
Incr. revenue at 25 USD per bbl revenue	570646	-	-	449929	-	-	327548	-

However, as fluid efficiency drops, the effective half-length drops as well, causing less efficient fracture and longer cleanup. This situation may end up in fracture being non-profi table 11 as reservoir depletes below 60 atm in drainage zone, even if all precautions and mitigation measures were taken (mentioned in section 5).

Table 11 – Profitability of the project (if FE drops)

P res (psi/atm)	1617	110	P res (psi/atm)	1029	70	P res	808.5	55
P wf (psi/atm)	882	60	P wf (psi/atm)	441	30	P wf	367.5	25
S	-5.1	-	S	-4.2	-	S	-4	-
Rate, bopd	153	-	Rate, bopd	92	-	Rate, bopd	65	-
Rate, m3/d	24	-	Rate, m3/d	15	-	Rate, m3/d	10	-
Incremental prod in 1 year	22889	-	-	13751	-	-	9772	-
Incr. revenue at 25 USD per bbl revenue	572481	-	-	343773	-	-	244292	-

Conclusions on the 5th section

Fluids and Laboratory:

– consider decrease of gel loading of guar-based polymer by 5 pounds per thousand gallons, and increase of breaker delivered into the fracture (e.g. putting extra breaker into the flush) – to increase the Effective fracture length;

– consider performing Intermediate laboratory tests between the fracturing jobs in High-pressure – high temperature equipment, at least once every 5 jobs, or when new fluid is involved, and/or reservoir temperature changes by more than 10ºC.

Fracturing Treatment Strategy in depleting formation:

– as shown by production decline analysis, the key mechanism of the production decline for given fractured wells is the reservoir depletion;

– increase of pumping rate and proppant volume (from 45 t to 65 t) provides less than 10% of fracture half-length increase due to increased leak-off in depleted reservoir. Propped half-length gain per 1 ton of extra proppant is decreasing significantly once the job volume exceeds 60-70 tons. The significant portion of the effect from added propped half-length proppant is compensated by the added damage from the added polymer required to deliver extra proppant;

– consequently, main strategy to deal with depleting reservoir is to increase the effective fracture half-length via several options, the most remarkable are: i) to minimize fluid volumes pumped into formation, use more aggressive PAD percentage, eliminate extra pumping stages like SRT, double injection test, because injection combined with SDT or SRT may be enough; ii) use cleaner fluids, like the ones based on Cellulose or on the Viscoelastic Surfactants; iii) use bigger proppants whenever possible, or more conductive proppant type;

From the calibrated model, the following recommendations should be considered for lower permeability, higher fluid efficiency (>45%) wells like A-233, in order to increase the effective half-length:

– consider gradual replacement of some PAD volume from crosslinked to linear gel in the beginning of PAD stage. Start with replacement of 20% of X-linked PAD to linear gel, on first well, then try 30% on the next well. After each job analyse the net pressure gain. Stop increasing linear gel percentage if the net pressure gain becomes too aggressive;

– consider addition of 20/40 or 30/50 proppant in the initial stages of jobs if the fracture half-length exceeds 100 meters for wells with efficiency more than 45%. It may help to prop the near-tip region (10-20 m) of the fracture;

– consider channel fracturing technique, which can provide up to 50% effective fracture half-length increase (based on well A-210 estimation) for the same volume of proppant pumped in comparison with the conventional propped fracturing techniques; in addition, channel fracturing techniques will allow to optimize future costs by replacement of expensive proppant by the regular cheap sand;

– there is a certain limit of profitability, which may happen at fluid efficiencies below 13%, and assuming clean revenue less than 30 USD/bbl, independently on measures taken to increase the fracture effective length.

Fracture and Reservoir understanding:

1. Fracture height was successfully determined with acoustic methods. It was revealed that good calibration can provide frac height which is in satisfactory match with the actual fracture height. Acoustic methods showed higher precision than temperature logs [82].

2. WNW-NW is the max stress direction in the zone of well A-210.

3. Multiphysics advanced proppant transport modelling was applied for analysis of the internal fracture structure. It helped to reveal the effective half-length, and proppant distribution.

4. Fracture length was derived from the actual frac height. Maximum propped frac length is in range 90-95 m for well A-210, and 115 meters for well A-233; effective half-length is about 60% of this length.

5. Temperature logs helped to calibrated fracture height for well A-233 with

good precision, because logs were recorded with higher frequency than on well A-210.

6. Reservoir pressure and kh/mu were determined (refer to technical details in report).

7. Fracture geometry development during injection test were defined: the strong PKN type in linear gels, with extent of height into the whole net pay at viscous stages, and further continuation of PKN-type growth.

8. Refracturing doesn’t result in fracture propagation in different azimuth, or fracture plane twisting. Most probably, refracturing will happen in parallel to existing fracture, close to it.

CONCLUSIONS

The goal of this dissertation is optimization of fracturing treatments in depleted Arystan field reservoirs and to identify the optimal combination of factors that is resulted in the largest increase in production at the lowest incremental cost.

The process of optimizing a well stimulation treatment is complex and involves evaluating a large number of variables and their interactions. There are typically many possible solutions to this problem, as the different stimulation materials and their associated costs can be combined in various ways to achieve the desired result. The challenge is to consider all of the relevant variables and their associated risks to arrive at the true optimal solution. This requires the use of advanced computer technology and modeling techniques to simulate the reservoir and fracture behavior and to evaluate the impact of different design parameters on the overall performance of the well. By leveraging the power of modern computer technology enables accurately and efficiently evaluate different stimulation treatment options to arrive at the optimal solution.

A wide range of factors was considered, including Intersect based reservoir simulation and fracturing model(by utilizing EZ frac), fluid properties, wellbore configuration, fracture design, material selection, and economic considerations.

Her is a list of main outcomes:

1. The objectives of the simulation study has been defined.
2. The key parameters that impact oil recovery and well productivity has been identified [83].
3. The results of the simulation model to identify the most sensitive parameters has been analyzed [84].
4. The parameter values one at a time to determine their individual impact on oil recovery and well productivity has been adjusted.
5. The results of the sensitivity analysis to identify the most influential parameters has been analyzed [85].
6. The sensitivity analysis results to develop a plan to optimize oil recovery and well productivity has been performed [86].
7. Hydraulic fracturing approach and model to incorporate the insights gained from the sensitivity analysis has been reviewed.
8. Integrated laboratory and simulation methods for scale analysis to understand well productivity decline has been performed.
9. The findings from the well productivity analysis into the hydraulic fracturing modeling and simulation study has been incorporated.
10. Advanced methods of fracture geometry analysis and fracture parameter sensitivity study to further optimize the hydraulic fracturing approach and simulation model has been performed.

Recommendation

During dissertation work the main concerns were related to reservoir characterization, HF design and fractures properties, actual contributed factor for well productivity decline , re-frac sensitivities(stress rotation that effect fracture orientation after significant local pressure decline). Additional study of petrophysical properties of horizons J-V, J-VI, J-VII, J-VIII, J-IX. Highly recommend taking core samples and execute special core analysis (SCAL) which should provide measurement:

1. Relative Permeability.
2. Capillary pressure.
3. Wettability Determination.
4. Reservoir Condition Corefloods.
5. Permeability relationships for downhole logging calibration.
6. Archie Exponents - a, m, n.
7. Core Mechanical Properties.
8. Pore Volume Compressibility.

To reduce uncertainty in water production of ARYSTAN crestal part wells:

Production Logging Tool (PLT) which provides a complete solution for acquiring, recording, and processing downhole well production data to indicate flow intervals. But in mechanical exploitation PLT applicable in casing more than 95/8 inches with using Y-tool.

Pulsar – standalone cased hole formation evaluation and reservoir saturation monitoring in low resistivity pay. Provides all the necessary measurements thru casing to estimate mineralogy, accurate porosity, water-, oil- and gas-saturation and current fluid contact positions. Recommended for evaluation of bypassed hydrocarbon reservoirs or reservoir saturation monitoring thru casing.

USIT (or IBS) ultrasonic imager delivers an accurate, comprehensive, high-resolution confirmation of the pipe-to-cement bond quality and downhole pipe condition in real time. Casing inspection and monitoring applications include corrosion detection, identification of internal and external damage or deformation, and casing thickness analysis for collapse and burst pressure calculations.

Extended data acquisition could include CMR Plus and Dielectric Scanner estimate independent porosity and saturation analysis. Combined interpretation provides porosity, pore size distribution, water saturation, irreducible water saturation, movable and residual hydrocarbons.

REFERENCES

1 Durmagambetov B., Urmanova D., Temirkhasov A. Geological and geochemical features of an oil field of precaspian region // Neft i Gaz. – 2022. – Vol. 2. – P. 32-41.

2 Urmanova D. et al. Geological and hydrodinamic modeling of an oil field of the pricaspian region of the republic of Kazakhstan // News of the National Academy of Sciences of the Republic of Kazakhstan. – 2022. – Vol. 5, №455. – P. 266-288.

3 Economides M.J., Nolte K.G. Reservoir stimulation. – Ed. 3rd. – NY.: John Wiley & Sons, 2000. – 856 p.

4 Avansi G.D., Maschio C.L., Schiozer D.J. Simultaneous history-matching approach by use of reservoir-characterization and reservoir-simulation studies // SPE Reservoir Evaluation and Engineering. – 2016. – Vol. 19, №4. – P. 694-712.

5 Nagar A., Verma N., Shrivastava P. et al. Effective Wellbore Cleanup and Improvement of Injection Performance and Conformance Using Coil Tubing Conveyed Tool for Waveform Dominated Fluid Dispersion and Pin-Point Chemical Placement During Well Stimulation // Procced. the SPE/ICoTA Well Intervention conf. and Exhibition. – Texas, 2020. – P. 36-53.

6 Zeng L. et al. Variation in the orientation of the maximum horizontal stress in thick channel-fill sandstones with low-permeability: A case of the Bonan Oilfield in the Bohai Bay Basin, eastern China // Mar Pet Geol. Elsevier Ltd. – 2019. – Vol. 107. – P. 32-40.

7 Chao Z. et al. Prediction of the shale gas permeability: A data mining approach // Geomechanics for Energy and the Environment. – 2023. – Vol. 33. – P. 100435.

8 Slotte P.A., Smørgrav E. Response Surface Methodology Approach for History Matching and Uncertainty Assessment of Reservoir Simulation Models // https://onepetro.org/SPEEURO/proceedings-abstract/08EURO. 10.05.2020.

9 Sakha M., Nejati M., Driesner T. On the initiation of hydraulic fractures in anisotropic rocks // International Journal of Rock Mechanics and Mining Sciences. – 2023. – Vol. 169. – P. 105429.

10 Li M. et al. Modeling method for rock heterogeneities and multiple hydraulic fractures propagation based on homogenization approach and PHF-LSM // Geomechanics for Energy and the Environment. – 2023. – Vol. 33. – P. 100442.

11 Laloui L. et al. Geomechanics for Energy and the Environment: Current developments // Geomechanics for Energy and the Environment. – 2022. – Vol. 32, №8. – P. 100345.

12 Li J. et al. Numerical simulation of 3D fracture propagation in wellbore strengthening conditions // J Pet Sci Eng. – 2017. – Vol. 156. – P. 258-268.

13 Ju W., Wu C.F., Wang K. et al. Prediction of tectonic fractures in low permeability sandstone reservoirs: A case study of the Es3m reservoir in the Block Shishen 100 and adjacent regions, Dongying Depression // J Pet Sci Eng. – 2017. – 2017. – Vol. 156. – P. 884-895.

14 Li S., Zhou Z. et al. One CT imaging method of fracture intervention in rock hydraulic fracturing test // J Pet Sci Eng. Elsevier B.V. – 2017. – Vol. 156. –

P. 582-588.
15 Wrobel M., Papanastasiou P., Dutko M. On the pressure decline analysis for hydraulic fractures in elasto-plastic materials // Geomechanics for Energy and the Environment. – 2023. – Vol. 33. – P. 100421.
16 Adachi J.I., Detournay E. Plane strain propagation of a hydraulic fracture in a permeable rock // Eng Fract Mech. – 2008. – Vol. 75, №16. – P. 4666-4694.
17 Xu C., Li P., Lu D. Production performance of horizontal wells with dendritic-like hydraulic fractures in tight gas reservoirs // J Pet Sci Eng. – 2017. – Vol. 148. – P. 64-72.
18 Ostojic J., Rezaee R., Bahrami H. Production performance of hydraulic fractures in tight gas sands, a numerical simulation approach // J Pet Sci Eng. – 2012. – Vol. 88-89. – P. 75-81.
19 Sarmadi N., Mousavi Nezhad M. Phase-field modelling of fluid driven fracture propagation in poroelastic materials considering the impact of inertial flow within the fractures // International Journal of Rock Mechanics and Mining Sciences. – 2023. – Vol. 169. – P. 105444.
20 Guha Roy D., Singh T.N. Effect of heat-treatment on the pure- and mixed-mode fracture properties of a homogeneous sandstone // Geomechanics for Energy and the Environment. – 2023. – Vol. 33. – P. 100430.
21 Adachi J. et al. Computer simulation of hydraulic fractures // International Journal of Rock Mechanics and Mining Sciences. – 2007. – Vol. 44, №5. – P. 739-757.
22 Nolte K.G. Hydraulic fracturing modeling: A review of recent work // Journal of Petroleum Technology. – 1979. – Vol. 31, Issue 2. – P. 235-242.
23 Hatambeigi M. et al. Wellbore cement fracture permeability as a function of confining stress and pore pressure // Geomechanics for Energy and the Environment. – 2023. – Vol. 33. – P. 100428.
24 Roque W.L. et al. Production zone placements based on maximum closeness centrality as strategy for oil recovery // J Pet Sci Eng. – 2017. – Vol. 156. – P. 430-441.
25 Le D.H. et al. Removal of fracturing gel: A laboratory and modeling investigation accounting for viscous fingering channels // J Pet Sci Eng. – 2012. – Vol. 88-89. – P. 145-155.
26 Chen Z. Finite element modelling of viscosity-dominated hydraulic fractures // J Pet Sci Eng. – 2012. – Vol. 88-89. – P. 136-144.
27 Dontsov E., Peirce A. Development of a hydraulic fracture model with a level set representation of the propagating crack // Computational Mechanics. – 2015. – Vol. 56, Issue 6. – P. 1021-1037.
28 Guo C. et al. Experimental study and numerical simulation of hydraulic fracturing tight sandstone reservoirs // Fuel. – 2015. – Vol. 159. – P. 334-344.
29 Osiptsov A.A. Fluid Mechanics of Hydraulic Fracturing: a Review // J Pet Sci Eng. – 2017. – Vol. 156. – P. 513-535.
30 Yang C. et al. Rapid multistage hydraulic fracture design and optimization in unconventional reservoirs using a novel Fast Marching Method // J Pet Sci Eng. – 2017. – Vol. 156. – P. 91-101.
31 Adachi J., Siebrits E., Tijsseling A. Numerical simulation of hydraulic

fracturing using the extended finite element method // Computers & Geosciences. – 2010. – Vol. 36, Issue 4. – P. 474-482.

32 Chen Y. et al. Thermal mechanical behavior of energy piles with cap under embedded depth // Geomechanics for Energy and the Environment. – 2023. – Vol. 33. – P. 100425-1-100425-12.

33 Worthington P.F. A scaled perspective on permeability: How to get the best from what we have // J Pet Sci Eng. – 2017. – Vol. 156. – P. 212-219.

34 Hashemi A., Sutman M., Medero G.M. A review on the thermo-hydro-mechanical response of soil–structure interface for energy geostructures applications // Geomechanics for Energy and the Environment. – 2023. – Vol. 33. – P. 100439.

35 Li Y. et al. A particle-scale investigation of mechanical behavior of cemented hydrate-bearing sediment using Discrete Element Method // Geomechanics for Energy and the Environment. – 2023. – Vol. 33. – P. 100436.

36 Guo J., Yang H., Yan H. Sealing failure of a cement sheath under temperature variation // Geomechanics for Energy and the Environment. – 2023. – Vol. 33. – P. 100429-1-100429-14.

37 Paredes M.P. et al. A Novel Chemical Treatment and Well Completion Strategy to Prevent Scale and Production Losses in Shushufindi Aguarico Field // https://search.spe.org/i2kweb/SPE/doc/onepetro:0994E248/. 11.04.2021.

38 Kamali F., Hussain F. Field-scale simulation of CO2 enhanced oil recovery and storage through SWAG injection using laboratory estimated relative permeabilities // J Pet Sci Eng. – 2017. – Vol. 156. – P. 396-407.

39 Elgaddafi R., Ahmed R., Shah S. Modeling and experimental studies on CO2-H2S corrosion of API carbon steels under high-pressure // J Pet Sci Eng. – 2017. – Vol. 156. – P. 682-696.

40 Zhang D. et al. Investigation of Multi-Scale Approach for Damage Control in Ultra-Deep Tight Sandstone Gas Reservoirs Based on the Multi-Scale Formation Damage Mechanisms // Proceed. 11th internat. Petroleum Technology conf. – Beijing, 2019. – P. 1-17.

41 Azari V. et al. Scale Treatment Optimization in Geothermal Wells // https://onepetro.org/SPEEURO/proceedings-abstract/20EURO/2-20. 10.09.2020.

42 Jarrahian K. et al. Building a Fundamental Understanding of Scale-Inhibitor Retention in Carbonate Formations // SPE Production and Operations. – 2020. – Vol. 35, №1. – P. 85-97.

43 Jordan M.M. Management of Scale Control in Produced Water Reinjection - The Near Wellbore Scale Challenge Overcome // https://onepetro.org/SPEOSS /proceedings-abstract/18OSS/2-18OSS/D021S006R001/216101. 10.08.2020.

44 Crowe C. et al. Scale Inhibition in Wellbores // https://onepetro.org /speutcpes/proceedings-abstract/94UTCPES/All-94UTCPES/SPE-27996. 10.08.2020.

45 Heath S. et al. The Importance of Scale Inhibitor Analysis in Scale Management-A State of the Art Overview to Provide Cost Effective Scale Control from Simple to Complex Production Scenarios // https://onepetro.org/SPEOSS /proceedings-abstract/16OSS/All-16OSS/192655. 05.07.2020.

46 Wang Z. et al. How and Why Does Scale Stick-Can the Surface Be Engineered To Decrease Scale Formation and Adhesion? // https://onepetro.org/

SPEOSS/proceedings-abstract/05OSS. 10.04.2020.
47 Oddo E. Why Scale Forms and How To Predict It // SPE Prod & Fac. – 1994. – Vol. 9, №01. – P. 47-54.
48 Wang W., Wei W. Silica and Silicate Scale Formation and Control: Scale Modeling, Lab Testing, Scale Characterization, and Field Observation // https://www.sci-hub.ru/10.2118/179897-ms. 05.04.2020.
49 Sedaghat A. A novel and robust model for determining rheological properties of Newtonian and non-Newtonian fluids in a marsh funnel // J Pet Sci Eng. – 2017. – Vol. 156. – P. 896-916.
50 Mi L. et al. An Enhanced Discrete Fracture Network model to simulate complex fracture distribution // J Pet Sci Eng. – 2017. – Vol. 156. – P. 484-496.
51 Chen D. et al. Characteristic of anisotropic coal permeability and its impact on optimal design of multi-lateral well for coalbed methane production // J Pet Sci Eng. – 2012. – Vol. 88-89. – P. 13-28.
52 Zhang W., Al Kobaisi M. A two-step finite volume method for the simulation of multiphase fluid flow in heterogeneous and anisotropic reservoirs // J Pet Sci Eng. – 2017. – Vol. 156. – P. 282-298.
53 Azadi M., Aminossadati S.M., Chen Z. Development of an integrated reservoir-wellbore model to examine the hydrodynamic behaviour of perforated pipes // J Pet Sci Eng. – 2017. – Vol. 156. – P. 269-281.
54 Luo X., Jiang G., Yang L. Experimental investigation of formation damage during drilling of ultradeep fractured carbonate reservoir // Geomechanics for Energy and the Environment. – 2023. – Vol. 33. – P. 100437.
55 Wang S. et al. Experimental study on fracture characteristics of coal due to liquid nitrogen fracturing // Geomechanics for Energy and the Environment. – 2023. – Vol. 33. – P. 100438.
56 Bijay K.C., Ghazanfari E., Frash L.P. Experimental study of fracture slip due to stress perturbation in fractured geo-resources // Geomechanics for Energy and the Environment. – 2023. – Vol. 33. – P. 100423.
57 Yang H., Kim J., Choe J. Field development optimization in mature oil reservoirs using a hybrid algorithm // J Pet Sci Eng. – 2017. – Vol. 156. – P. 41-50.
58 Wu K., Olson J.E. Numerical investigation of complex hydraulic-fracture development in naturally fractured reservoirs // SPE Production and Operations. Society of Petroleum Engineers (SPE). – 2016. – Vol. 31, №4. – P. 300-309.
59 Musso G. et al. Hydro-mechanical behaviour of a cement–bentonite mixture along evaporation and water-uptake controlled paths // Geomechanics for Energy and the Environment. – 2023. – Vol. 33. – P. 100413.
60 Kadkhodaie A., Rezaee R. Have you ever heard the sound of well logs or reservoir data? // J Pet Sci Eng. – 2017. – Vol. 156. – P. 340-347.
61 Shedid S.A., Saad M.A. Comparison and sensitivity analysis of water saturation models in shaly sandstone reservoirs using well logging data // J Pet Sci Eng. – 2017. – Vol. 156. – P. 536-545.
62 Wang X. et al. Studying reservoir heterogeneity by Analytic Hierarchy Process and Fuzzy Logic, case study of Es1x formation of the Wang guan tun oilfield, China // J Pet Sci Eng. – 2017. – Vol. 156. – P. 858-867.

63 Durmagambetov B.O., Tulebayeva R.A., Mukhanov A.Zh. Use of a special log complex for studying the properties of reservoir fluids and rocks of the sediments of the cretaceous and jurassic ages of the Arystanovskoye field // Neft i Gaz. – 2022. – Vol. 132, №6. – P. 6-18.

64 Lai Y. et al. Fractal characteristics of rocks and mesoscopic fractures at different loading rates // Geomechanics for Energy and the Environment. – 2023. – Vol. 33. – P. 100431.

65 Khan J.A. et al. Hydraulic fracturing with low and high viscous injection mediums to investigate net fracture pressure and fracture network in shale of different brittleness index // Geomechanics for Energy and the Environment. – 2023. Vol. 33. – P. 100416.

66 Lai F., Li Z., Wang Y. Impact of water blocking in fractures on the performance of hydraulically fractured horizontal wells in tight gas reservoir // J Pet Sci Eng. – 2017. – Vol. 156. – P. 134-141.

67 Guo X. et al. Investigation of the temperature effect on rock permeability sensitivity // J Pet Sci Eng. – 2017. – Vol. 156. – P. 616-622.

68 Weng X. Modeling of complex hydraulic fractures in naturally fractured formation // Journal of Unconventional Oil and Gas Resources. – 2015. – Vol. 9. – P. 114-135.

69 Zhao Q. Research and Application of Numerical Simulation of Hydraulic Fracturing in Low Permeability Fracture Reservoirs // IOP Conference Series Earth and Environmental Science. – 2019. – Vol. 384, №1. – P. 012138.

70 Stolyarov S. et al. A Novel Technology for Hydraulic Fracture Diagnostics in the Vicinity and Beyond the Wellbore // https://onepetro.org/SPEHFTC/proceedings-abstract/19HFTC/3-19HFTC/D031S007R005/218373. 05.06.2021.

71 Durmagambetov B., Abdrazakov D., Urmanova D. Advanced methods of fracture geometry analysis and parameters sensitivity study // News of the National Academy of Sciences of the Republic of Kazakhstan. – 2022. – Vol. 6, №456. – P. 45-57.

72 Metelkin D.A. et al. Borehole Acoustics as a Key to Perfect Hydraulic Fracturing in Achimov Formation // https://search.spe.org/i2kweb. 04.05.2020.

73 Zhang A. et al. An evaluation method of volume fracturing effects for vertical wells in low permeability reservoirs // Petroleum Exploration and Development. – 2020. – Vol. 47, №2. – P. 441-448.

74 Huang J. et al. Three-Dimensional Effects of Reservoir Depletion on Hydraulic Fracture Propagation // https://www.sci-hub.ru/10.2118. 20.07.2020.

75 Ray B. et al. An Investigation into Proppant Dynamics in Hydraulic Fracturing // https://onepetro.org/SPEHFTC/proceedings-abstract. 10.05.2020.

76 Gabdrakhmanova K.F., Izmaylova G.R., Samigullina L.Z. Probabilistic statistical model for predicting the effectiveness of hydraulic fracturing // IOP Conference Series: Materials Science and Engineering. – 2020. – Vol. 952, №1. – P. 012045-1-012045-8.

77 Webster P. et al. Developments in Diagnostic Tools for Hydraulic Fracture Geometry Analysis // Procced. Unconventional Resources Technology conf. – Denver, Colorado, 2013. – P. 1229.

78 Lecampion B., Bunger A., Zhang X. Numerical methods for hydraulic fracture propagation: A review of recent trends // Journal of Natural Gas Science and Engineering. – 2018. – Vol. 49. – P. 66-83.

79 Cipolla C.L., Warpinski N.R., Mayerhofer M.J. Hydraulic Fracture Complexity: Diagnosis, Remediation, and Exploitation // https://onepetro.org/ SPEAPOG/ proceedings-abstract/08APOG/All-08APOG/SPE-115771. 01.05.2020.

80 Shady M. et al. Reviving a Fractured Water Injection Well: The First Use of Clay Acid Stimulation in a Major Oil Field in Algeria // https://onepetro.org /SPEMEOS/proceedings-abstract. 01.05.2020.

81 Rezaei A., Dindoruk B., Soliman M.Y. On parameters affecting the propagation of hydraulic fractures from infill wells // J Pet Sci Eng. – 2019. – 2019. – Vol. 182. – P. 106255-1-106255-23.

82 Zhang Z., Li H., Zhang D. Reservoir characterization and production optimization using the ensemble-based optimization method and multi-layer capacitance-resistive models // J Pet Sci Eng. – 2017. – Vol. 156. – P. 633-653.

83 Wang P. et al. Lithofacies classification and its effect on pore structure of the Cambrian marine shale in the Upper Yangtze Platform, South China: Evidence from FE-SEM and gas adsorption analysis // J Pet Sci Eng. – 2017. – Vol. 156. – P. 307-321.

84 Pavlyukov N. et al. TIV-Anisotropy in Geomechanical Modeling for Planning of Hydraulic Fracturing at the Kharampurskoye Field // https://search.spe.org/i2kweb/SPE/doc/onepetro:5748BA0F. 10.05.2020.

85 Durmagambetov B., Urmanova D. Investigation of the salt formation issue in the oil field of the Precaspian region // Neft i Gaz. – 2022. – Vol. 131, №5. – P. 40–64.

86 Durmagambetov B., Ismailova D., Drozdov N. About the possibility of implementing water-alternating-gas injection using pump-jet systems at the Arystan field // Neft i Gaz. – 2023. – Vol. 134, №2. – P. 108-121.